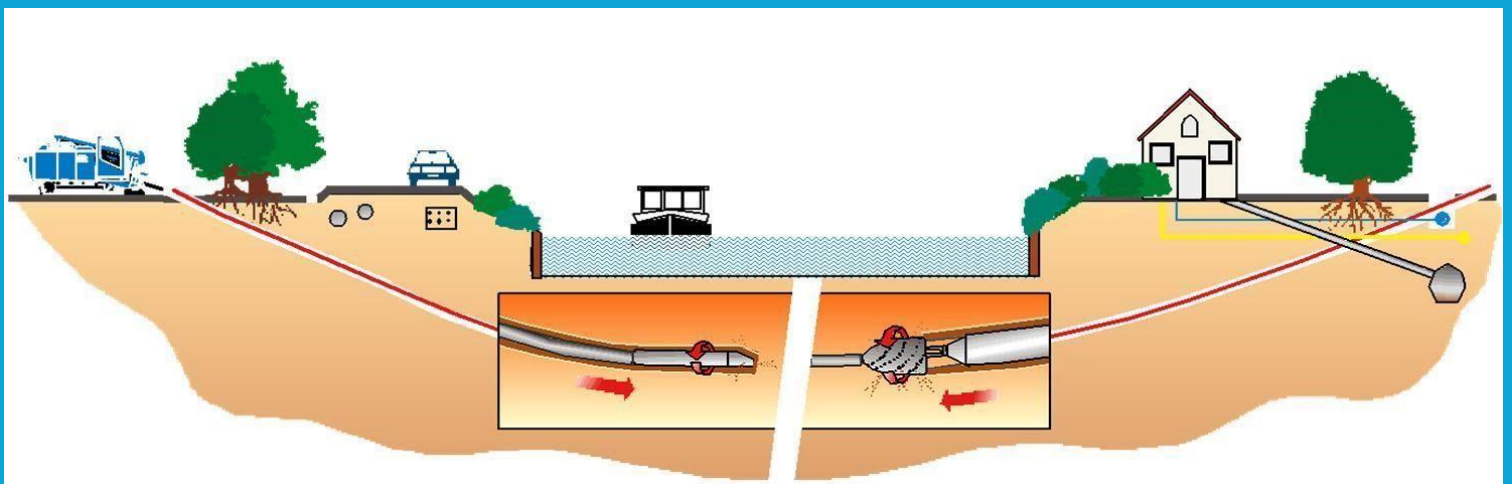


MSc thesis in Geo-Engineering

# A study on factors affecting pullback forces in Horizontal Directional Drilling

Adam Lisowski  
2024





A STUDY ON FACTORS AFFECTING PULLBACK FORCES IN  
HORIZONTAL DIRECTIONAL DRILLING

A thesis submitted to the Delft University of Technology in partial fulfillment  
of the requirements for the degree of

Master of Science in Geo-Engineering

by

Adam Lisowski

August 2024

Adam Lisowski: *A study on factors affecting pullback forces in Horizontal Directional Drilling* (2024)

The work in the following thesis was conducted in collaboration with:

**Deltares**



Department of Geo-Engineering  
Faculty of Civil Engineering  
Delft University of Technology

Supervisors: Dr. Ir. Wout Broere  
Dr. Ir. Guy G. Drijkoningen  
Henk Kruse  
Hans Landwehr  
Jörg Himmerich

## ACKNOWLEDGEMENTS

Words cannot express my gratitude to my professor and chair of my committee for his mentorship, patience and most of all for the constant feedback throughout the process. Furthermore, this journey could not have been successful without the other members of the defense committee, who have generously provided me with their knowledge and expertise of the Horizontal Directional Drilling industry. Additionally, this endeavour was possible thanks to the generous support of Deltares and the Drilling Contractors Association (DCA), who provided financial aid during the research.

I am also grateful to Robert Osikowicz Engineering (ROA) and Zakład Remontowo-Budowlany Janicki (ZRB Janicki) for support and consulting during the development of the research. Moreover, I would also like to thank my classmates for the inspiration and mutual feedback sessions conducted over the duration of the project.

Lastly, I would be remiss in not mentioning my family and closest friends. Their unwavering belief and support during the process have kept my spirits and motivation high. Their emotional support was invaluable.



## ABSTRACT

This thesis aims to explore the influence of borehole alignment accuracy and other soil and pipe parameters on the pullback forces during the pullback phase in Horizontal Directional Drilling (HDD) operations. To that end a model inspired by PipeForce V1 was implemented and expanded upon in Python. The model was used to calculate the pullback forces based on the measured product pipe navigational coordinates obtained from actual HDD projects. Calculated pullback force data was compared to actual measurements. It was found that pullback forces tend to decrease with increasing borehole alignment accuracy. The extent of the influence depends on the length of the installation under consideration. Furthermore, through analysing ballasting and specific gravity of slurry, it was found that a balance between those factors resulted in a decrease in the maximal pullback forces, through optimising the effective vertical force on the product pipe. Lastly, it was found that the originally proposed model PipeForce V1 should not be applied to longer installations due to an almost quadratic growth in one of the calculated factors, which was not checked for in the original publication.



# CONTENTS

1	INTRODUCTION	1
2	BACKGROUND INFORMATION ON HORIZONTAL DIRECTIONAL DRILLING	5
2.1	Procedure	5
2.1.1	Geotechnical Investigation	5
2.1.2	Optimal Path Design	6
2.1.3	Pilot Hole Drilling	7
2.1.4	Borehole Reaming	8
2.1.5	Product Pipe Preparation	12
2.1.6	Product Pipe Pullback	12
2.2	Application	14
2.3	Limitations	14
3	LITERATURE STUDY	17
3.1	Most Frequently Used Navigational Instruments	17
3.1.1	Walkover locating systems	17
3.1.2	Magnetic tracking	18
3.1.3	Gyroscopic surveys	19
3.1.4	Combination of tracking and survey methods	20
3.1.5	Accuracy and error propagation in navigational instruments	20
3.2	Description of Physical Phenomena and Effects Influencing the Pullback Force	24
3.2.1	Influence of product pipe feeding system outside of the bore	24
3.2.2	Influence of product pipe friction inside the bore	24
3.2.3	Influence of soil clamping on the drilling equipment (Chock Effect/ Wedging Effect)	24
3.2.4	Influence of bending due to bore geometry (Capstan Effect)	25
3.2.5	Influence of slurry circulation	25
3.2.6	Influence of product pipe ballasting	25
3.2.7	Influence of reamer and drill string exiting the bore	25
3.2.8	Influence of penetration of different geological structures or strata	26
3.3	Description of Currently Available Models Analysing the Pullback Force	26
3.3.1	ASTM F1962 Model	26
3.3.2	PRCI Model	27
3.3.3	Driscopipe Model	28
3.3.4	Drillpath Model	29
3.3.5	NEN Model	30
3.3.6	Additional Theoretical Models	31
3.3.7	Comparison of Described Models	31
3.4	Description of the Implemented Numerical Model Analysing the Pullback Force	33
3.4.1	Friction due to pipe weight on the ground $(T_g)_i$	33
3.4.2	Pulling force component due to friction of the ballasted pipe inside the borehole $(T_b)_i$	34
3.4.3	Resisting force due to slurry $(T_r)_i$	35
3.4.4	Resisting force due to bend negotiation $\Delta T_{f-k}$	35
3.4.5	Resisting force due to drill string exiting the borehole $(T_s)_i$	37
3.4.6	Total pullback force $T_i$ formulation	38
3.4.7	Implemented model Limitations	38
4	DATA AVAILABLE	41
4.0.1	Raw Data	41

4.0.2	Preliminary Data Investigation . . . . .	46
5	RESULTS AND ANALYSIS . . . . .	53
5.1	Validation of the Model with Real Data . . . . .	53
5.2	Relationship Between the Accuracy of Borehole Alignment and the Pullback Force . . . . .	56
5.2.1	Approach to borehole alignment adjustment . . . . .	56
5.2.2	Influence of trajectory with real ballast and specific gravity of slurry data . . . . .	58
5.2.3	Influence of trajectory with optimal ballast and specific slurry gravity data . . . . .	60
5.3	Influence of Ballast and Specific Gravity of the Slurry on the Pulling Force . . . . .	63
5.4	Additional Relationships Between Parameters . . . . .	65
6	DISCUSSION . . . . .	69
6.1	Data Available . . . . .	69
6.2	Model employed in the research . . . . .	69
6.3	Results . . . . .	70
6.4	Recommendations for further research . . . . .	71
7	CONCLUSION . . . . .	73
A	PYTHON CODE . . . . .	75
A.1	Model . . . . .	75
A.2	Beam Calculation . . . . .	87
A.3	Data Resampling . . . . .	89
B	ADDITIONAL VISUALISATIONS OF CHANGING MAXIMAL PULLING FORCES WITH VARYING GENERATED TRAJECTORIES . . . . .	91

# ACRONYMS

<b>HDD</b> Horizontal Directional Drilling . . . . .	1
<b>DCA</b> Drilling Contractors Association . . . . .	2
<b>BHA</b> Bottom Hole Assembly . . . . .	7
<b>CPT</b> Cone Penetration Test . . . . .	5
<b>SPT</b> Standard Penetration Test . . . . .	5
<b>RMS</b> Root Mean Square . . . . .	20
<b>HDPE</b> High Density Polyethylene . . . . .	31



# 1

## INTRODUCTION

Horizontal Directional Drilling ([HDD](#)) was developed in the United States in the 1970's by Martin Cherrington. He utilized a modified vertical drilling rig, previously used for oil drilling, to develop a rig for horizontal directional drilling. Upon finding a very distinctive niche within the market and with the help of environmental movements which opposed any engineering techniques making use of trenches in order to preserve nature, Cherrington was employed by Sacramento Municipal Utility District and later by Pacific Gas & Electric Co., where the method proved its usefulness. At that point the [HDD](#) rig was deployed in order to dig an approximately 500 ft. (152.4 m) long borehole which was designated to store a 4 in. (10.16 cm) diameter gas pipe. After a certain amount of struggles the work was completed successfully marking the first trenchless river crossing in the industry. News about such an achievement quickly spread throughout the industry putting more attention towards the method itself ([Farr \[2012\]](#)).

Throughout the years, since the first utilization of the [HDD](#) method, it was constantly being upgraded in order to accommodate for wider and longer works, however, the steering technology was very inaccurate and in a general sense archaic as it was based on using hand-held air drills in order to create small vertical openings from the surface in the hope of crossing paths with the drill string leading to extracting information on the path and angle of the drill head based on the change of depth at which contact was established. Such a method was applicable at the time, but it left a lot of room for errors and inaccuracies, however back then it was acceptable as the subsurface remained quite spacious and devoid of underground infrastructure. A breakthrough in the steering technology was achieved in the late 1980s in the form of a magnetic steering tool developed by a company called Tensor. The navigational device based on using an artificial magnetic field that allowed a steering tool position to be determined in relation to a source, such as the drill head. That was the threshold upon which the workers were able to assess the position and angle of inclination of the drilling head without actually hand-drilling vertically down to reach the drill string. Such development boosted the accuracy and the general ease of work with trenchless horizontal drilling. Since then a number of milestones has been reached regarding the variety of navigational devices along with their respective readout accuracies.

[HDD](#) has been used in the Netherlands since 1983. Since the introduction of this technique, Deltares (formerly GeoDelft) has been involved in research and further development of this trenchless technique. Furthermore, as the method was introduced into the European market, it has gained great popularity due to its simplicity and cost effectiveness. Additionally, trenchless methodology in general, entails minimal disturbance to the subsurface compared to previously applied cut and cover installations, which on the European continent is quite crucial due to the amount of buried artifacts, such as for example, explosives left over after the World Wars along with archaeological wonders still very strongly present in certain regions. Horizontal directional drilling has been utilized to create small diameter horizontal boreholes which then are filled with polyethylene or steel piping, conduits or cables in order to move previously overground infrastructure like electric lines or water/gas pipes, into the underground domain.

Throughout the years thousands of [HDD](#) works have been completed all around the world especially in the highly urbanised areas. Such actions led to the sub-

surface becoming increasingly occupied. Furthermore, the amount of underground infrastructure is projected to be increasing even more in the coming years leading to potential issues concerning the space availability and risk of damaging installations already in place. Thanks to the European Green Deal and Paris Climate Accords, the European Union aims to be climate-neutral by year 2050. Such a complex goal comes with a lot of issues regarding a massive restructurization of (but not limited to) the electrical grids in order to accommodate for all electric based devices which are about to replace previously utilized fossil fueled ones. Such high demand in electrical energy will result in the installation of thousands of kilometers of high and low voltage cables in the subsurface. Therefore, the scale of this endeavour might potentially benefit from any scientific developments in the field. With such issues in mind, there are at least two potential solutions, namely: the drilling will have to be conducted at higher depths where no piping is present or the accuracy of the process will have to be enhanced.

The main focus of the following research is the analysis and discussion surrounding the pullback force in the final stages of the HDD process, when the product pipe is being pulled in. The most crucial research question is whether the borehole alignment accuracy (smoothness of the bore path) influences the pullback force, by manipulating which soil and operational parameters, the pullback force can be influenced. The main thesis of the following work is that the borehole alignment accuracy has a significant impact on the pullback forces and that through smoothing of the drilling trajectory along with variations of certain influential parameters the overall pullback force can be lowered.

The most crucial research questions are:

1. Does the borehole alignment accuracy (smoothness of the bore path) influence the pullback force?
2. Which other soil and pipe parameters influence the pullback force and in what way?

In the following work, the Chapter 2 provides comprehensive background information on the topic of HDD process itself, along with the most common applications of the method and its inherent limitations. Chapter 3 consists of a comparison and descriptions of the advantages and disadvantages of navigational devices currently in use. Additionally, the descriptions of the phenomena and effects influencing the pullback and thrust forces can be found there as well. In Section 3.2 the partial forces and the basic mechanics behind them, along with their influence on the pullback forces are described. Lastly, recent findings regarding the modeling and estimation of the pullback force are described, along with the detailed specifications of the models chosen to be implemented in the work. In Chapters 4 through 5 the available data, the undertaken step by step analysis and the results of said analysis are described. These chapters as well as the discussion Chapter 6 can be considered the core of the work. In the discussion Chapter 6 the results uncovered in the previous chapters are discussed, while pointing out their advantages and weaknesses with regard to the utilized models and past case data. Furthermore, it is also mentioned how this research might be beneficial in the future when combined with further developments in the field. Finally, the conclusion chapter consists of the most crucial discoveries of the whole work along with its advantages and shortcomings.

In terms of methodology, a promising numerical model found in the literature study was implemented in Python programming language. Namely, PipeForce Version 1 model created by Liangxue Cai and Maria Anna Polak ([Cai, 2011]). Models have been run based on data from past installations supplied by Deltares and the Drilling Contractors Association (DCA). After the model being ran successfully with the real life data and benchmark values for ballasting, specific gravity of the drilling

mud and the trajectory smoothness coefficient, the values of mentioned parameters have been varied in order to find relations and dependencies between them and the overall pullback force. Results of the mentioned analysis were then visualized and presented further in [Chapter 5](#).



# 2

## BACKGROUND INFORMATION ON HORIZONTAL DIRECTIONAL DRILLING

### 2.1 PROCEDURE

HDD is a steerable trenchless method utilized for subsurface drilling works together with insertion of previously manufactured pipe. Essentially the HDD rigs can be considered as adjusted small oil drilling rigs with a few key differences. An addition of a ramp for directional drilling instead of a mast keeping the drill string vertical. Furthermore, while the drill string is kept in tension by the gravity in oil drilling, a similar result is achieved by the HDD rig pushing the string segments one by one. In terms of pushing systems, the earlier rig models used cables, which later were replaced by hydraulic systems and finally electric mechanisms utilizing racks and pinions.

A typical HDD project consists of six steps. Said six steps can be categorized into two stages. Before breaking the ground two steps have to be conducted, namely, the geotechnical investigation in order to establish the geotechnical parameters of the soil and with accordance to the findings from the first step an optimal path design can be constructed. As soon as the preparation stage is complete the next four steps can commence. These four steps consist of, a small-diameter bore being drilled along the predesigned bore path using a steerable and tractable drill bit (pilot drill), afterwards, the bore is reamed to a diameter typically 30-50% greater than the intended pipe diameter through one or multiple reaming passes, then the pipe string is prepared in order to finally be pulled into the already reamed borehole. After that step, one could consider the cleanup procedure like mud extraction and treatment along with removal of all heavy equipment an additional stage, however it was omitted in the following research.

#### 2.1.1 Geotechnical Investigation

The target of a geotechnical investigation is not only to establish whether or not a HDD crossing is feasible, but also to determine the most appropriate way of conducting the installation itself, bearing in mind choice of equipment (drilling head, mud, etc.) is based on the soil conditions in place. The geotechnical report has to consist of encountered soil strata analysis, which is conducted by taking soil samples at chosen intervals along the theoretical bore path, yet far enough as not to create escape routes for the drilling mud to follow, when the drilling is taking place. The amount and spacing of the samples taken is dependent on the size of the installation, along with general geological conditions in the area of interest. Apart from sampling the soil, geotechnical engineers often use practices like the Cone Penetration Test (CPT) and Standard Penetration Test (SPT), where by reading certain values off of the graphs provided by the test, one can deduct the penetrated soil types continuously. Such examinations tend to give a cross-sectional in-depth look into the geology on site. Typical benchmark values based on which a preliminary soil investigation can be conducted based on the CPT and SPT results can be seen in Table

2.1

Table 2.1: General values associated with different soil types (Drilling Contractors Association (DCA) [2009])

Soil Type/ Test Type	CPT	SPT	Young's Modulus
Parameters [Units]	qc [MPa]	N <sub>30</sub> [Blows/30cm]	E <sub>s</sub> [MPa]
<b>dense sand</b>	>20	>50	100 - 200
<b>medium dense sand</b>	10 - 20	25 - 50	50 - 100
<b>loose sand</b>	5 - 10	10 - 25	20 - 50
<b>stiff clay</b>	> 2	> 8	10 - 25
<b>medium stiff clay</b>	1 - 2	2 - 8	5 - 10
<b>soft clay</b>	< 1	< 2	0 - 5

### 2.1.2 Optimal Path Design

As soon as the geotechnical report of the site under consideration is finished, the appropriate, detailed path design can commence. The path needs to be adjusted considering the geological conditions along with the bending radii that both the drill string and the final product pipe can endure. In general a rule of thumb is to take the radius as big as it is possible in order to minimize the influence of bends on the overall process. Small curvature radii cause additional bending stresses on the drill string and the product pipe itself, while also introducing higher pullback forces due to the so-called Capstan Effect. The Capstan Effect is the phenomenon of generating additional drag forces as a pipe negotiates a curve due to a component of the pulling force acting normal to the curvature (more on the topic of Capstan Effect can be seen in Section 3.2.4). Deciding on the appropriate geometry of the installation is complicated as it consists of finding the optimal path by compromising between the total available length for the project, the required depth for safe cover at which the pipe should be installed and the maximal bending radii of both the drilling string and the product pipe (Internal Sources [2022]).

In general there are about five most common configurations for designing the bore path. Most of the time the path is designed in a manner consisting of a series of straight and curved segments as seen in Figure 2.1. Most of the time the curved elements consist of either sag or over bends. The bent segments should be designed in a way of being both gradual (not to exceed minimal bending radii of the product pipe as mentioned in Section 2.3) and sufficiently short as not to generate too much additional resisting forces. A crucial aspect of designing a bore trajectory is to find balance between low bending radii and as much of straight segments as possible as those generate the least amounts of resisting forces. Straight segments in cohesive and stronger geological conditions additionally limit the potential of subsurface deformations during the installation.

Furthermore, on top of the already popular combinations of elements used, a new one was introduced in a study focused on the topic of borehole trajectory conducted by Wiśniowski, Skrzypaszek, Łopata and Orłowicz (Łopata P. & Orłowicz G. [2020]). Said method is one focusing on the concept for designing HDD trajectories related to the natural deflection of the pipe described by a chain curve. A catenary curve method is based on a natural curve that a cable, chain, or any other line of uniform weight assumes when suspended between two points, example of which can be seen in Figure 2.2. Such a solution is claimed to enable easier insertion of the pipeline into a wellbore and to ensure its longer life due to a more natural stress distribution along the length compared to the mixture of straight and curved elements traditionally in use. Furthermore, a smoother bore trajectory limits the amount of bending leading to potentially lower pullback force requirements.

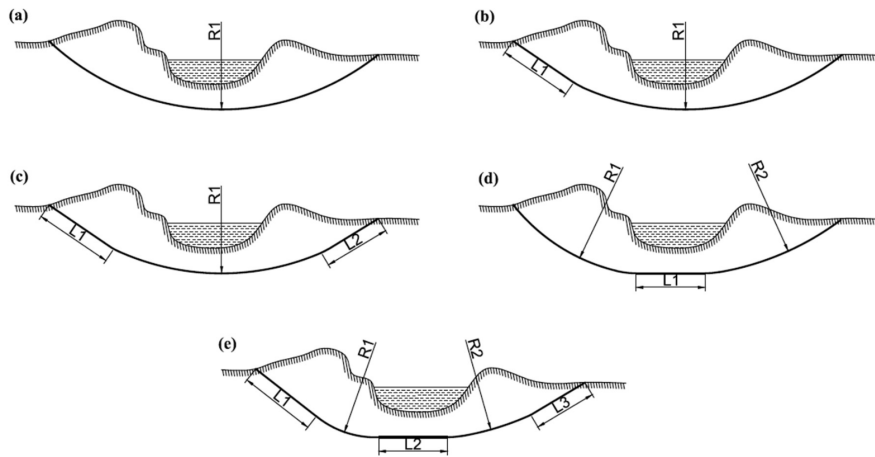


Figure 2.1: Most commonly used path trajectories as a combination of straight and curvilinear sections: (a) curvilinear section; (b) straight section and a curvilinear section; (c) two straight sections and a curvilinear section; (d) straight section and two curvilinear sections; (e) three straight sections and two curvilinear sections. (Łopata P. & Orłowicz G. [2020])

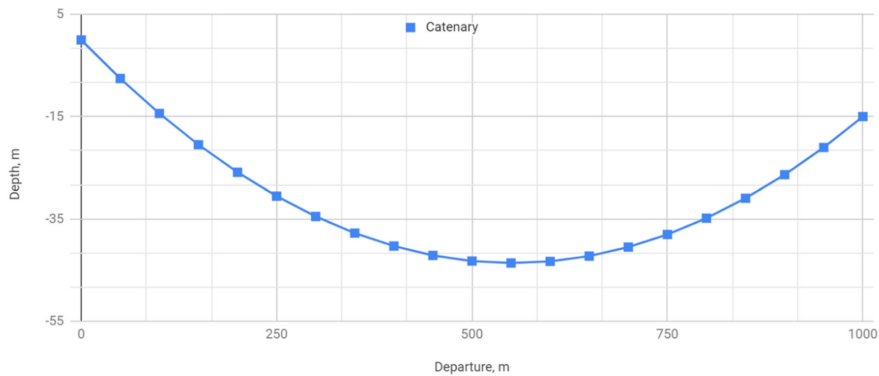


Figure 2.2: Example of a catenary path design (Łopata P. & Orłowicz G. [2020])

### 2.1.3 Pilot Hole Drilling

As soon as the planning steps are concluded, the more practical, drilling part can commence. The first procedure after finishing the preliminary investigation and path design, is the pilot drilling. It is considered as the most complex and the one of the slower steps in the entire process of installation. In general the process focuses on making an initial, small diameter bore (0.1 - 0.25 [m] in diameter) along the designated path, as accurately as the conditions allow. The speed of the pilot process may vary dependent on the rig in use and the surrounding geological formations, but should remain around the value of 100 m/h for smaller rigs (Broere [2021]). In case of bigger drilling operations an average value of 300 m/h can be assumed. The equipment used to said end is contained in Bottom Hole Assembly (BHA), schematized example of which can be seen in Figures 2.3 and 2.4. The BHA in case of the pilot drill is always made up of a few parts, a drilling tool at one end, a bent sub-assembly, a steering tool and finally, dependent on the navigation tool in use, an additional non-magnetic drill pipe can be added in order to limit the magnetic field disturbances due to relative movements of drill pipe connections (visible in Figure 2.5). Following the BHA, segments of a hollow drill pipe are mounted by the piece at the drilling rig, pushing the entire drill string in. Through the hollow drill pipe segments drilling mud is pumped in order to remove the cuttings from the excavated borehole. The most commonly used drill heads are, jet drill bits and a regular

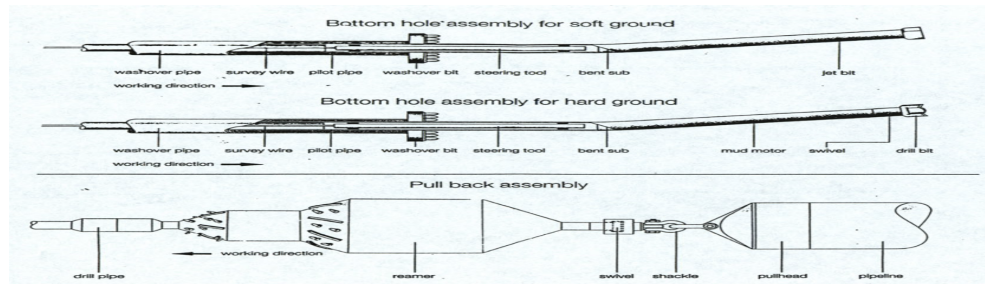


Figure 2.3: Older bottom hole assembly schematic Broere [2021]

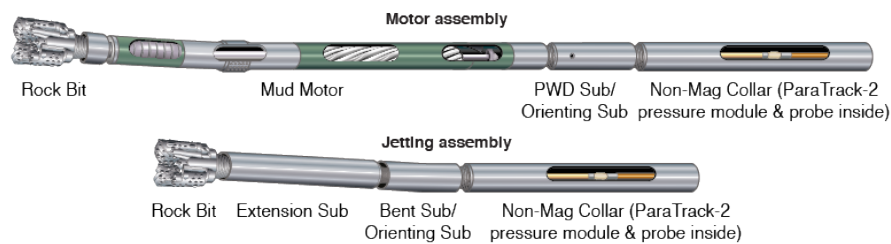


Figure 2.4: Newer bottom hole assembly schematic Prime Horizontal [nd]

drill bits combined with a mud motor. Jet drill bits are mainly utilized in soft soils as they use highly pressured mud to dig through the soil. The Mud motor is a tool which transforms the energy created by mud pumps into fast rotation of the drill bit. A mud motor is an expensive piece of equipment mostly utilized in harder soils and rocks as it lowers the stress on the drill pipe while maintaining high torque at the drill head. The pilot bore directional control is realised differently for a jetting tool and a mud motor. With a jetting tool a piece drill string with an asymmetrical leading edge is applied, inducing a steering bias. Whereas, with a mud motor the shaft connected to it can be set at different angles, creating the steering bias. When there is a need to change the direction of the drilling tool, the asymmetrical tool is rotated so that the new direction aligns with the steering bias of the leading to an effective change of direction. If no path adjustment is required the whole drilling string is rotating so that no steering bias is established. Finally, a schematic of the pilot phase can be seen in Figure 2.6.

#### 2.1.4 Borehole Reaming

Upon the small diameter pilot bore being completed, the reaming phase can commence. As the drill string punches out of the soil on the side opposite to where the drilling rig is placed, the pilot drilling head is dismantled and a reamer is attached to the drill string. Examples of rock reamers can be seen in Figure 2.7. Said tool is meant to enlarge the already existing borehole up to appropriate size which ranges between 1.3 up to 1.5 times the diameter of the product pipe to be pulled in. The magnitude of the borehole over-sizing depends on a multitude of attributes like, soil types, soil stability, depth, type of drilling mud, borehole hydrostatic pressure and possibly more specific characteristics of the area under consideration for the project (Internal Sources [2022]). The speed of the reaming process may vary dependent on the rig in use, yet should oscillate around 50 m/h (Broere [2021]). Naturally, installations conducted with bigger drilling rigs and higher pipe diameters will prove slower. Dependent on the diameter of the reamer in use, this step might even take longer than the pilot drilling. While the over-sizing is crucial in order for the product pipe to be pulled in without major issues, the bigger the produced bore is, the harder the maintenance of the opening in the soil can be. Dependent on the particular case and conditions during installation, the reaming phase might consist of one



Figure 2.5: Example of drill pipe connectors utilized in the industry [Bormill Inc. \[2019\]](#)

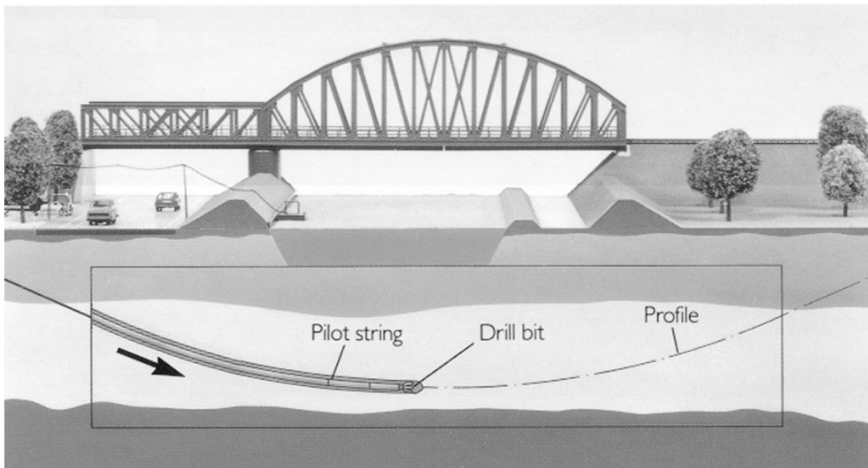


Figure 2.6: Pilot phase schematic ([Broere \[2021\]](#))

or multiple passes (using the same or an increasing reamer size) of the reamers in order to achieve the desired bore diameter. Upon encountering problems in terms of borehole instabilities, additional swab passes are applied in order to smooth the internal surface of the borehole and remove any additional debris, in such cases it is also recommended to apply drilling mud with more yield and with faster gelling capabilities to provide more support to the excavation. A schematic of the reaming phase can be seen in Figure 2.8.



Figure 2.7: Example of rock reaming tools utilized in the industry (Drillingbits.eu [2019])

Furthermore, the drilling mud such as, for example fluid bentonite is injected into the borehole, while the installation is progressing. The injection of drilling fluid has a number of effects which are expected based on its properties. Firstly and most importantly, due to its characteristics it keeps the soil cuttings in suspension and brings them out of the borehole through circulation induced by mud pumps. Secondly, it is meant to add lubrication between the pipe and excavation walls while also supporting and stabilizing the borehole by increasing the pressure within. Thirdly, the accumulation of so-called "mudcake" on the walls of the borehole in order to prevent ground water from entering the drilled path. Finally, it is worth to mention that a lot of energy in the form of heat is created due to friction between the borehole and the drill string or a product pipe being pulled in. To that end, drilling mud provides additional cooling capacity leading to limiting the wear of tools in use. The most common products utilized as drilling mud are either different kinds of clays or polymers, in case of clays the most commonly used one is sodium

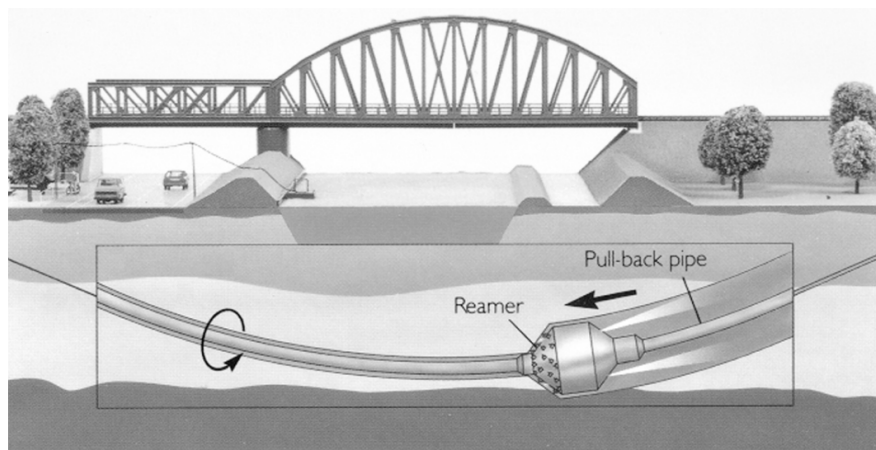


Figure 2.8: Reaming phase schematic (Broere [2021])

montmorillonite (bentonite) which owes its name to Fort Benton in the United States where it was first mined for its water absorption properties for the oil and gas industry. In both cases fresh water needs to be added, for drilling mud to be created. Based on soil and cutter parameters, appropriate drilling mud is designed for the installation at hand. During the boring, mud is consistently monitored in order to keep the borehole open, maintain circulation and omit any risks regarding the failure of the pumping systems. Figure 2.9 visualises the circulation of the drilling mud inside of the borehole. Furthermore Figure 2.10 shows the movement of the drilling mud around an installation site. In that figure it can be seen that in the mud tank (element number 5 Figure 2.10), the bentonite or polymers are being mixed with fresh water, then the drilling mud is pumped through the drill string into the borehole. Then as the mud circulates within the borehole it flows out by the entrance and is being sucked away into the mud pit (element number 14 in Figure 2.10) and further into the recycling unit (element number 6 in Figure 2.10) where separation of soil cuttings and mud is conducted. From the recycling unit, left-over bentonite is fed back to the tank and the cycle continues.

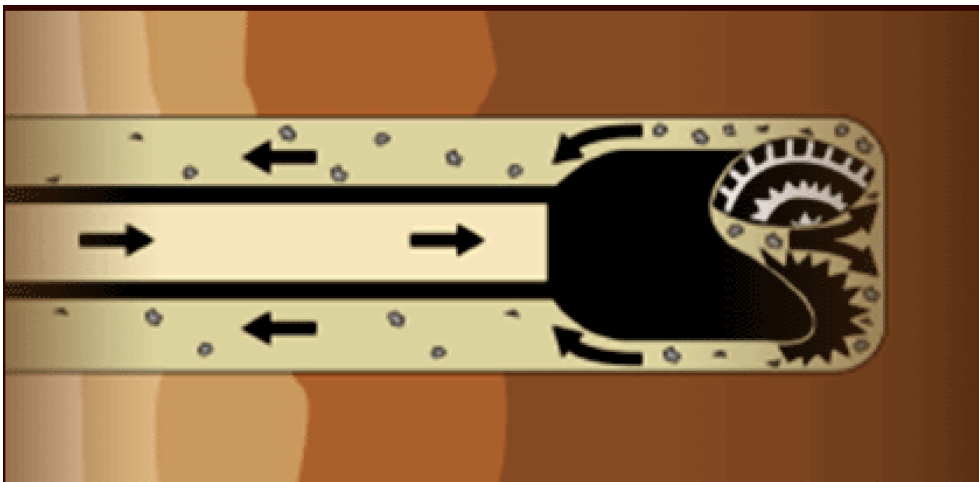


Figure 2.9: Visualisation of mud flow around the drilling head (Oil & Gas UK [nd])

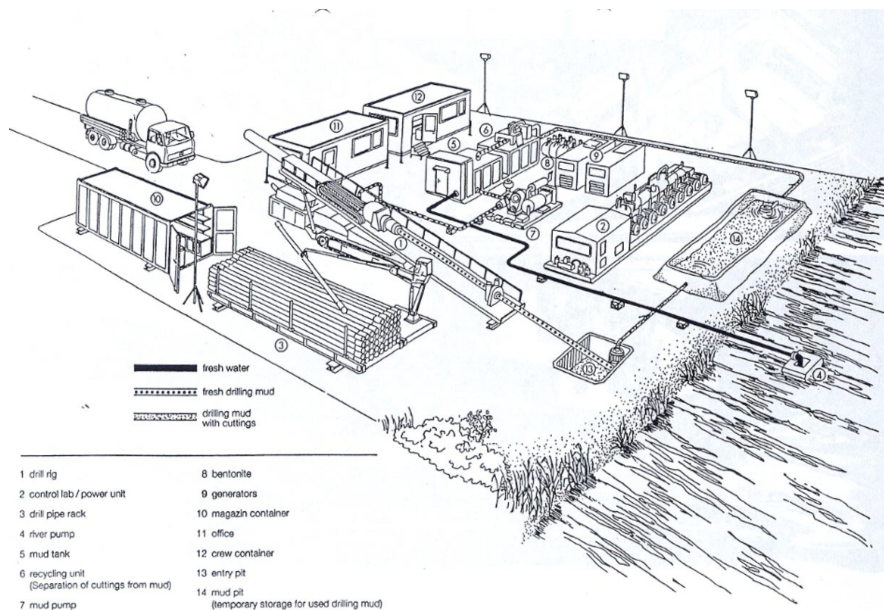


Figure 2.10: General drilling installation site layout (Broere [2021])

### 2.1.5 Product Pipe Preparation

Before the completion of the bore excavation, comes the time to prepare the product pipe, intended to be pulled into the opening. Pipe segments are laid out on rollers or on the ground and welded together in order to create a continuous segment. Furthermore, the pipe is also tested keeping in mind certain safety factors in order to determine whether all prerequisites are met for the installation at hand. The process benefits greatly from being able to be conducted as soon as possible after the bore is prepared, additionally it is crucial to keep the velocity of insertion constant. In order to better visualise the step of product pipe preparation, an exemplary pipe preparation layout site can be seen in Figure 2.11. As seen in the figure another very useful aspect is the slight overbend feeding the pipe into the opening (known also as catenary) which can be spotted just before the pipeline insertion point into the ground in the figure. The feeding system is constructed in such way in order to limit the bending path before an optimal depth is reached.

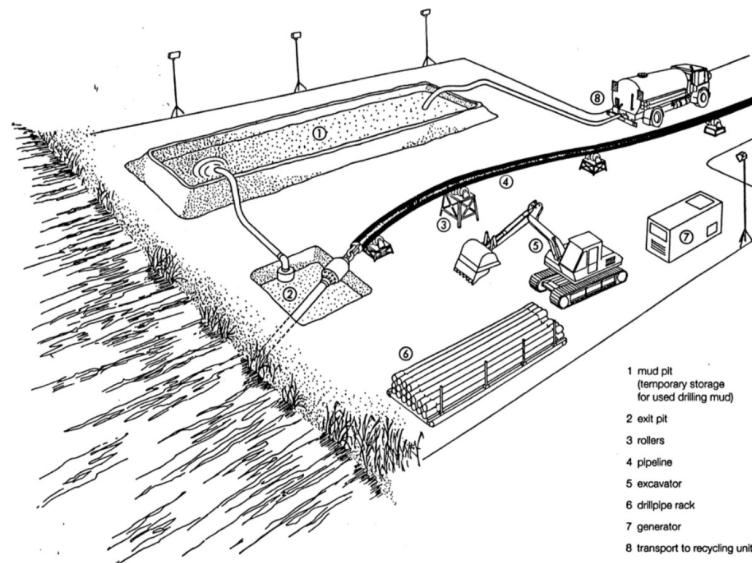


Figure 2.11: Product pipe preparation site layout (Broere [2021])

### 2.1.6 Product Pipe Pullback

The final step of the HDD entails pulling the product pipe laid out in a single segment, mentioned in the previous step, into the already prepared borehole. In order to pull the pipe most commonly a reaming tool along with a swivel are connected between the drill string and the product pipe, an example of such configuration can be seen in Figure 2.12. The reamer is present in order for the final smoothing of borehole walls just before the product pipe slides along. The role of the swivel connection is to keep the product pipe from rotating along with drill string. The product pipe has to be pulled in carefully as not to exceed its material specifications. Some of the most crucial aspects to look at are, the insertion velocity, how much the pipe is bending in the hole, whether the drilling mud circulation works properly without any hindrance and finally axial tension forces along with the length of pipe inserted compared to how far into the borehole the pipe is, should be monitored. The constant insertion velocity is crucial in order to avert a standstill during which, due to the characteristics of the drilling mud, its yield strength will increase leading to more force required for movement to commence once more. A standstill additionally poses a threat of damaging the product pipe upon relaunch of the pullback

operation. During this phase dependent on the type of rig used, the velocity is expected to be approximately 100 m/h (Broere [2021]).



Figure 2.12: Reamer connected with a swivel to the product pipe (Kezdi [2020])

## 2.2 APPLICATION

Among trenchless technologies, HDD has a good standing applicability in most of underground operations (Najafi [2010]). HDD constitutes about 15% of all trenchless operations installing water, gas distribution systems, oil/gas transmission, telecommunications systems and electric cables. However, in the case of sewage installations, it constitutes around 12% (Carpenter [2011]).

Specific sizes of HDD rigs are suggested to be used for specific soil conditions, project conditions including diameter, depth, length of borehole, and type of product pipe to complete the job successfully. HDD technology has many benefits compared to open cut especially in urbanized areas, where the open method might prove problematic or downright impossible due to site constrictions. Parameters related to HDD rigs of different sizes can be seen in Table 2.2. Furthermore, even larger rigs are currently being used in the industry having > 500 t of maximal tension force, able to conduct installations of over 5000 m in length. However, machines of such size are used in special projects, hence absent from Table 2.2.

Table 2.2: General values associated with different rig sizes (Broere [2021])

Drilling Rig Type	Mini	Midi	Midi large	Maxi
<b>max. tension force [kN]</b>	7.5 - 10	15	30	200
<b>entry angle [°]</b>	8° - 40°	8° - 25°	8° - 15°	8° - 15°
<b>min. bending radius [m]</b>	20	50	100 - 150	250
<b>drill string diameter [mm]</b>	33 - 53	43 - 53	75	100
<b>max. product pipe diameter [m]</b>	0.2	0.2 - 0.4	0.4 - 0.6	0.6 - 1.5
<b>max. drilling length [m]</b>	200	400	400	1500
<b>length of drill pipe [m]</b>	3	6	6	9.5
<b>max. pump flow [L min<sup>-1</sup>]</b>	150	150 - 500	500 - 1250	2500

## 2.3 LIMITATIONS

HDD is a widely used method that gained a lot of popularity throughout the past 50 years, but it does not mean that the method is truly universal, it comes with its own drawbacks. Firstly, a crucial issue comes with the presence of coarse-grained material and excessive presence of bedrock material, which may cross the path of the installation. Coarse-grained material does not fluidize with drilling mud and water, therefore it causes more friction and wear to the used tools. Furthermore cobbles and boulders being encountered during drilling provide additional ways for pressured mud to escape creating potential risks of cave-ins along with a chance for deviations from the design path of the installation. Any changes to the initially designed trajectory might cause prolongation of the installation and additional costs, through the need of reversing and correcting the drilling path.

Secondly, keeping the equilibrium between the mud pressure inside the borehole and the forces acting on the soil outside of it might prove problematic. Careful estimations and safety factors need to be introduced as to avert the possibility of a frac-out and collapse of the bore. Upon mud pressure inside of the bore being too high, an uncontrollable spillage of drilling mud of varying rheological properties to the surroundings may occur. If the mud pressure within the bore is too low, the walls of the drilled opening might cave in as the support from within is too low. Important in any case of bore disruption the drilling mud despite its natural origins is considered to be industrial waste needing treatment and recycling. The condition of the pressure and force calculations is dependant on the quality of the geotechnical investigation (mentioned in Section 2.1.1), as that is where most of the parameters

in use come from. Even with safety factors taken into account, the unpredictability of geological formations present in heterogeneous soil has to always be taken under consideration.

Thirdly, due to the effectiveness and the method being noninvasive, a multitude of HDD projects are conducted in congested urban areas. Understanding the staging areas along with the maintenance of traffic in said locations are as crucial for the installing company as a successfully drilled operation itself. Hence, an ever increasing role of site planning and trajectory design should be acknowledged. While careful staging of installation site in urban areas proves crucial, it might still benefit projects conducted outside of urban areas.

Finally, as the trajectory during any installation is bending, there is a limitation present due to the minimal bending radii of the product pipe in question. Upon exceeding the minimal bending radii the product pipe might deform in a plastic manner, leading to potential ruptures. Hence, a general approach to safe minimal bending radii estimation can be seen below, in Equations 2.1 through 2.4.

In accordance with the current guidelines, Ruhrgas AG (Broere [2021]) has recommended a rule of thumb, which is used by most of the contractors and designers. This rule of thumb links the minimum bending radius with the external diameter of the pipe. The results of this recommendation can be seen in Equations 2.1 and 2.2.

For a diameter  $\leq 0.7\text{m}$ :

$$R_{min} = 1000 \cdot D_{ext} \quad (2.1)$$

For a diameter  $> 0.7\text{m}$ :

$$R_{min} = 1400 \cdot \sqrt{D_{ext}^3} \quad (2.2)$$

where,  $D_{ext}$  is the external diameter of the product pipe.

Furthermore, as any HDD installation is a three dimensional issue, not only does the bending in the horizontal plane play a role, but also the one in the vertical plane. Therefore, in order not to exceed the material safety during installation, a combined bending radius needs to be calculated. Formulation for the combined bending radius can be seen in Equation 2.3.

$$R_{combine} = \sqrt{\frac{R_h^2 \cdot R_v^2}{R_h^2 + R_v^2}} \quad (2.3)$$

where,  $R_h$  is the bending radius of the product pipe in horizontal direction and  $R_v$  is the bending radius of the product pipe in vertical direction.

Although, the above rule of thumb is based on experience, the influence of the soil conditions is not taken into account. An updated design guideline from the DCA (Drilling Contractors Association (DCA) [2009]) does take this into account (Broere [2021]). The formulation proposed in the DCA guidelines can be seen in 2.4, while also considering values present in Table 2.3 (supplement to Table 2.1).

$$R_{combine} = C \cdot \sqrt{D_a \cdot s} \quad (2.4)$$

where,  $C$  is the soil dependent constant present in Table 2.3,  $D_a$  is the outer diameter of the product pipe and  $s$  is the wall thickness of the pipe.

Table 2.3: Values of Soil Constant C[-] associated with different soil types (Drilling Contractors Association (DCA) [2009])

<b>Soil Type/ Test Type</b>	<b>Soil Constant</b>
<b>Parameters [Units]</b>	<b>C [-]</b>
<b>dense sand</b>	8500
<b>medium dense sand</b>	9400
<b>loose sand</b>	10200
<b>stiff clay</b>	10500
<b>medium stiff clay</b>	11500
<b>soft clay</b>	12500

# 3

## LITERATURE STUDY

### 3.1 MOST FREQUENTLY USED NAVIGATIONAL INSTRUMENTS

In this chapter the focus is shifted towards the process of locating and steering of the drill head over the duration of the installation. Locating and steering systems are working very much in tandem as steering is based on the readings of the locating devices. Said two processes come together under a general term 'navigation'. There are actually two completely separate navigational systems. The initial system is the downhole survey device which is quite small nowadays, which takes up the form of an insulated copper wireline inside the drill string which is used to read measurements from the steering probe (part of the BHA). The copper wire runs through the entirety of the drill string up to the drill cab, where it is connected to a computer on which the readings can be interpreted by the drilling personnel. The steering probe measures inclination and azimuth of the BHA based on Earth's gravitational and magnetic fields. However it can be easily influenced by any magnetic fields or ferromagnetic materials in the subsurface. Furthermore, as a magnetic survey not based on calculating the current position in a field, but calculating it based on the last known position along with the new azimuth and inclination, this magnetic survey method suffers from a cumulative error propagation, as error from one calculation propagates to the next. Due to the limited accuracy of the measurements taken by internal sensors in the form of the steering probe, additional external navigational devices are widely recommended and used in order to work in tandem with the internal one. In this chapter the focus is put towards the most popular modern navigational instruments, their advantages and limitations. Each of the navigational instruments is described in a separate subsection as each method is widely used in the field and therefore is applicable for mentioning in the following research.

Navigational devices under consideration are: Walkover Locating Systems, Magnetic Tracking, Gyroscopic Surveys and a combination of said methods. Navigation instruments are widely used in HDD installations in order to correctly ascertain the position, speed and direction in which the BHA is moving. Such measures ensure that the path of the installation is the right one with accordance to the design plans. Without such instruments in place it would be almost impossible to navigate the subsurface considering how densely it has become over the past 50 years, especially in urban regions. In the past, before the devices listed below were in use, one would bore on much smaller depths and in order to check the direction and general position of the BHA, internal magnetic locating tools of limited range and reliability would be used. In extreme cases a series of boreholes would be drilled vertically to confirm the drill head's position. While short and shallow installations could be done using such classic ways of taking measurements, as the industry scaled the need for better types of navigational tools arose. Nowadays these navigational instruments are absolutely crucial for performing any kind of subsurface installations accurately, leading to safest and most economically feasible works.

#### 3.1.1 Walkover locating systems

A walkover system consists of a transmitter which is placed in a protecting housing, as part of the BHA and a receiver, with which a member of the crew has to walk along the bore path in order to minimise the total distance between the two

parts of the walkover device. The optimal positioning of the receiver is directly over the transmitter so that only the depth of the bore is what separates the two. Walkover systems are very popular in the industry and are regarded quite highly as a limited but accurate device. Said system is mainly used for shallow installations that are performed under a generally accessible landmass as the measurement error associated with this method increases with the increase in the distance between the transmitter and the receiver (depth). Additionally, obstacles like for example ferromagnetic rebars or other types of underground artifacts located in the path of the measurements can lead to temporary errors, however, errors in this particular case do not accumulate over the amount of measurements. One very important limitation of the walkover system compared to any other navigational instrument used in HDD is that it has a maximal depth rating (varies amongst producers), above which the device might not work properly anymore and the readings are not to be trusted. Furthermore, surface elevation differences encountered while measuring with this method can render the consecutive readings not comparable. Hence, installations requiring a very specific bending radius or slope, under uneven terrain, should be conducted using a different instrument. Another major drawback of the system is the access to area above the transmitter, upon conducting installations under, amongst others, busy roads, railways and waterways, the use of walkover devices can be problematic. A walkover system is presented in Figure 3.1, where the receiver is being held by a worker and the device is pointed towards a transmitter in the subsurface which is not present in the figure.



Figure 3.1: Walkover locating system in use (Underground Infrastructure Magazine [2012])

### 3.1.2 Magnetic tracking

Magnetic wireline tracking/ steering is one of the most popular navigational instruments in HDD. This instrument can be split into two categories, based on whether direct current (DC) or alternating current (AC) is being used. In terms of accuracy, systems using direct current (DC) yield better results than ones utilizing alternating current (AC) (Sullivan [2023]). In both cases the instrument consists of an inline survey probe located in the BHA and a large loop made out of an insulated copper wire which is laid out along the bore alignment with a slight offset on both sides. An example of how the magnetic tracking wire can be set up is visible in Figure

3.2. Upon running electrical current through the wire a magnetic field is induced that the downhole survey probe uses to calculate its position relative to the wire. Additionally, there is also an opportunity to utilize a solenoid to generate the magnetic field making this method much more flexible in terms of terrain requirements (magnetic tracking wiring requires a lot of space), however it yields less accurate results compared to the wire in place. In terms of error generation, this is once again a method which calculates the current location of the drill string based on the current data and not on previous readings, leading to the magnitude of error being dependent on the distance to the source (in this case the magnetic field generated in the wire on the surface). This method's limitations are related to the availability of space around the bore path (a lot of space is needed for the loop and bodies of water might interfere) and the presence of strong sources of magnetic field like a power station for example.

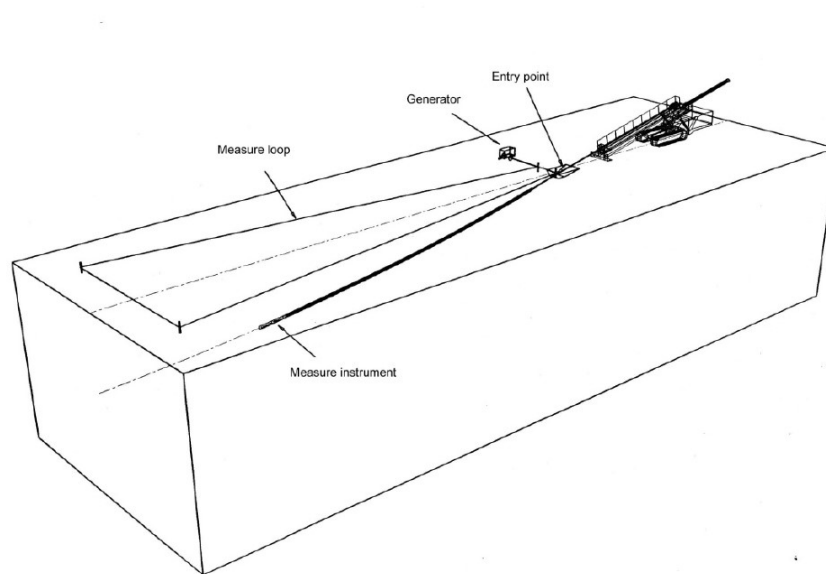


Figure 3.2: Magnetic tracking system in use Broere [2021]

### 3.1.3 Gyroscopic surveys

Gyroscopic steering can be considered as the most technologically advanced and universal navigational instrument. It consists of an optical fibre wire transmitting the calculated positions to the drilling crew, an optical gyro that resides in a solid-state device and additionally there are also three fibre-optic gyroscopes present that measure pitch, yaw and roll of the BHA (Sullivan [2023]). Said method has a lot of advantages like for example the placement of the navigational device in the BHA, as placing it just after the jetting assembly lets it sit closer to the drill head, which is helpful to the crew, as it provides information on the changes of the behaviour of the drill head the quickest. Apart from that this method is very flexible, it does not require any specific site conditions to operate. Moreover, it is also remains unaltered by strong magnetic fields in the surroundings. Finally, the gyroscopic device can be utilized where the installations require utilization of additional casings for bore stability. On the other hand it can also be considered as the most expensive method available on the market. Furthermore, the internal process is quite complicated as it conducts its calculations based on its last calculated position, the readings from the gyroscopes and the length of drill string that enters the bore. Such calculation methodology has one major disadvantage, where the calculation error accumulates over the amount of measurements taken, leading to higher uncertainties regarding

the positioning of the drill string closer to the exit of the bore. While, in shorter installations that might prove inconsequential, longer operations could find it problematic. Additionally this method can be coupled with a GPS tracker to mitigate the arising errors. Finally, the method is costly, yet faster and yields either the same or more accurate results than magnetic wireline tools.

#### 3.1.4 Combination of tracking and survey methods

Considering the error accumulation mentioned in case of each of the navigational instruments, a logical approach is to combine certain steering methods in order to offset their respective disadvantages leading to readings as accurate as possible. In this regard two such combinations can be distinguished, namely:

- Magnetic Tracking + Gyroscopic Survey
- Gyroscopic Survey + GPS tracking

Both cases rely on the presence of Gyroscopic survey which provides accurate information at the beginning with a calculation error propagating with the bore length, leading to lower errors in the beginning and higher errors by the end of the bore and a tracking system which measures the position relative to an external frame of reference one point at a time, which gives higher errors with larger depths of boring, leading to maximal errors occurring somewhere in the middle section of the bore, with best accuracy achieved at either ends.

#### 3.1.5 Accuracy and error propagation in navigational instruments

In the following subsection further comparison in terms of error propagation, accuracy, susceptibility to interference, ease of setup, speed of installation and cost can be seen. Table 3.1 stands as a quick summary of points mentioned previously regarding all navigational instruments. Table 3.2 shows further numbers regarding the internal error of pitch and direction measurements. Due to the cumulative error related to survey methods (gyroscopic instruments), measurements can be visualized as a normal distribution pattern where, 99.7% of the results fall within  $3\sigma$  values from the mean, leading to a value of  $\pm 0.01^\circ$  in terms of inclination and  $\pm 0.4^\circ$  in terms of direction. On the other hand, as magnetic and walkover tracking are both methods with direct error measurements, the Root Mean Square (RMS) over the results leads to  $\pm 0.1^\circ$  in terms of inclination, while respectively  $\pm 0.4^\circ$  and for the walkover device it is not specified.

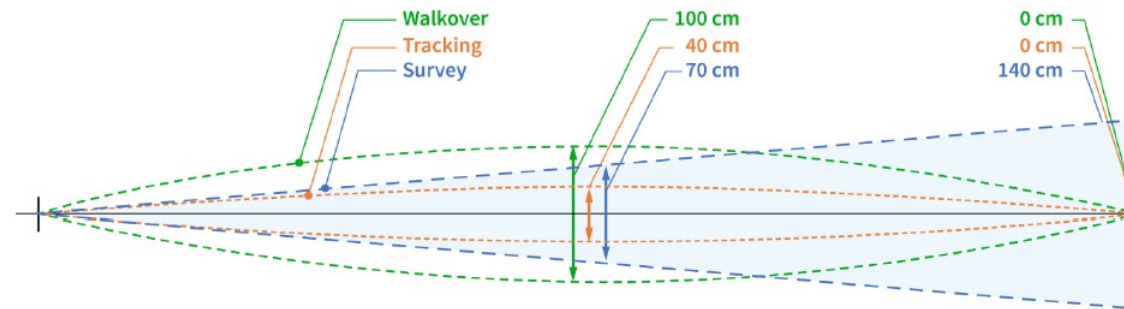
**Table 3.1:** Accuracy in navigational instruments (Drilling Contractors Association (DCA) [2022])

Guidance Method	Accuracy over Length			Accuracy over Depth				Susceptibility to Interference	Ease of Setup	Speed	Cost
	<250m	250 - 1000m	>1000m	<15m	15-50m	50-100m	>100m				
<b>Walkover</b>	High	High	High	High	Medium	Low	Low	Medium	High	High	High
<b>Magnetic Tracking</b>	High	High	High	High	High/ Medium	Medium	Medium	Medium	Medium	Medium	Medium
<b>Gyroscopic Survey</b>	High	High	Medium	High	High	High	High	High	High	Medium	Medium
<b>Magnetic Tracking + Gyroscopic Survey</b>	High	High	High	High	High	High	High	High	Medium	Medium	Medium/ Low
<b>Gyroscopic Survey + GPS Tracking</b>	High	High	High	High	High	High	High	High	High	Medium	Medium/ Low

Table 3.2: Accuracy of pitch and azimuth measurements (Drilling Contractors Association (DCA) [2022])

	Walkover Instruments	Magnetic Instruments	Gyroscopic Instruments
<b>Inclination</b>	+/- 0.1°	+/- 0.1°	+/- 0.01°
<b>Pitch</b>	(RMS)	(RMS)	(3σ)
<b>Direction</b>		+/- 0.4°	+/- 0.4°
<b>Azimuth</b>		(RMS)	(3σ)
<b>Depth</b>	max. 50m	No limits	No limits
<b>Accuracy</b>	5% of depth	2% of distance to cable	70cm at 1000m
<b>Sensitivity for interference</b>	Yes	yes, active and passive	No

Bore Depth: 10m, Bore Length: 1000m



- Gyro Survey uncertainty accumulates with length ( $0.04^\circ$ )
- Tracking uncertainty increases with distance from magnetic source (2%)
- Walkover uncertainty increases with distance from magnetic source (5%)

Figure 3.3: Measurement error visualisation for a 1000m bore at 10m depth (Drilling Contractors Association (DCA) [2022])

## 3.2 DESCRIPTION OF PHYSICAL PHENOMENA AND EFFECTS INFLUENCING THE PULLBACK FORCE

Considering the evolving urban drilling industry in the past decades, along with technology development, also the complexity and risk potential increased over the years. One of the main characteristics describing any HDD installation is the drilling rig size. The ability of correct estimation of the maximal pulling forces required for a certain installation is therefore a crucial element during the designing and cost calculation stages of any project. Based on the maximal pulling force estimations, the correct rig size (general rig specifications seen in Table 2.2) for the job is chosen. Picking an adequate rig for the installation is the optimal outcome, yet more often than not the choice lands on a conservatively bigger rig in order not to make the mistake of having an insufficient pulling force at the machine and having to replace it, while every day out in the field is costly. Furthermore, the maximal pulling forces influence decisions regarding the strength of the product pipe along with procedures to be employed during installation, such as methods for drag reduction (Xu [2018]). In the following section, the focus is shifted towards the phenomena and effects influencing the pullback forces, to which special attention should be paid as initial estimations as close to the true values are essential for an optimal design and later on installation.

### 3.2.1 Influence of product pipe feeding system outside of the bore

As the product pipe is being laid out and prepared to be pulled into the bore, it introduces additional resistances to the pulling process. The interaction of pipe with the ground in the form of friction will counteract the pulling force applied from the drilling rig, hence impeding the process. On the other hand, in order to minimise such impediment, rollers can be applied. Pipe on rollers has effectively a much smaller resisting force leading to an overall smaller pullback force than in the case of simply being dragged on the ground.

### 3.2.2 Influence of product pipe friction inside the bore

As soon as the product pipe is being pulled into the prepared bore, the outer edges of the pipe will eventually touch the walls of the borehole leading to a friction force, resisting the pulling process. Furthermore, walls of the prepared bore are generally covered with a film of drilling mud which supplies lubrication and cooling to the entire process, leading to an overall smaller friction coefficient. On the other hand, as the installation proceeds the mud-cake is eroded away, leading to an increase in friction with time.

### 3.2.3 Influence of soil clamping on the drilling equipment (Chock Effect/ Wedging Effect)

Upon removal of a certain amount of soil in order to put the product pipe into the bore, an opening in the soil can be temporarily maintained by the presence of a mixture of polymers along with drilling mud. It can be kept open only up to an extent as some material will constantly be chipping away from the walls of the bore. Upon introducing the product pipe into the subsurface, said pipe will apply forces to the bore itself leading to deformations. The extent of the forces applied to the walls of the bore depend on the quality of ballasting conducted during the installation, along with the trajectory of the bore. Due to the fact that pipes more often than not, will negotiate bore path bends imperfectly, the soil surrounding the bore will be further displaced. Upon displacement the bore, might start to clamp

around the pipe which leads to additional resisting forces, increasing the overall pullback force.

#### 3.2.4 Influence of bending due to bore geometry (Capstan Effect)

Apart from the clamping of the soil due to bore deformations during the installation phase, another phenomenon takes place increasing the overall pullback forces due to the pipe adjusting to the geometry of the bore. Said phenomenon is called the Capstan Effect (Cai [2011]), it is an additional wall contact force created due to the tension/ compression in pipe through the curvature of the bore profile. It can be understood as additional friction present in locations, where the product pipe bends and is in contact with the walls of the bore. In the contact locations the pipe applies additional normal force to the walls due to the tension or compression it endures. Therefore, it can be summarized as, the more deviations from as smooth of a trajectory as possible, the more resisting forces will be present. Detailed analysis of the bore geometry influence is present in Section 5.2.

#### 3.2.5 Influence of slurry circulation

The presence of slurry (drilling mud) is a vital element of HDD installations (Shu [2016]). Firstly it lowers the overall pullback force by creating a lubricating film around the bore, leading to lower friction forces encountered downhole. Furthermore, the drilling mud helps in creating additional downhole pressure, which is crucial for keeping the bore from caving in. Finally through circulation of the slurry the cuttings are removed from the bore resulting in a clear passage for the product pipe installation. On the other hand, mud circulation has an additional effect of applying pressure and mud drag to the drill string and the product pipe being pulled in, however its contributions to the process outweigh the slight increase in resisting forces.

#### 3.2.6 Influence of product pipe ballasting

During the product pipe pullback operation, due to the pipe's own self weight, it tends to hover around the upper part of the bore. Such phenomenon can be witnessed through the buoyancy of the hollow cylinder (pipe) filled with air. Through the constant contact between the piping and the bore, excessive resisting forces are generated. Ballasting became a method of mitigating said forces up to a certain extent through optimal positioning of the pipe within the bore. With correct ballasting the amount of contact between the pipe and the walls of the bore can be limited along with the effective down or upward force acting on the pipe. Dependent on the material in use along with the amount of ballasting, three essential outcomes can be achieved: one where, the upward force on the pipe is the largest leading to friction with the upper part of the bore; a case where, the downward force is larger leading to pipe friction against the lower part of the bore; finally a case where, the effective force in either direction is minimized and the pipe is in as much of a floating state in the mud suspension as possible. Hence, correctly conducted ballasting can reduce the pullback force by keeping the product pipe suspended in the drilling mud. Detailed analysis of the ballasting influence is present in Section 5.3.

#### 3.2.7 Influence of reamer and drill string exiting the bore

As the product pipe is being pulled in, the drill string along with the reamer are exiting the bore. The drill string and the reamer undergo analogical processes to the product pipe, therefore all of the effects influencing the forces acting on the product pipe should also be extended to the reamer and drill string, acknowledging the

differences like size and material properties. Therefore the drill string along with the reamer can be considered to be increasing the overall resisting forces in a similar fashion to the product pipe. Furthermore, the buoyancy of the drill string always remains negative considering its weight and shape. Hence, forces arising due the drill string being pulled out of the bore might vary greatly and cannot be omitted.

### 3.2.8 Influence of penetration of different geological structures or strata

The subsurface can be considered as a heterogeneous medium, due to presence of a variety of geological and other structures. In most cases around the globe HDD installations are performed in soft soils. Said soils introduce an issue of sagging under the weight of the drill string, reamer and the product pipe leading to consecutive changes to the bore trajectory after it has been initially established. These deviations from the original trajectories might influence the pullback force as a new path needs to be created for the pipe. This phenomenon can have a negative or a positive effect on the overall pullback forces dependent on the installation.

## 3.3 DESCRIPTION OF CURRENTLY AVAILABLE MODELS ANALYSING THE PULLBACK FORCE

In the following section a brief description and comparison of the available pullback force prediction models is presented. While, not all existing models have been mentioned in this section, most popular models in terms of publications have been chosen. Furthermore, additional promising, yet untested models have been mentioned as optional reading material in Section 3.3.6.

### 3.3.1 ASTM F1962 Model

The "Standard Guide for Use of Maxi- Horizontal Directional Drilling for Placement of PE Pipe or Conduit Under Obstacles, Including River Crossings" (ASTM F1962) method proposes a set of equations for pullback force determination, including the Capstan Effect (described in Section 3.2.4). The ASTM Model considers the bore profile to be made up of two curved and one horizontally straight segments (as the middle section). Moreover it is also assumed that the pipe entry and exit points are level, as shown in Figure 3.4. Said assumptions prove difficult in application outside of the theoretical as real conditions are rarely up to the standard required for this models accuracy (according to F1962 [2011] referenced by Rabiei [2016]).

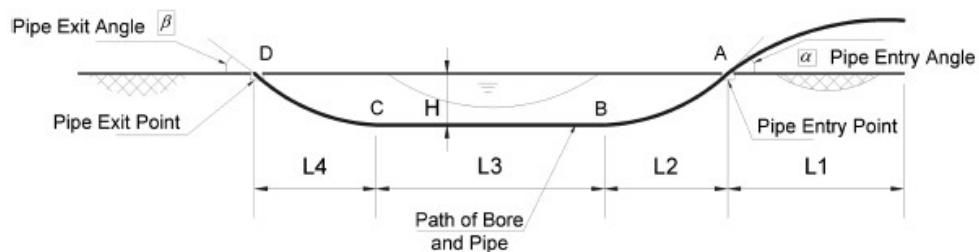


Figure 3.4: General bore schematic of ASTM Model (Rabiei [2016])

The model assumes peak pullback forces manifesting in the points marked 'A', 'B', 'C' and 'D' seen in Figure 3.4. Therefore, the model proposes a set of equations in order to calculate the forces in each of the mentioned points and an additional formulation acknowledging the fluidic drag is added. Mentioned formulations can be seen in Equations 3.1 through 3.6.

$$T_A = e^{v_a \cdot \alpha} \cdot [v_a \cdot w_a \cdot (L_1 + L_2 + L_3 + L_4)] \quad (3.1)$$

$$T_B = e^{v_b \cdot \alpha} \cdot (T_A + v_b \cdot |w_b| \cdot L_2 + w_b \cdot H - v_a \cdot w_a \cdot L_2 \cdot e^{v_a \cdot \alpha}) \quad (3.2)$$

$$T_C = T_B + v_b \cdot |w_b| \cdot L_3 - e^{v_b \cdot \alpha} \cdot (v_a \cdot w_a \cdot L_3 \cdot e^{v_a \cdot \alpha}) \quad (3.3)$$

$$T_D = e^{v_b \cdot \beta} \cdot [T_C + v_b \cdot |w_b| \cdot L_4 - w_b \cdot H - e^{v_b \cdot \alpha} \cdot (v_a \cdot w_a \cdot L_4 \cdot e^{v_a \cdot \alpha})] \quad (3.4)$$

where,  $\alpha$  and  $\beta$  are the pipe entry and exit angles as shown in Figure 3.4,  $v_a$  and  $v_b$  are respectively, internal bore coefficient of friction and the coefficient of friction between pipe and the ground/ rollers outside of the bore,  $w_a$  and  $w_b$  are in and out of bore unit effective (buoyant) weights of the pipe,  $L_1$  through  $L_4$  are lengths of the respective pipe segments as seen in Figure 3.4,  $H$  is the depth of installation. For estimating the fluidic drag component an additional equation is provided in the form of:

$$\Delta T = \Delta P \frac{\pi}{8} (D_b^2 - D_p^2) \quad (3.5)$$

where,  $\Delta P$  is the hydrokinetic pressure estimated to be 70[kPa],  $D_b$  is the borehole diameter and  $D_p$  is the outer pipe diameter. Finally the total pullback force that occurs in the installation is the sum of all mentioned equations, hence:

$$T_{tot} = T_A + T_B + T_C + T_D + \Delta T \quad (3.6)$$

ASTM method acknowledges a lot of aspects related to the increase of the pullback force over the length of the bore, yet due to its discrete nature it is hard to estimate the pullback force more or less continuously throughout the bore, as an assumption of linear increase over the spaces between the calculated forces in points 'A', 'B', 'C' and 'D' cannot be accepted as an accurate result. Therefore, despite the method being in general more complex than the other discussed in this section, it still leaves space for improvement.

### 3.3.2 PRCI Model

The "Pipelines Research Council International" (PRCI) method is based on research conducted for the American Gas Association. The method assumes that the pullback force at the pipeline entry point is always zero (the above-ground pipeline contribution is assumed insignificant) and that it gradually increases along the pipe as the leading end approaches the exit point. The increase in tension along a straight pipe segment is given as (according to Huey [1996] referenced by Rabiei [2016]):

$$\Delta T_s = |T_s| + T_{drag} \pm w_b \cdot L_s \cdot \sin \theta_s \quad (3.7)$$

where,  $T_s$  is the force of friction between the pipe and the surrounding borehole,  $T_{drag}$  is the shear force acting on the pipe's outer surface due to the pipe's interaction with the drilling slurry;  $w_b$  is the effective (buoyant) unit weight of the pipe,  $L_s$  represents the length of the pipe segment under consideration and  $\theta_s$  is the angle of the pipe/ borehole axis with respect to the horizontal.

Representing a curved pipe segment as a three-point beam undergoing large deflections, with the maximum center deflection of:

$$h = R \cdot \left(1 - \cos\left(\frac{\alpha}{2}\right)\right) \quad (3.8)$$

where,  $\alpha$  is the angle of a curved segment, the PRCI method provides the following equation for tensile force change along a curved pipe segment:

$$\Delta T_c = 2|T_c| + T_{drag} \pm w_b \cdot L_c \cdot \sin\theta_c \quad (3.9)$$

where,  $T_c$  is the force of friction between the pipe and the surrounding borehole evaluated using certain iterative procedure,  $L_c$  is the length of the pipe's curved segment and  $\theta_c$  is the angle of line bisecting the pipe segment with respect to the horizontal. PRCI method proposes the following equation to calculate the fluidic drag force  $T_{drag}$ :

$$T_{drag} = \pi D_p \cdot L \cdot \mu_{mud} \quad (3.10)$$

where,  $D_p$  is the product pipe's outer diameter,  $L$  is the length of the pipe segment under consideration and  $\mu_{mud}$  is the fluid drag coefficient with the recommended value of 350 Pa, but with certain speculation regarding the use of 172 Pa to get a more accurate result.(Puckett [2003])

Finally with Equations 3.7 through 3.10 in place, one can calculate the total pullback force by taking a sum of both components over the amount of straight and curved sections leading to Equation 3.11 below:

$$T_{pullback} = \sum \Delta T_s = \sum \Delta T_c \quad (3.11)$$

The PRCI method acknowledges both the presence and effect of mud and the effect of bending to a certain extent. However by reviewing the formulations utilized in the method, it can be seen that this model can be considered as the simplest one out of the ones mentioned in this section. While simplicity and conservative approach prove to be crucial in many domains, modern solutions involve more parameters and acknowledge a higher count of influences in the general process leading to more realistic results.

### 3.3.3 Driscopipe Model

The Driscopipe (name indicating focus on polyethylene pipe installation) method is an approximate analytical method for estimating the pipe pullback loads in HDD installation. The pipe is treated as a series of straight-line segments along its centerline that are linked together, as shown in Figure 3.5. All the segments are assumed to be in static equilibrium. A force balance analysis for each segment, e.g., the  $i^{th}$  segment, gives the relationship between the axial forces  $T_i$  and  $T_{i-1}$  at the two ends of the segment (according to Performance Pipe [1993] as referred to by Yang [2014]) as seen in Equation 3.12.

$$T_i = T_{i-1} + W_s \cdot L_i \cdot (\mu \cdot \cos\theta_i \pm \sin\theta_i) \quad (3.12)$$

where,  $W_s$  is the net weight of the pipe per unit length,  $L_i$  is the length of the pipe segment under consideration,  $\mu$  constitutes the friction coefficient between the pipe and the borehole and  $\theta_i$  is the inclination angle. Assembling all the segments, one can obtain the pulling force, following Equation 3.13 seen below:



$$N_i = \sqrt{[(T_{i-1} \cdot \Delta\Phi_i \cdot \theta_{Ni})^2 + (T_{i-1} \cdot \Delta\theta_i + W_s \cdot L_i \cdot \cos\theta_{Ni})^2]} \quad (3.15)$$

Finally, the total pullback force is given by the sum of the increments along the entire bore resulting in Equation 3.16:

$$T_{tot} = \sum_{i=1}^n \Delta T_i \quad (3.16)$$

Once again, analogically to the previously mentioned Driscopipe model, the Drill-path method does not acknowledge the additional forces due to the pipe bending (described in Section 3.2.4) inside the borehole and forces arising due to the fluidic drag (described in Section 3.2.5).

### 3.3.5 NEN Model

The final model described in this section might not be fully considered as a pulling force prediction model, it should be more regarded as a set of regulations set by the Netherlands Standardization Organisation in NEN 3650-1 (NEN [2020]).

According to the regulations, frictions exerted on the pipe which is located in three different regions, i.e. ground surface, straight section and curved section of borehole, are calculated separately, denoted by  $T_1$ ,  $T_2$ , and  $T_3$ . The friction between the pipe and the roller system or the ground surface is treated as  $T_1$ . The friction due to the drilling fluid and the friction between the pipe and the borehole wall are two components for the frictional resistance  $T_2$  exerted on the pipe inside straight sections of the borehole. In analysis of  $T_3$ , the same frictional resistance as  $T_2$ , friction resulting from pipe bending, and friction due to Capstan Effect (described in Section 3.2.4) are calculated, denoted by  $T_{3a}$ ,  $T_{3b}$  and  $T_{3c}$  separately. The total pulling force is equal to the sum of three friction components. (Cai [2017]) The formulations for this model can be seen in Equations 3.17 through 3.22, below:

$$T_1 = f \cdot L \cdot g \cdot f_1 \quad (3.17)$$

$$T_2 = f \cdot L_2 \cdot (\pi D_0 \cdot f_2 + g_{eff} \cdot f_3) \quad (3.18)$$

$$T_{3a} = f \cdot L_b \cdot (\pi D_0 \cdot f_2 + g_{eff} \cdot f_3) \quad (3.19)$$

$$T_{3b} = f \cdot 2q_r \cdot D_0 \cdot \frac{\pi}{\lambda} \cdot f_3 \quad (3.20)$$

$$T_{3c} = f \cdot L_B \cdot g_t \cdot f_3 \quad (3.21)$$

$$T_{tot} = T_1 + T_2 + T_{3a} + T_{3b} + T_{3c} \quad (3.22)$$

where,  $f$  is a total factor of 1.4 or 2.0, for normal crossing cases or cases with a gravel layer;  $L$  is the length of the pipe outside the borehole;  $g$  is the weight of the pipe per unit length;  $f_1$  is the friction coefficient between the pipe and ground surface, 0.3 is recommended while 0.1 is used when the roller system is adopted;  $L_2$  is the pipe

length in a straight section of borehole;  $D_o$  is the outside diameter of the pipe;  $f_2$  is the viscous friction due to drilling fluid, 50 Pa is suggested;  $g_{eff}$  is the net weight of the pipe considering the buoyancy force;  $f_3$  is the friction coefficient between the pipe and the borehole wall,  $f_3 = 0.2$ ;  $L_b$  is the length of the bend;  $q_r$  is the maximum soil reaction pressure near the end of the bend;  $L_B$  is the chord of the bend;  $g_t$  is the thrust force,  $T_{tot}$  is the total pullback force in the installation.

### 3.3.6 Additional Theoretical Models

Apart from the models proven in the industry mentioned in Sections 3.3.1 through 3.3.5, a number of proposed theoretical solutions can be found. Interestingly more accurate models than the ones currently in use have been introduced in: Rabiei [2016]; Yang [2014]; Rabiei [2015]; Xu [2018] and Cai [2011]. The last proposed theoretical solution mentioned is described in detail below, in Section 3.4.

In each of the mentioned articles new aspects have been taken into account, however not all of them were applicable considering the data at hand. The Rabiei [2016] model mainly focuses on redefining the Capstan Force influence to accommodate for High Density Polyethylene (HDPE) piping, hence was not chosen due to the limited scope that HDPE piping entails. Furthermore, Yang [2014] solution proposed the use of advanced physical models in combination with advanced dynamic computations, proving too complex to implement within a limited time frame. Moreover, the Rabiei [2015] model introducing the advantage of a lack of iterative process for pull force increment evaluation was considered for implementing in this research, yet the higher practicality potential of the model was not valuable enough for this research. Lastly, the Xu [2018] model proposed another influential phenomenon in the form of soil wedging around the pulled pipe, however such aspect was already partially adopted in the model chosen for this study.

### 3.3.7 Comparison of Described Models

In the following section a brief comparison in the form of Tables 3.3 and 3.4 is presented, giving an overall indication of what are the advantages and disadvantages of each model.

Table 3.3: Applicability of the pullback calculation models based pipe material type in use (Cai [2017])

Prediction Models	Driscopipe	Drillpath	PRCI	NEN 3650	ASTM F1962	PipeForce V1
Steel pipe	N	Y	Y	Y	N	Y
Plastic pipe	Y	Y	N	Y	Y	Y

Note: 'Y' - indicates that an aspect is taken under consideration in a certain model, while 'N' - indicates that an aspect is not taken into consideration.

Table 3.4: Comparison of models based on the influencing parameter acknowledged (Cai [2017])

Prediction Models	Weight friction between pipe and ground	Weight friction between pipe and borehole	Pipe weight and buoyancy	Fluidic drag friction	Friction due to the Capstan Effect	Friction due to the pipe's stiffness	Resistances exerted on drill string
Driscopipe	Y	Y	Y	N	N	N	N
Drillpath	Y	Y	Y	N	Y	N	N
PRCI	N	Y	Y	Y	N	Y	N
NEN 3650	Y	Y	N	Y	Y	Y	N
ASTM F1962	Y	Y	Y	Y	Y	N	N
PipeForce V1	Y	Y	Y	Y	Y	Y	Y

Note: 'Y' - indicates that an aspect is taken under consideration in a certain model, while 'N' - indicates that an aspect is not taken into consideration.

### 3.4 DESCRIPTION OF THE IMPLEMENTED NUMERICAL MODEL ANALYSING THE PULLBACK FORCE

In the following research, a theoretical solution to calculate pulling forces introduced by Liangxue Cai and Maria Anna Polak from University of Waterloo was adapted, taking into account fundamental differences between the data types available in both projects. The original name of the model is PipeForce Version 1 (Cai [2011]), however said model has been significantly changed in order to accommodate for lack of high resolution design and pilot drilling data as well as other differences in available information. The model was implemented in Python programming language. The code for said model is in Appendix A.

Firstly, the definition of the coordinate system for the discretization of points along the bore that has been utilized in the following model is given. Pilot bore profile, i.e. the centerline of pilot bore, is assumed to be a broken line formed by straight line segments. The discrete points where the coordinates are determined during pilot bore drilling phase are the key points of the broken line. Let the entry point be selected as the origin of the  $x$  and  $y$  coordinates, as shown in Figure 3.7. Key points from entry point to exit are denoted by  $K_1, K_2, \dots, K_n$ , successively. A pilot bore profile including  $n$  key points is formed of  $n - 1$  straight segments and the two end points of segment  $S_i$  are points  $K_i$  and  $K_{i+1}$ .

Secondly, the numerical pullback force model in this thesis is based on two additional physical models, where the product pipe is treated as an isodiametric cylindrical shell, the two physical models utilized in the analysis are: (1) infinite pipe with outer radius  $r_p$ , wall thickness  $t_p$ , pipe density  $\rho_p$  and elastic modulus  $E_p$  is located in an unlimited borehole, and (2) a simply supported, intermediate loaded beam with slopes  $\theta_1, \theta_2$  and a normal force  $P$  causing a beam deflection consistent with the given mentioned slopes at the ends of beam segment. The choice of assumed physical models in this thesis was the first deviation from the original PipeForce programme. In the original instead of a simply supported, intermediate loaded beam a cantilever is used, however due to the fact that in this project instead of information on a pilot bore, data on the final alignment of the bore is presented, a different approach to calculating the normal forces had to be adopted to yield more accurate results. Further information on the normal force calculation can be seen in Section 3.4.4.

#### 3.4.1 Friction due to pipe weight on the ground $(T_g)_i$

Moving on to the actual calculations incorporated in the model, the friction due to the weight of pipe laying on the ground outside of the borehole, waiting to be pulled in, was taken into account. Following Equation 3.23 seen below:

$$(T_g)_i = (w_p \cdot \mu_g \cdot \cos\beta_0 + w_p \cdot \sin\beta_0) \cdot [L - \sum_{k=1}^{i-1} L_k] \quad (3.23)$$

where,  $w_p$  is the weight of pipe per unit length,  $\mu_g$  is the friction coefficient between pipe and ground,  $L$  is the total length of pipe,  $L_k$  is the length of borehole segment  $S_k$  representing portions of pipe that has been pulled into borehole and  $\beta_0$  is the angle between horizontal line and the ground surface in front of pipe entrance.

Upon further investigation angle  $\beta_0$ , which is the angle between the horizontal line and the ground surface, has been assumed to be zero for simplicity, and the value of the friction coefficient between the pipe and the ground  $\mu_g$  was taken to be 0.1[–] which differs from the original Pipeforce Version 1 model input parameters, however the presence of rollers and not simply ground is applied and according to the NEN 3650-1 regulations (NEN [2020]). Such assumptions led to Equation 3.23 simplifying to:

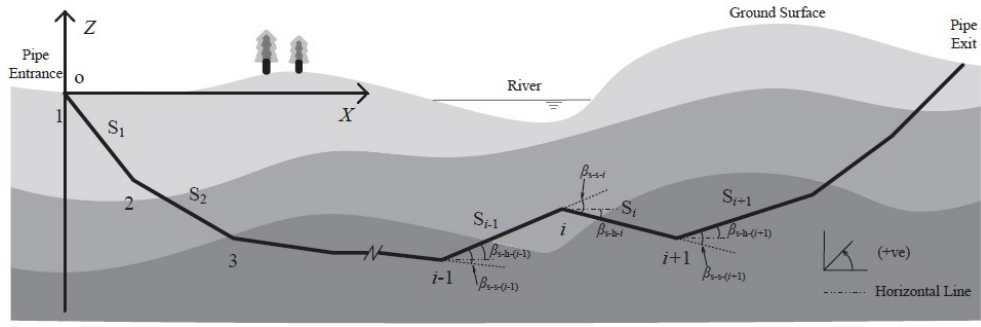


Figure 3.7: Example of bore profile

$$(T_g)_i = w_p \cdot 0.1 \left( L - \sum_{k=1}^{i-1} L_k \right) \quad (3.24)$$

### 3.4.2 Pulling force component due to friction of the ballasted pipe inside the borehole $(T_b)_i$

The next component in the calculations to find the pullback force was the resisting force component caused by friction between the ballasted product pipe being pulled in and the lubricated inner surface of the bore.

$$(T_b)_i = \sum_{k=1}^{i-1} (|K_{c-k} \cdot L_k \cdot w \cdot \mu_{b-k} \cdot \cos \beta_{s-h-k}| + L_k \cdot w \cdot \sin \beta_{s-h-k}) \quad (3.25)$$

where,  $K_{c-k}$  is the coefficient of chock effect relevant to borehole segment  $S_k$ , it indicates the clamping/ sticking effect of soil on the pipe,  $w$  is the submerged weight of pipe per unit length acknowledging the ballasting of the pipe with water,  $\mu_{b-k}$  is the friction coefficient between soil and pipe at borehole segment  $S_k$  and  $\beta_{s-h-k}$  is the angle between borehole segment  $S_i$  and horizontal line.  $\beta_{s-h-k}$  can be seen in Figure 3.7.

$$w = w_p - w_g (\pi r_o^2 \cdot \gamma_s - n_{bal} \cdot \pi r_i^2) \quad (3.26)$$

where,  $w_p$  is the weight of pipe per unit length,  $w_g$  is the unit weight of water assumed at  $1000 \text{ [N/m}^3]$   $r_o$  is the outer radius of the pipe,  $\gamma_s$  is the specific gravity of the slurry in use,  $n_{bal}$  is the ballast in percentage and  $r_i$  is the inner diameter of the product pipe. The ballast is assumed to be done with water.

Once again changes to the original mathematical model were made. The value of the coefficient of chock effect mentioned already as one of the influential phenomena in Section 3.2, was assumed to be 0.5 with accordance to the NEN3650-1 regulations (NEN [2020]). Additionally, the friction coefficient  $\mu_{b-k}$  instead of being calculated for every segment separately, was assumed to be 0.24. Such assumptions led Equation 5.1 to the form of:

$$(T_b)_i = \sum_{k=1}^{i-1} (|0.12 L_k \cdot w \cdot \cos \beta_{s-h-k}| + L_k \cdot w \cdot \sin \beta_{s-h-k}) \quad (3.27)$$

### 3.4.3 Resisting force due to slurry $(T_r)_i$

The next factor contributing to the resisting forces, hence increasing the pullback forces over the length of the bore is the resistance due to slurry. Due to the way in which, the reamer and product pipe are located with respect to each other, additional resisting forces arise at the connection of said two elements. Apart from that, friction due to slurry can be divided between friction against the product pipe and friction against the sides of the borehole. Such a situation in the subsurface leads to a general equation in the form of:

$$(T_r)_i = C \cdot A_a \cdot P_1 + \frac{\pi}{4} D_p^2 \cdot P_1 \quad (3.28)$$

where,  $C$  is the ratio of the shear force of slurry on the outer surface of the pipe to the total shear force on the outer surface of the pipe and the borehole wall, which is assumed to be 0.5 by ASTM F1962-11, 0.465 is recommended here according to theoretical analysis of slurry flow in horizontal directional drilling installations;  $A_a$  is the cross section area of annulus between pipe and borehole;  $P_1$  is the pressure of slurry at the position where the pulling head of pipe is located and  $D_p$  is the outer diameter of the product pipe.

Furthermore, the downhole slurry pressure changes along the borehole can be derived from Equation 3.29:

$$\frac{dp}{dz} = \frac{47.82(v_p \cdot v_a)}{(D_B - D_p)^2} + \frac{6\tau_f}{D_B - D_p} \quad (3.29)$$

where,  $\tau_f$  is the yield point assumed to be 14.305 [Pa],  $v_p$  is the plastic viscosity assumed at value of  $1.6e^{-5}$  [Pa · s] (Hijnekamp [2016]);  $D_p$  and  $D_B$  are the outer diameter of product pipe and the diameter of borehole respectively;  $v_a$  is the average velocity of drilling fluid flowing in the annulus, described by Equation 3.30:

$$v_a = \frac{1.272Q}{D_B^2 - D_p^2} \quad (3.30)$$

The final equation for this partial resistance force is the calculation of the pressure of slurry at the position where the pulling head of pipe is located. As seen in Equation 3.31:

$$P_1 = C_p \cdot s \cdot \frac{dp}{dz} \quad (3.31)$$

where,  $C_p$  is a scale coefficient accounting for the unpredictable factors, a value of 2 is recommended;  $s$  is the length of annulus between pipe (or drill string) and borehole;  $dp/dz$  is the pressure drop gradient.

### 3.4.4 Resisting force due to bend negotiation $\Delta T_{f-k}$

The next partial force under consideration can be split into two separate pieces, one of them is the Capstan Effect (already mentioned in Section 3.2.4), which is small per unit length, however it accumulates over the entirety of the bore length, whereas the other part constitutes the resistance due to pipe bending along the bore path. Bore paths are bending and deflecting from any arbitrary centre due to the heterogeneity of the subsurface, however only bigger bends contribute to high resisting forces due to bending, small deviations do not contribute much into it. The overall resisting force due to the pipe bending in the bore seen in Equation 3.32 is hence the sum of the two partial forces seen in Equation 3.33 through 3.35:

$$T_{f-k} = F_1 + F_2 \quad (3.32)$$

where,  $T_{f-k}$  is the sum of the two partial resisting forces  $F_1$  and  $F_2$  occurring due to the product pipe bending in the bore. Said two forces are further described by Equations 3.33 and 3.35)

$$F_1 = T_{K_i} \cdot (e^{\mu_{b-i} \cdot K_{c-i} \cdot \gamma_{s-s-i}} - 1) \quad (3.33)$$

where,  $T_{K_i}$  is the total resistance force acting on pipe before it negotiates the corner  $K_i$ ,  $\mu_{b-i}$  is the friction coefficient between soil and pipe (assumed at 0.24[-]) at  $K_i$ ,  $K_{c-i}$  is the corresponding coefficient of chock effect (assumed at 0.5[-]) at point  $K_i$  and  $\gamma_{s-s-i}$  is the angle between the extension of the pipe segment before point  $K_i$  and the one after. Plugging in the assumed values brings Equation 3.33 to the form of:

$$F_1 = T_{K_i} \cdot (e^{0.12\gamma_{s-s-i}} - 1) \quad (3.34)$$

The second part of the resisting force due to bending, was changed as the original authors calculate the normal forces over many iterations of varying bore deformations. Calculations are then ended when forces at certain contact points converge. This approach calculates the potential forces acting on the piping, however, as the resolution and general data on the pilot bores was of insufficient quality. Another approach was taken for this research, the deformed pieces of product pipe already in place were taken under consideration and the normal forces were back calculated based on their shape under the assumption of a simply supported, intermediate load beam being present. The changed equation then takes up the form of:

$$F_2 = K_{c-i} \cdot \mu_{b-i} \cdot P_i \quad (3.35)$$

where,  $\mu_{b-i}$  is the friction coefficient between soil and pipe (assumed at 0.24) at  $K_i$ ,  $K_{c-i}$  is the corresponding coefficient of chock effect (assumed at 0.5) at point  $K_i$  and  $P_i$  is the normal force calculated from the simply supported intermediate loaded beam. Similarly to Equation 3.34, plugging in the values of constants leads to equation:

$$F_2 = 0.12P_i \quad (3.36)$$

Furthermore, taking the simply supported intermediate loaded beam formulations into consideration, Equation 3.36 for the resisting forces due to bending effect changes into (MechaniCalc [nd]):

$$F_2 = 0.12 \frac{6E \cdot I \cdot L \cdot \theta_2 \cdot (\theta_1 - \theta_2)}{\left(L^2 - \frac{(-L \cdot \theta_1 - 2L \cdot \theta_2)^2}{(\theta_1 - \theta_2)^2}\right) \cdot (-L \cdot \theta_1 - 2L \cdot \theta_2)} \quad (3.37)$$

where,  $E$  is the Youngs Modulus,  $I$  is the moment of inertia of a hollow tube given by Equation 3.38,  $L$  is the length of pipe segment under consideration,  $\theta_1$  and  $\theta_2$  are respectively slopes at either ends of the pipe segment. The formulation for the moment of inertia  $I$  is given by:

$$I = \frac{\pi}{64} (D_p^4 - d_p^4) \quad (3.38)$$

where,  $D_p$  is the outer diameter of the product pipe and  $d_p$  is the inner diameter of the product pipe.

Equation 3.36 seen above is achieved a series of algebraic manipulations shown in Equations 3.39 through 3.43, using the fact that for a simply loaded beam:

$$\theta_1 = \frac{P \cdot a \cdot b \cdot (L + b)}{6L \cdot E \cdot I} \quad (3.39)$$

$$\theta_2 = \frac{P \cdot a \cdot b \cdot (L + a)}{6L \cdot E \cdot I} \quad (3.40)$$

where,  $P$  is the applied normal force required to achieve recorded beam deflection according to the data,  $a$  is the distance from the left edge of the pipe segment under consideration to the location of applied normal force, while  $b$  is the distance from the right edge of the pipe segment under consideration to the location of applied force. From the slope formulations seen in Equations 3.39 and 3.43 solving for  $P$  (normal force) and substituting  $L - a$  for  $b$  yields:

$$P = -\frac{6E \cdot I \cdot L \cdot \theta_1}{a \cdot (2L^2 - 3L \cdot a + a^2)} \quad (3.41)$$

$$P = \frac{6E \cdot I \cdot L \cdot \theta_2}{a \cdot (L^2 - a^2)} \quad (3.42)$$

Equating formulations 3.41 and 3.42 to each other and solving for  $a$  yields:

$$a = \frac{-L \cdot \theta_1 - 2L \cdot \theta_2}{\theta_1 - \theta_2} \quad (3.43)$$

Plugging the distance  $a$  into Equations 3.41 or 3.42 results in achieving the initially introduced Equation 3.37.

### 3.4.5 Resisting force due to drill string exiting the borehole $(T_s)_i$

The final element constituting to the overall pullback resistance force is the friction due to the drill string exiting the bore, while the product pipe is being pulled in. One major difference between the drill string and product pipe is the fact that the former one rotates, greatly reducing the required pullback force, while the other one does not. However, in this research this aspect was encompassed in a different manner. Due to the lack of specifications of the drill strings and reamers used in the installations, deviations from the original model had to be made. While, originally in PipeForce V1 all of the resisting factors mentioned in subsections 3.4.1 through 3.4.4 were once again recalculated for the geometry of the drill string and reamer, in this research a different approach was utilized. At the beginning of the product pipeline pullback stage the entirety of the pipe is laid outside of the bore, while the entire drill string is inside of it. In such situation calculations of the influence of the drill string can be made by taking the total resisting force at the moment (found in the data) and the resisting force of the product pipe being laid outside of the bore (estimated by the model). By subtracting the total force at that first instant of movement and the resisting factor  $(T_g)_i$ , the total drill string resisting force  $(T_s)_i$  is found. Such an approach resulted in Equation 3.44 seen below:

$$(T_s)_i = (T_0 - (T_g)_0) \cdot \frac{\sum_{k=0}^{i-1} L_k}{L} \quad (3.44)$$

where,  $T_0$  is the total pulling force required to start the product pipe pullback stage,  $(T_g)_0$  is the resisting force due to the friction of the product pipe outside of the bore at the start of the pullback stage,  $L_k$  is the length of borehole segment  $S_k$ , under the sum it is representing portions of pipe that has been pulled into the borehole already,  $L$  is the total length of the installation.

Through this method of calculation of the final resisting factor  $(T_s)_i$ , the assumption was made that the resisting force is decreasing linearly throughout the installation as the drill string is being pulled out and replaced by the product pipe. Such an assumption could be taken due to a generally low magnitude of said force and its effect on the overall maximal pullback force.

Furthermore, an advantage of the chosen assumption and calculation method is the ability to begin the pullback force calculation at the same value as the actual measured forces from the field, which further shows the accuracy and trends present in the model calculation without a potential outlier of starting at different base values, potentially leading to a diverging result. The trends and model results will be further discussed in 5 and 6.

### 3.4.6 Total pullback force $T_i$ formulation

Finally, the total pullback force calculation as seen in Equation 3.45 is a sum of all the partial resisting forces described in Sections 3.4.1 through 3.4.5. The model is based upon dividing the complex phenomenon of pulling a pipe into an underground bore prepared beforehand into a number of much simpler problems calculated separately for the most part, keeping in mind that two partial resisting forces,  $F_1$  from Equation 3.32 along with  $(T_s)_i$  both are partially based on the other forces calculated in the model. This dependency would not have been different if the original model was fully implemented, therefore, proposed changes should yield similar results to the original in terms of accuracy of pullback force calculation. The final formula encompassing all the resisting factors can be seen in Equation 3.45, below:

$$T_i = (T_g)_i + (T_b)_i + (T_r)_i + \sum_{k=1}^{i-1} \Delta T_{f-k} + (T_s)_i \quad (3.45)$$

### 3.4.7 Implemented model Limitations

As mentioned beforehand, the proposed model was changed in order to accommodate for different data being supplied. Such approach changed the the models purpose, from calculating the expected pullback forces based on the designed trajectory of the installation, to analysing the impact of varying input parameters like, bore path accuracy/ smoothness, ballast coefficient and specific gravity of the slurry.

Firstly, a different formulation was applied for calculating the pulling force component due to friction of the ballasted pipe inside the borehole  $(T_b)_i$  seen in Section 3.4.2. The original equation was expanded by the additional functionality of varying the ballasting percentage and the specific gravity of the slurry. Such approach lets analyse the impact those parameters have on the overall calculation and the results in the form of maximal pullback forces. Therefore, a thorough sensitivity analysis should be conducted in order to uncover any errors in the model that might occur.

Secondly, changes to the calculation method of the normal forces acting upon product pipe bending  $P_i$  in Section 3.4.4, lead to uncertainties regarding additional resisting forces due to not only the bending of the product pipe but also to previous deformations of the bore. While, the original model proposes iterative calculation of soil displacements around bending zones leading to calculation of the normal forces with a finite element algorithm, in this research, they have been calculated

based on already existing bends in the product pipe trajectory. Hence forces prior the final state regarding soil deformations have been neglected.

Finally, the original model recalculated all of the resisting factors to achieve the resistance factor due to drill string exiting the borehole  $(T_s)_i$ . However, in this research it was assumed that subtracting  $(T_g)_0$  (the resisting force due to the friction of the product pipe outside of the bore at the start of the pullback stage) from  $T_0$  (the total pulling force required to start the product pipe pullback stage) results in the value of the maximal resisting force due to the drill string present in considered installation (Section 3.4.5). Such value would then decrease linearly over the length of the installation. Said approach does not account for the non-linearity of the real physical phenomenon, thereby rising uncertainties in the intermediate maximal pullback force calculation along the bore path.



# 4

## DATA AVAILABLE

In this chapter the database description along with the description of the past cases taken into account is presented. Direct, numerical examples of the data utilized in this study are absent from this section.<sup>1</sup>

### 4.0.1 Raw Data

The available data provided mostly by Deltares, along with other anonymous companies, was initially in the form of a spreadsheet with a multitude of parameters regarding each of the three main installation stages of a drilling project separately (pilot bore, reaming and product pipe pullback). Parameters include, but are not limited to:

- Drilling fluid type pilot/reamer
- Drilling fluid type pullback
- Entry point
- Exit point
- Entry bending radius
- Exit bending radius
- Entry angle
- Exit angle
- Horizontal pipe bend placement
- Product pipe material
- Young's Modulus
- Outer diameter of the product pipe/reamer/ drill string/ drill head
- Product pipe/ drill string wall thickness
- Number of joints
- Distance between joints
- Steering system in use
- Size of the bent sub
- Number of nozzles
- Design coordinates (three-dimensional)
- Reported coordinates of pilot bore (three-dimensional)
- Measured coordinates of product pipe in place (three-dimensional)
- Start/ end time
- Minimal/ maximal pump pressure
- Minimal/ maximal mid discharge
- Minimal/ maximal torque
- Minimal/ maximal RPM
- Unit weight of mud pumped in/ out
- Minimal/ maximal thrust force
- Type of product pipe feeding system
- Friction factor of pipe feeding system
- Unit weight of ballasting fluid
- Geological data regarding the encountered strata
- CPT readouts

Initially, a total of nine projects described in this way were shared for the purpose of the study, yet due to certain pieces of information missing or information that proved to be physically inaccurate or downright impossible, six out of the initial nine were left out of the study. In Figures 4.1 through 4.3 visualisation of the

<sup>1</sup> For further information regarding the data, an additional file will be shared upon request at most two years after the completion of this research as per the signed non-disclosure agreement.

mentioned raw data can be seen, to the left of the Figures is the trajectory three-dimensional plot, which in certain cases does not align perfectly, yet that remains as a testament to the troublesome nature of data gathering. In terms of trajectories, three lines are visible, the design, reported and measured path. While it is clear what the design path is, the reported path is the trajectory of the initial pilot bore and the measured path is the trajectory assumed by the pulled in product pipe. It was found throughout the preliminary data analysis that the measured path had the highest amount of data points without any obvious outliers, hence those types of coordinates were primarily considered in further analysis. Coordinate paths lack of convergence might potentially be due to the way the data was extracted or collected. Despite the deviations from a singular trajectory, for each installation the paths were similar in shape, therefore showing clearly that, differences in coordinate systems or reference points are the primary cause of differences between the plotted trajectories.

Furthermore, the geological strata encountered during the drilling operation can be seen in the upper right plots in Figures 4.1 through 4.3. The geological formations present during a drilling operation provides invaluable information regarding the level of difficulty of the installation and what potential threats were present. In the installations considered in this study the geological strata that have been encountered counts loose sand, medium sand, dense sand, peat, and weak clay. The soil layers were plotted as horizontal layers as borehole and CPT pieces of data were too sparse to create a geological cross-section of the area.

Finally, the last plot visible in Figures 4.1 through 4.3, depicts the thrust (push) and pullback forces and their magnitudes along the installation length. The thrust forces were recorded during the pilot boring, while the pullback forces were recorded during the product pipe pullback step. In most cases the thrust force recorded during the pilot phase have a much smaller sample size than the pullback forces, which explains the visual differences between the two. Said two forces were put side by side in order to visualise the initially received data. As visible in the figures, pull forces have a much higher resolution than the thrust/ push forces.

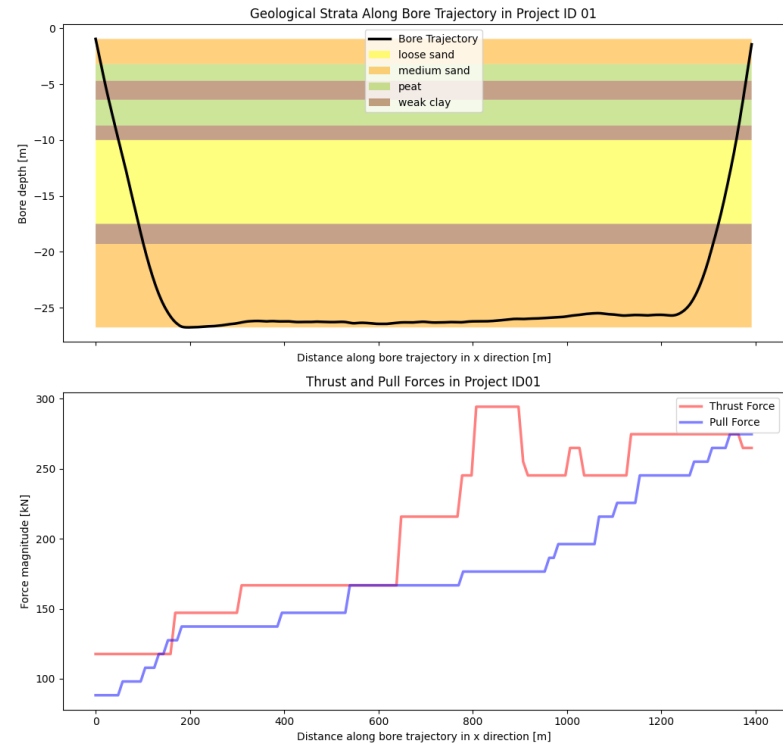
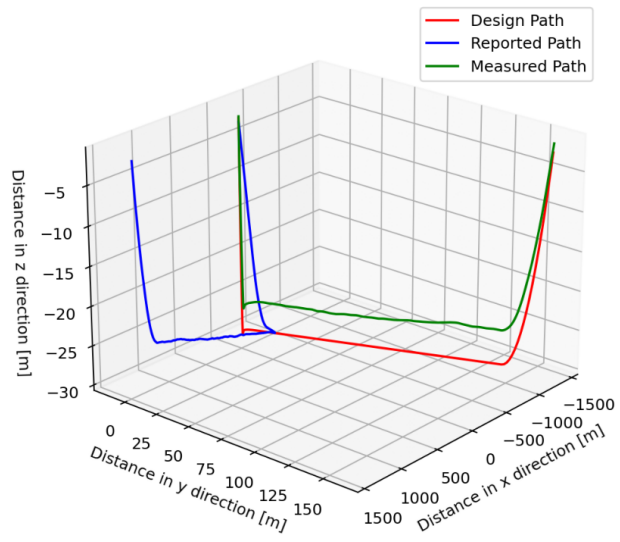


Figure 4.1: Raw data, after normalization for Installation 01

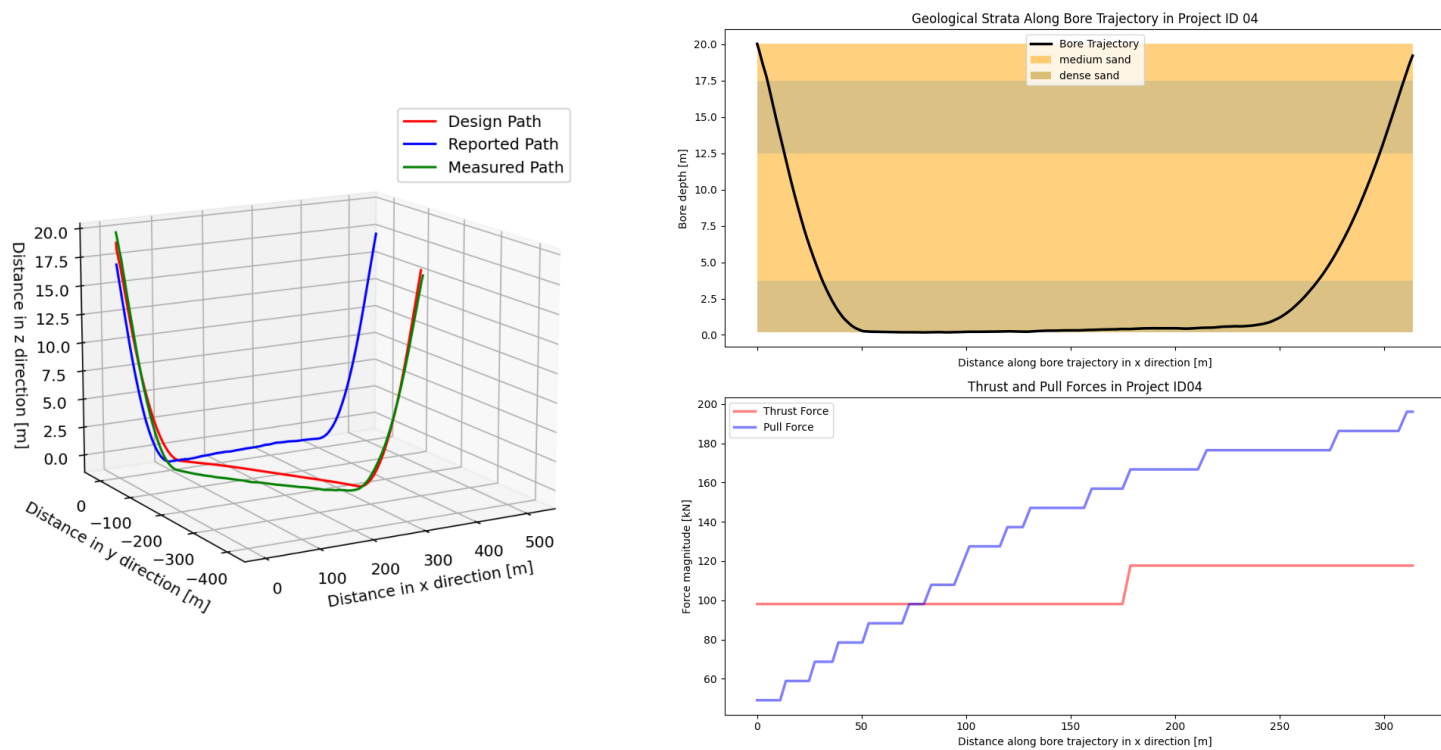


Figure 4.2: Raw data, after normalization for Installation 04

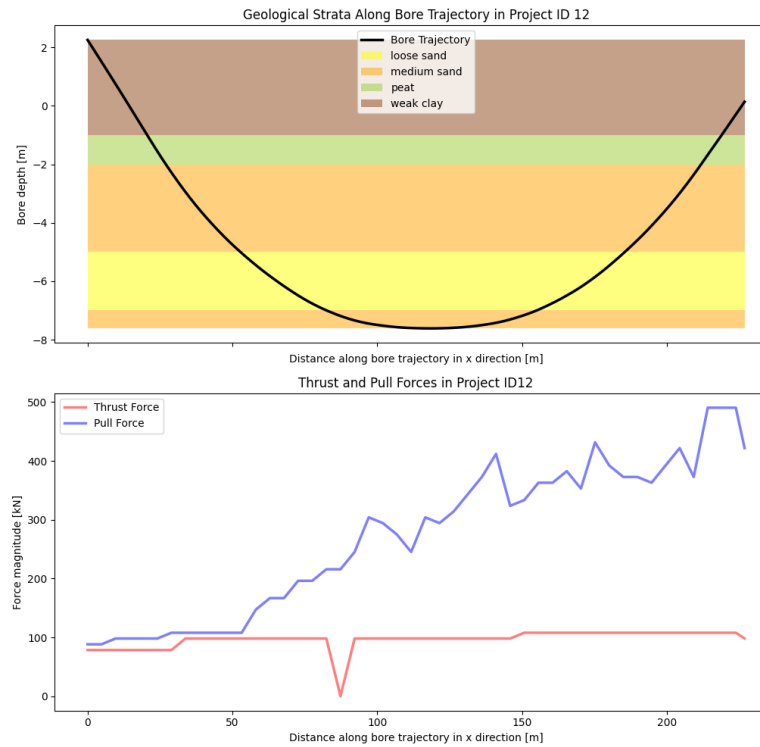
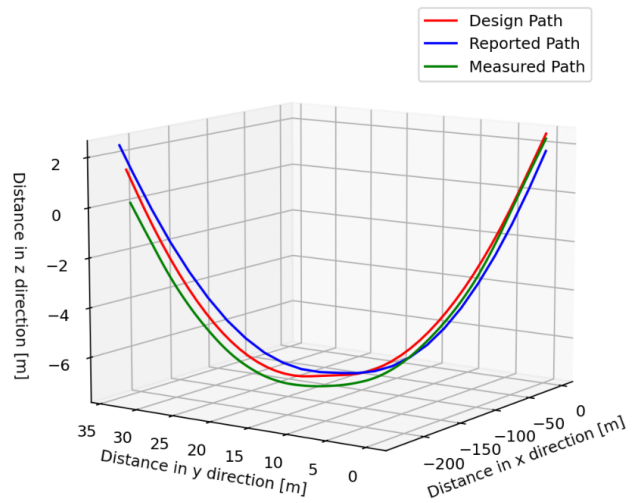


Figure 4.3: Raw data, after normalization for Installation 12

#### 4.o.2 Preliminary Data Investigation

After the initial reworking of the data, namely normalizing and rotating the installations using a rotation matrix in order to minimise the deviations in the top view of the trajectory (y-plane), the installations were considered as a two dimensional problem. In the preliminary data analysis other types of information that could be gathered from raw data were accessed, resulting in the plots found in Figures 4.4 through 4.6. In the first plot seen at the top of the series, the double gradient of the boring trajectory is plotted. Double gradient essentially meaning a double derivative over the x coordinate of the trajectory, leading to the absolute values of deviations (in any direction) from the centre of the borehole. Said plot is present to visualize how irregular the path of installation truly is and in which places the biggest unevenness occurs. As expected, both the beginning and the end of the installations are visibly more irregular than the middle sections. This observation is in line with prior reasoning, that initially the pipe has to bend in order to fit into the bore and after reaching an appropriate depth it needs to adjust its shape once again to establish a horizontal middle section. Then, bending is once again required in order to start moving upwards, towards the exit of the bore. The values seen in the double gradient plots can be considered as the sum of deviations in y and z-planes. The data used for the creation of the double gradient plots was discrete, however the plotting package "Matplotlib" connected the points with lines leading to a continuous visualisation.

The second plot visible in Figures 4.4 through 4.6 is the step plot of the thrust and pull forces recorded respectively, in the initial pilot phase of the installation and then in the final pullback phase. The step function visualizes the process behind the changes in forces, making it comparable to the other two plots seen above and below them. It can be seen that while the other two plots are peaking, changes in acting forces are also more frequent. In section 3.2 the factors influencing pullback forces have been mentioned, accordingly, as the directional changes during boring are one of the main parameters influencing the pullback forces, the previously mentioned observation was to be expected. The occurrence of a higher force activity related to higher magnitude of values in the other plots can be best seen in the Figures 4.4 and 4.5.

The third plot present in Figures 4.4 through 4.6 is a visualization of the pipe's bending radii changes along the length of the borehole. This plot should partially mimic and go in line with the double gradient plot described before. While the inverted bending radii and the double gradient plots can be considered similar, upon comparing the two to the pullback forces recorded, a relationship can only be seen in the case of Installation 01. With an increasing amount of irregularities, higher magnitudes of pulling forces can be expected to occur. However, in Installations 04 and 12 such dependency does not seem to manifest. Such a behaviour might be due to the relatively short lengths of the installations in question. In the figure the y-axis is actually the inverted bending radii of the pipe, meaning that the highest readout values, have effectively the smallest bending radii which points towards sharp bends and sudden changes in direction. The method for obtaining bending radii was to take each three consecutive coordinates and fit a circle through them. The radius of said circle would then be considered as the bending radius at the middle point's x coordinate. Such method was then additionally corrected for the scenario's where the bending radius would approach zero or infinity as it would mean respectively, breaking of the drill string or would show up as an outlier rendering the rest of the information within lost. As the irregularities even after correction proved highly irregular, a Gaussian filter was applied to each of the coordinate axis leading to a filtered outcome, which can be considered as more in line with reality. The filtered plots can be seen in Figures 4.7 through 4.9. Gaussian filter is popularly used to blur images and remove detail and noise, in this particular case the noise was the issue. Gaussian filter works similar to a mean filter where it takes the sur-

rounding coordinates and calculates a common new mean value, ridding the data of excessive changes in magnitude leading to a gentler curve. The Gaussian filter method of functioning is best described by Equation 4.1. By correcting the bending radii data for the sudden, high magnitude changes, which should not occur under the assumption that the drillstring remained in one piece, the outcome seems to have a much more gradual outline than the previously achieved plots. The Gaussian filter as used in this research was taken from Python "Scipy" package under the name of *gaussian\_filter1d*. (Fisher [2003])

$$G(x) = \frac{1}{\sqrt{2 * \pi * \sigma}} * e^{-\frac{x^2}{2\sigma^2}} \quad (4.1)$$

The last plot present at the bottom of the Figures 4.4 through 4.6 constitutes a colorbar which indicates the consecutive geological strata being penetrated by the drill during the installation. It is in place so that additional observations regarding the relationship between changes in the geology and irregularities or force changes present in the previously mentioned plots can be made.

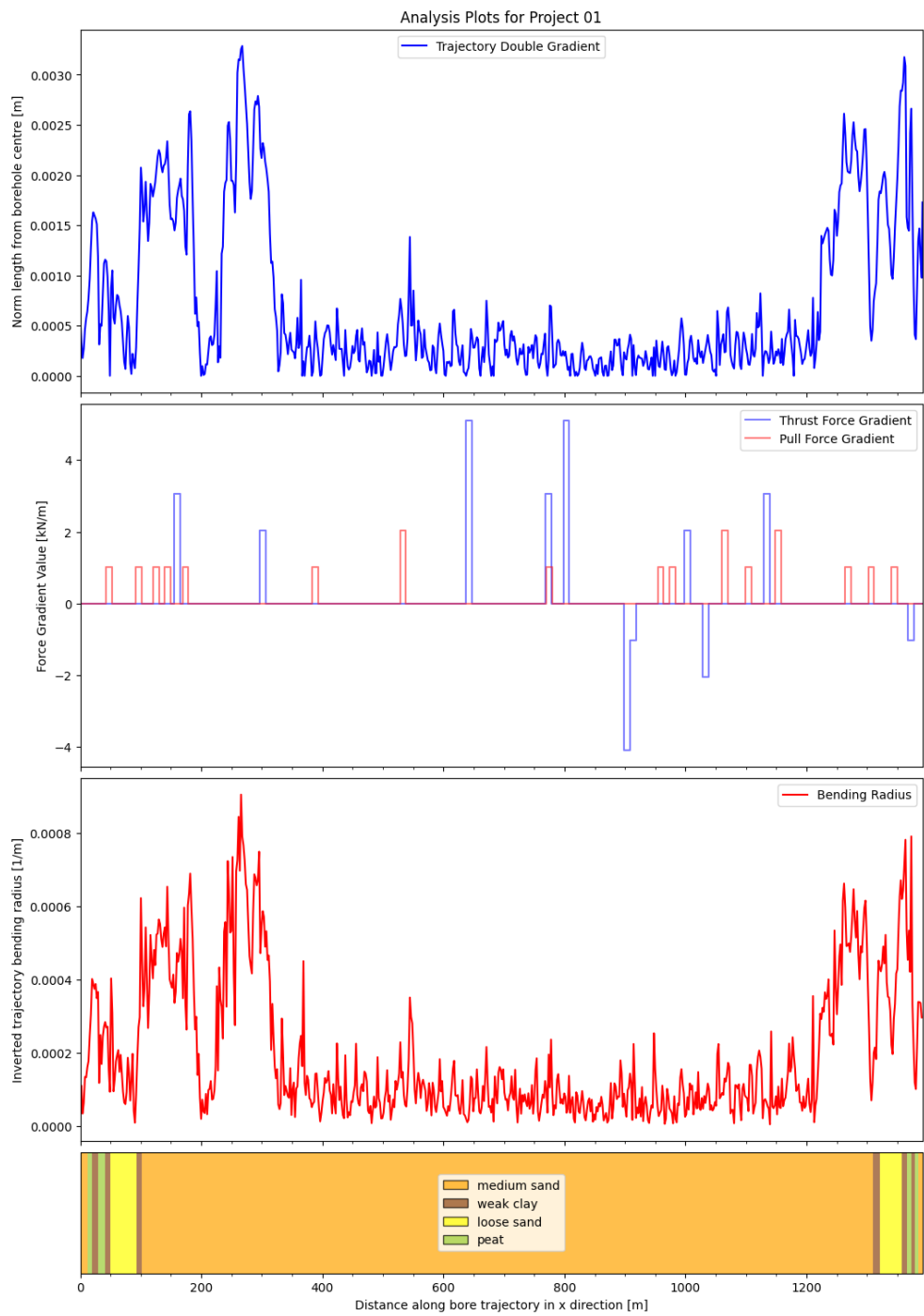


Figure 4.4: Data preliminary analysis for Installation 01

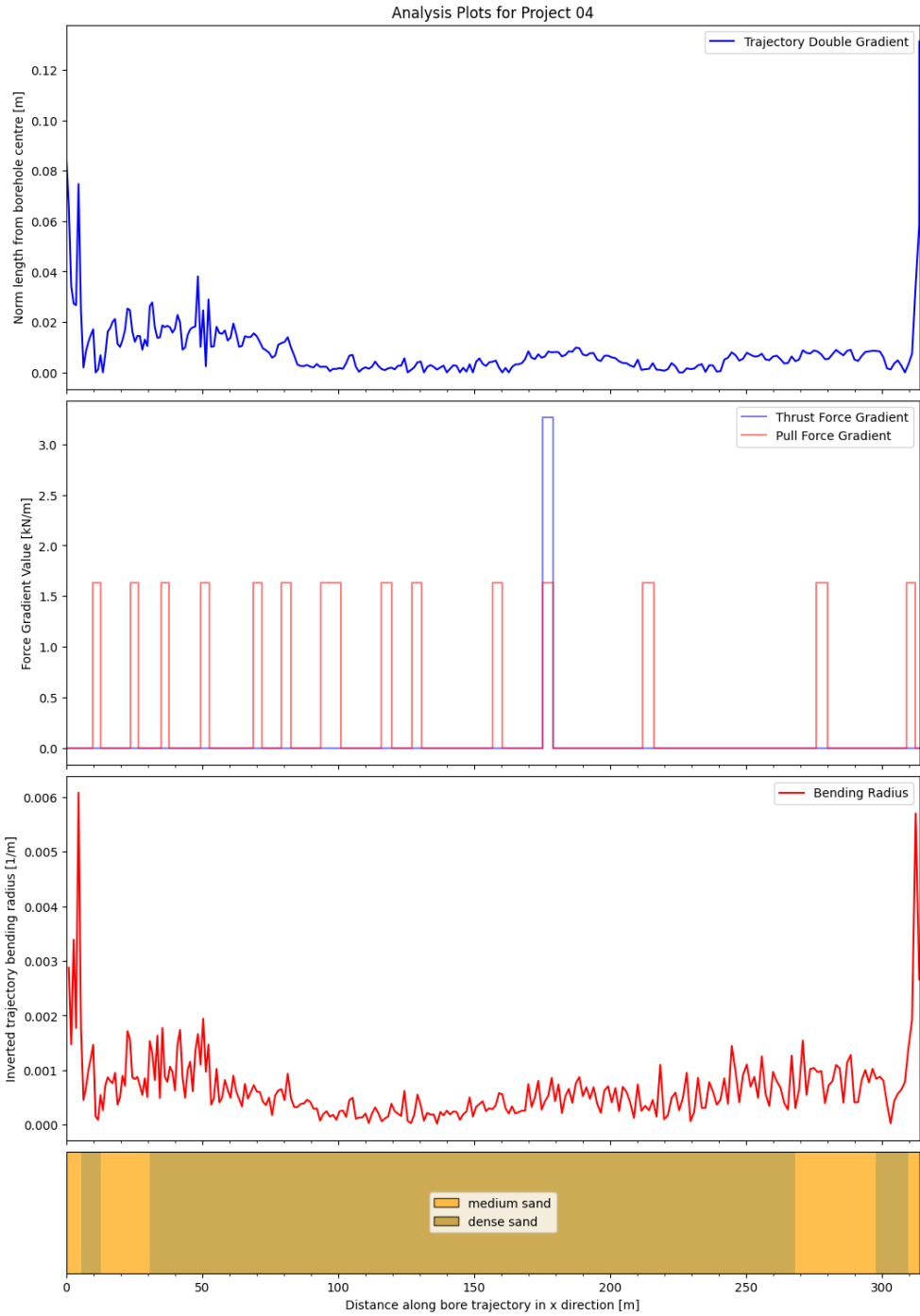


Figure 4.5: Data preliminary analysis for Installation 04

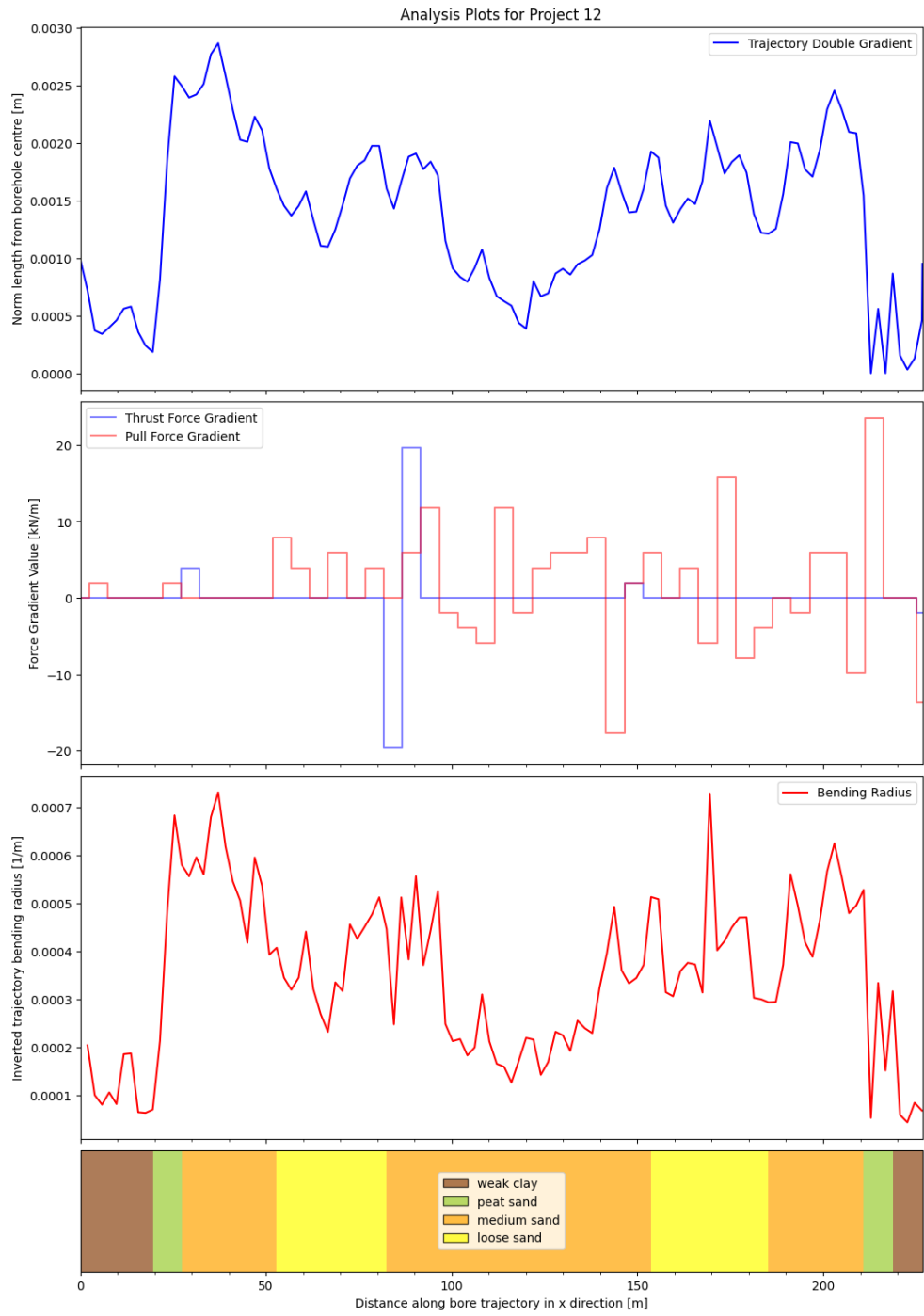


Figure 4.6: Data preliminary analysis for Installation 12

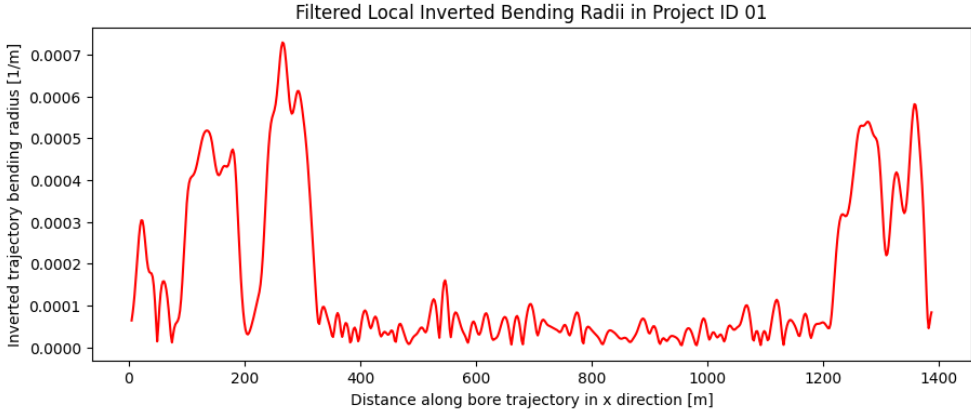


Figure 4.7: Bending radii after Gaussian filter in Installation 01

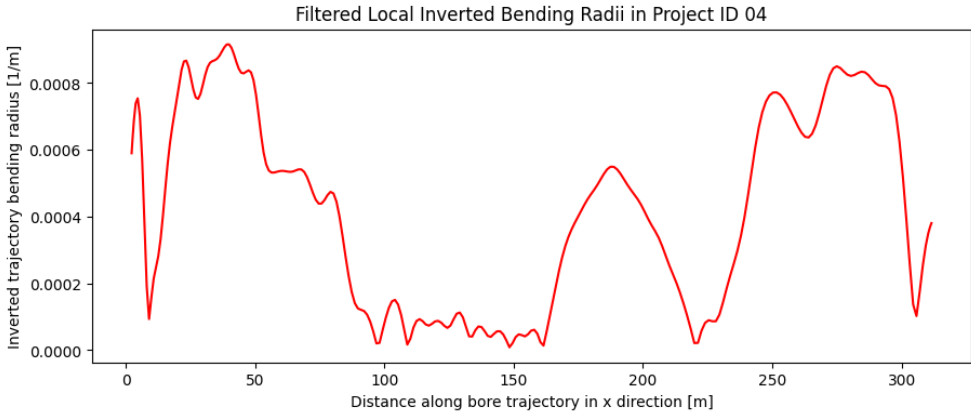


Figure 4.8: Bending radii after Gaussian filter in Installation 04

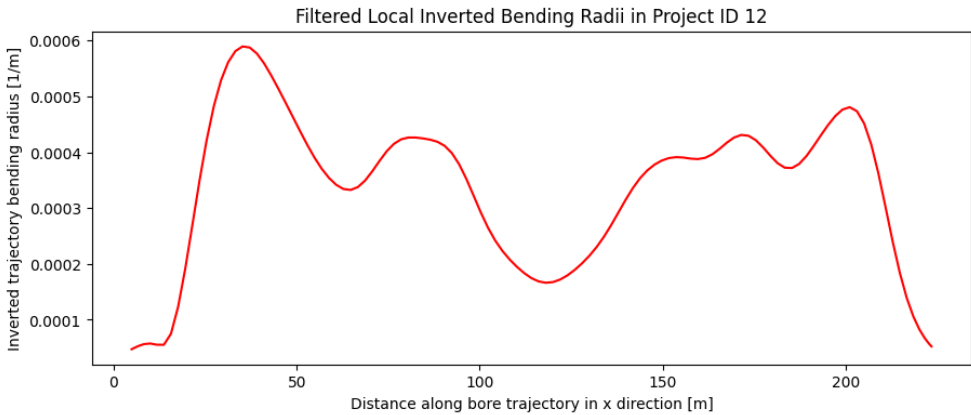


Figure 4.9: Bending radii after Gaussian filter in Installation 12



# 5

## RESULTS AND ANALYSIS

In this chapter, results of the research along with further analysis are described. Firstly the attention should be put towards the validation of the model, in Section 5.1 the results produced by the model were compared to the actual measured ones. In the next Section 5.2 the influence of the borehole alignment accuracy/ the smoothness of the bore trajectory on the pullback forces was analysed. Furthermore, the influence of varying ballast and specific gravity of the slurry on the pullback forces was considered and described in Section 5.3. Finally, the limitations of the utilized model have been described in the Section 3.4.7 found in this chapter. Due to the fact that multiple installations have been of insufficient quality to be run through the model and yield results appropriate for further deliberation, most of the analysis present in this chapter can be considered as a result of visual examination of generated plots and values. A thorough statistical analysis would require a much bigger sample size. More on recommendations and further research in the field can be found in Chapter 6, Section 6.4.

### 5.1 VALIDATION OF THE MODEL WITH REAL DATA

Firstly, in order to validate the outcomes produced by the implemented model, actual measured pulling forces were compared with the ones generated by the model for two different cases. Cases under consideration were:

- Forces simulated with found optimal values for ballasting and specific gravity of the slurry
- Forces simulated with actual measured values for ballasting and specific gravity of the slurry

Generated pulling forces can be seen in Figure 5.1, where "Simulated real" are pulling force values calculated with measured ballast and specific slurry gravity values in place, while "simulated optimal" are the pulling force values with optimal values of ballast and slurry specific gravity plugged into the model. As seen in the figure, in case of installation 01 the simulated pullback force with real values of ballasting and specific gravity of the slurry deviates from the measured values greatly, however, the pullback forces generated for installations 04 and 12 can be considered to be following expected paths. The values of pullback forces with optimal values plugged in are much lower than the measured and simulated real values and the latter two mentioned can be considered similar in shape and magnitude to each other. Naturally the measured and simulated real curves are not perfectly overlapping as the amount of parameter and phenomena accounted for in the implemented model are limited compared to the actual physical process.

Secondly, with the observations above in mind and additional analysis of the behaviour of every force component along the first installation a conclusion was derived that the model implemented in the current form, as described in Section 3.4, approximates the pulling forces in a similar fashion to the measured ones for shorter drilling operations, however when longer installations are introduced (more than 600m, found empirically with accordance to the length of bores available as data sets), the  $(T_b)_i$  coefficient, accounting for the pulling force component due to friction

of the ballasted pipe inside the borehole, increases in approximately quadratic order. This dependency can be further explained by the  $L_k$  factor, being the length of borehole segment  $S_k$  representing portions of pipe that have been pulled into the borehole. Said length factor is progressively increasing during the installation as more segments are being pulled in, which on its own does works well in the other partial forces calculated in the model, however in  $(T_b)_i$  an additional sum over the elements is taken with  $L_k$  factor inside leading to a doubling of the summation over the elements being pulled into the bore. The formulations for  $(T_b)_i$  can be seen in Section 3.4.2.

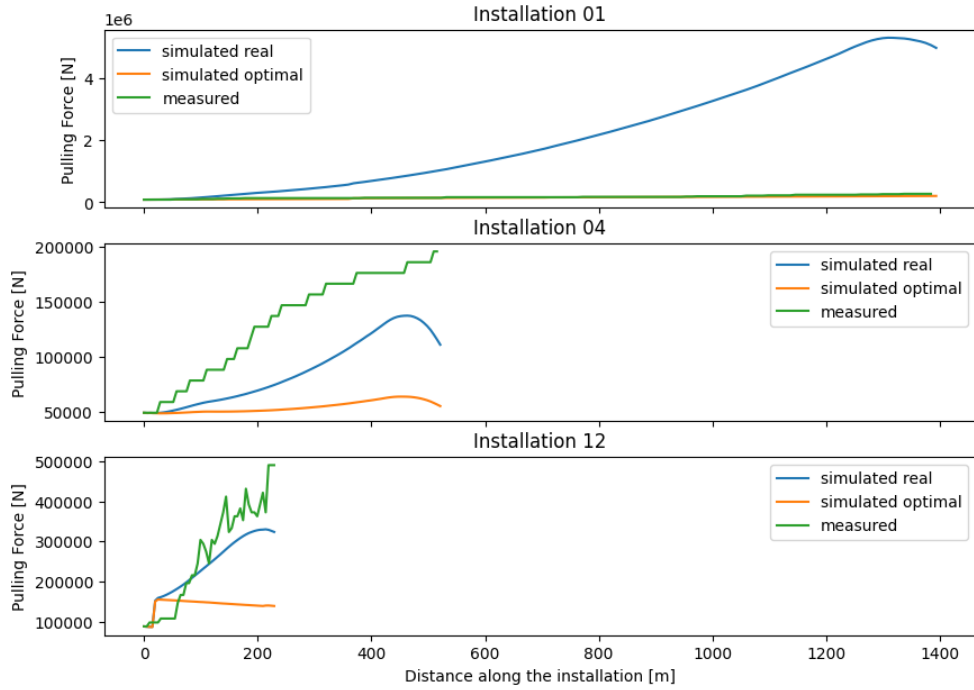


Figure 5.1: Pulling force plot appropriate for short installations

Thirdly, considering the previously mentioned analysis, an additional feature was introduced into the code, where the forces for the long installations would be calculated without the double summation and the forces in short installations would keep the calculation method as described in Section 3.4.2. Such approach led to the expansion of the code with a different formulation for the longer installations in the form of:

$$(T_b)_i = \sum_{k=1}^{i-1} (|K_{c-k} \cdot L_s \cdot w \cdot \mu_{b-k} \cdot \cos\beta_{s-h-k}| + L_s \cdot w \cdot \sin\beta_{s-h-k}) \quad (5.1)$$

where,  $L_s$  represents the length of pipe segment under consideration and not a progressively increasing length of product pipe already pulled into the bore.

With such a correction, after recalculation, the  $(T_b)_i$  term no longer increased so rapidly leading to a more realistic outcome, visible in Figure 5.2. In said figure, the two plots for installations 04 and 12 have not changed due to the utilization of the model as described before, while the simulated forces for the longest, installation 01, can be seen to be following the measured forces much closer than previously in Figure 5.1.

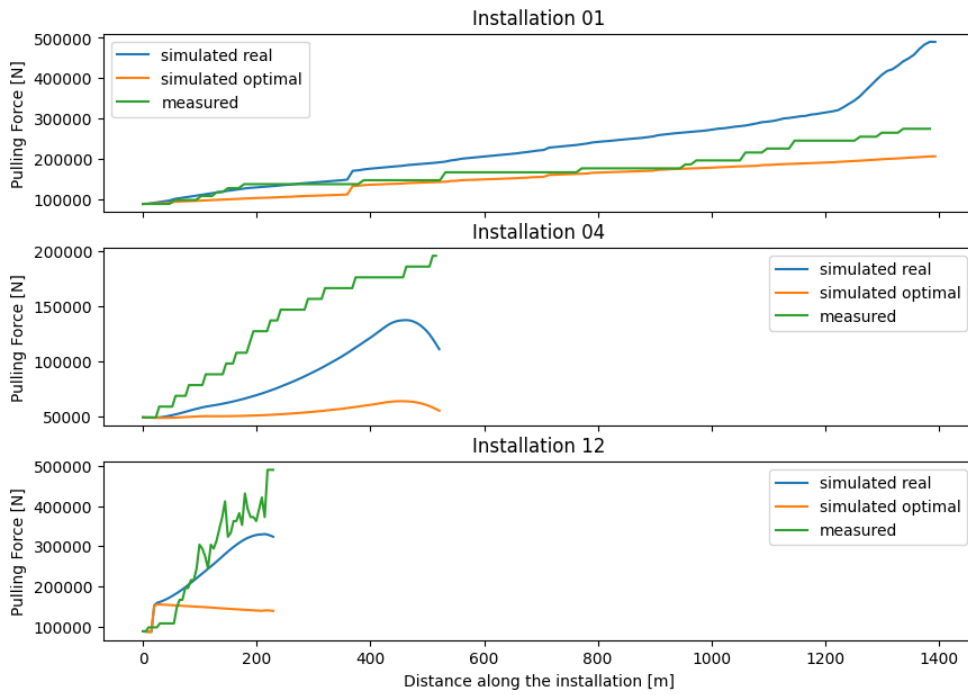


Figure 5.2: Pulling force plot for simulated and measured outcomes

Fourthly, in order to visualize the change applied to the code and show that the change was beneficial only in case of the longest installation, forces in installations 04 and 12 were simulated with the changed script, resulting in Figure 5.3. In the figure it can be seen that, while the generated forces in installation 01 follow the measured forces similarly, the ones in installations 04 and 12 differ much more from the original, compared to the case of utilizing the model before the change. Hence, a feature was added, where the model checks for the length of the installation and if it exceeds 600m the script with changed  $(T_b)_i$  formulation is used.

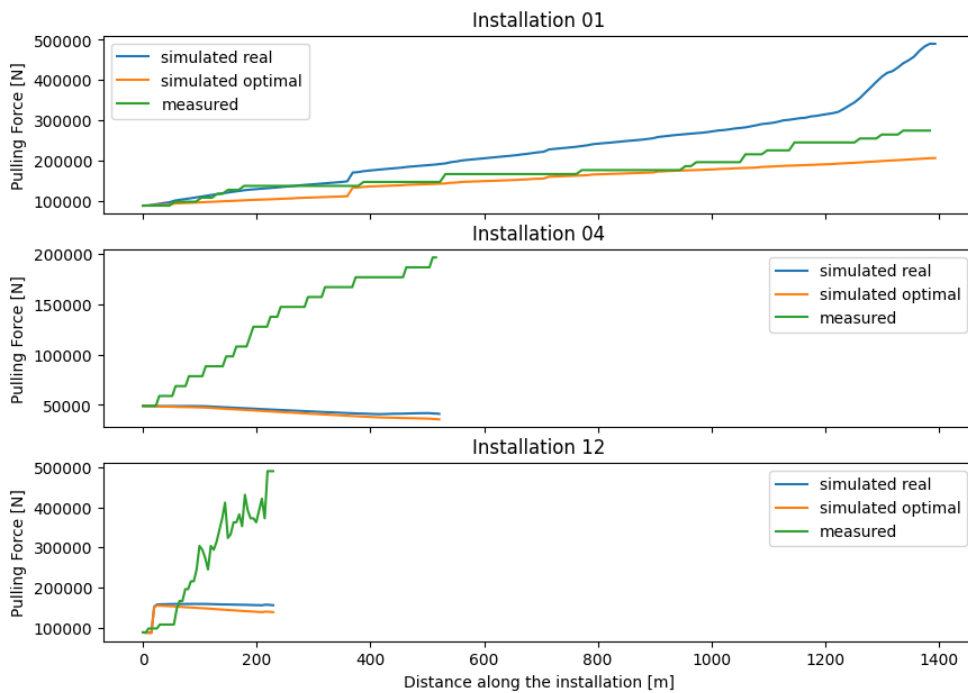


Figure 5.3: Pulling force plot appropriate for long installations

Finally, in all of the Figures 5.1 through 5.3, a visible tendency is present, where by the end of each installation the simulated pulling forces plateau or decrease, which also was found to be caused by the aforementioned  $(T_b)_i$  factor. The reasoning behind such phenomenon might be the presence of sine and cosine trigonometric functions in the formulations. The angle taken into the calculation is the one between the horizontal line and the pipe segment under consideration. Therefore, for certain pipe orientation, elements of the  $(T_b)_i$  formulation might prove negative, hence decreasing the overall pulling force value. Further research into said factor is recommended, however more on that can be seen in Section 6.4.

## 5.2 RELATIONSHIP BETWEEN THE ACCURACY OF BORE-HOLE ALIGNMENT AND THE PULLBACK FORCE

In the following section, the influence of accuracy of borehole alignment on the maximal occurring pullback forces was analysed. In Section 5.2.1, the methodology of creating smoother trajectories was described and visualised. Furthermore in Sections 5.2.2 and 5.2.3, the influence of a smoother/ more accurate trajectory were shown and quantified. In order to broaden the analysis with more parameters, in Section 5.3 the relationship between the ballasting and specific gravity of the slurry and the maximal pullback force occurring was described.

### 5.2.1 Approach to borehole alignment adjustment

Considering the fact that borehole alignment is a three dimensional path, as mentioned before one dimension was disregarded (namely the y-plane) by rotating the installation to minimise the deflections in said plane. The next step in making a smoother trajectory than the original one, was creating 1000 potential borehole alignments with `make_smoothing_spline` function from Python Scipy.interpolate package. Said function takes a value `lambda` as an argument, which indicates the level of 'smoothness' of the generated spline (trajectory). Initially generated trajectories in the fashion shown in Figure 5.4 then had to be filtered for admissible and inadmissible ones based on certain assumptions. In order to find and keep only the bore paths, which resembled the original one with an acceptable level of likeness, critical points were implemented (seen in the figure as red boxes). These critical points were created manually at the coordinates where the original trajectories would manifest a bend at the target depth of the installation. Additionally, an arbitrary value of 5% of the total length and depth of the bore under consideration was added to the critical points, creating a critical box through which trajectories would need to pass to be admissible. Furthermore, to achieve a closer match to the original trajectory, extra weight was added to the initial and final points. Such method allowed filtering out unrealistic and unwanted paths (due to their geometry), while maintaining the individuality of each project and providing a sufficient amount of acceptable alignments for comparison. Critical points should be assumed for each installation separately as the local site-dependent requirements change with location.

Henceforth, trajectories fulfilling the assumed conditions and ones that did not, were referred to as valid and invalid. As seen in Figures 5.5 through 5.7, a much more streamlined trajectory generation process took place leading to generated paths being much closer to the original ones than in the case visible in Figure 5.4. As seen in each of the figures, for each installation there is a range of valid and invalid trajectories present. Furthermore, the amount of critical points differs between the installations, that is due to the fact that the shortest installation, namely Installation 12, has a different overall geometry than the longer ones. Such short bores do not exhibit a long straight section placed at a designated depth in the middle of the

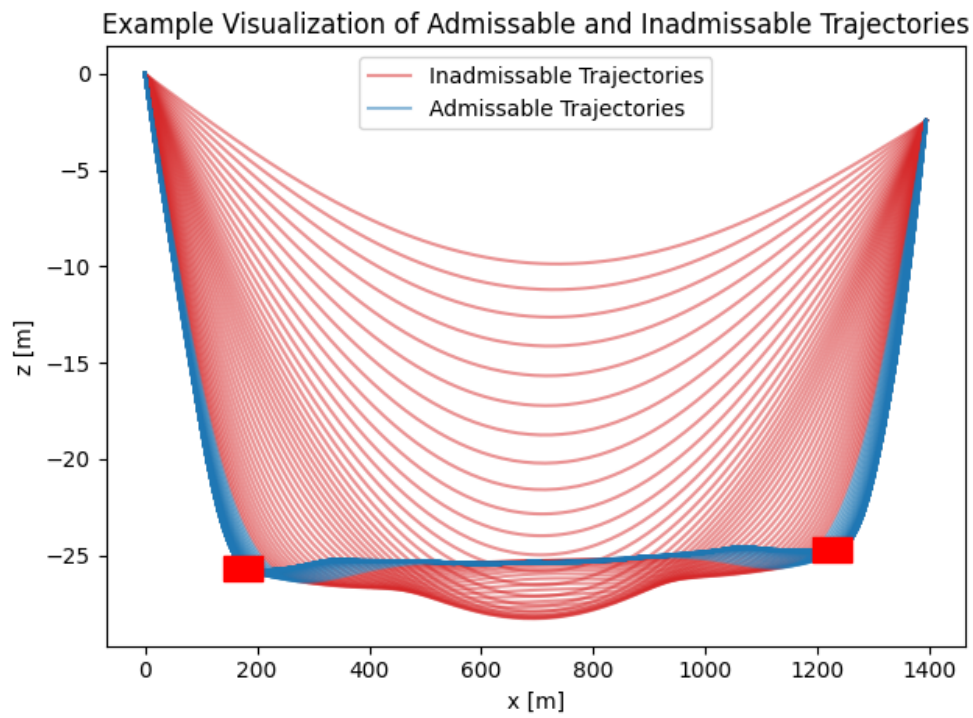


Figure 5.4: Visualisation of trajectory generation and validation

path. This fact led to the application of a single critical point as more intermediate points would result in generation of trajectories far too similar to the original one, making them redundant for further analysis.

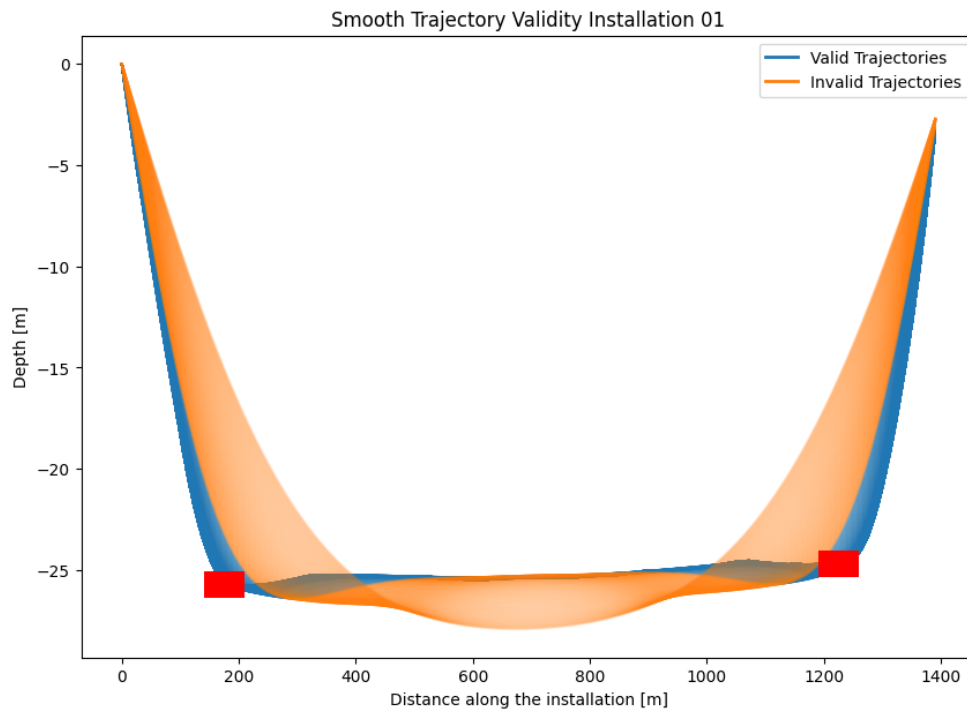


Figure 5.5: Plot showing the valid and invalid generated trajectories

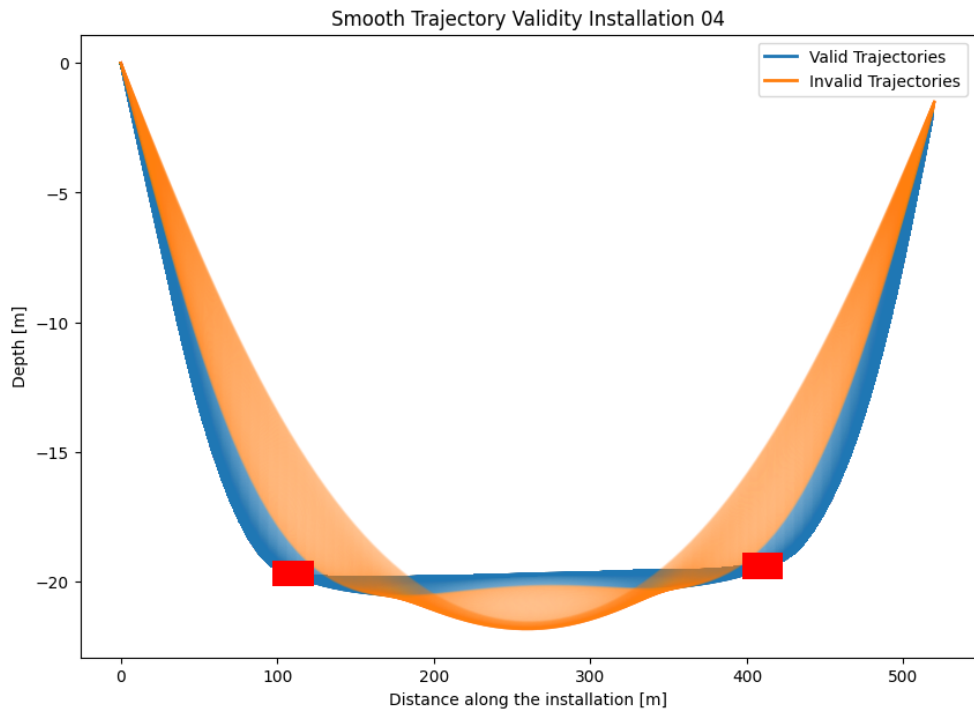


Figure 5.6: Plot showing the valid and invalid generated trajectories

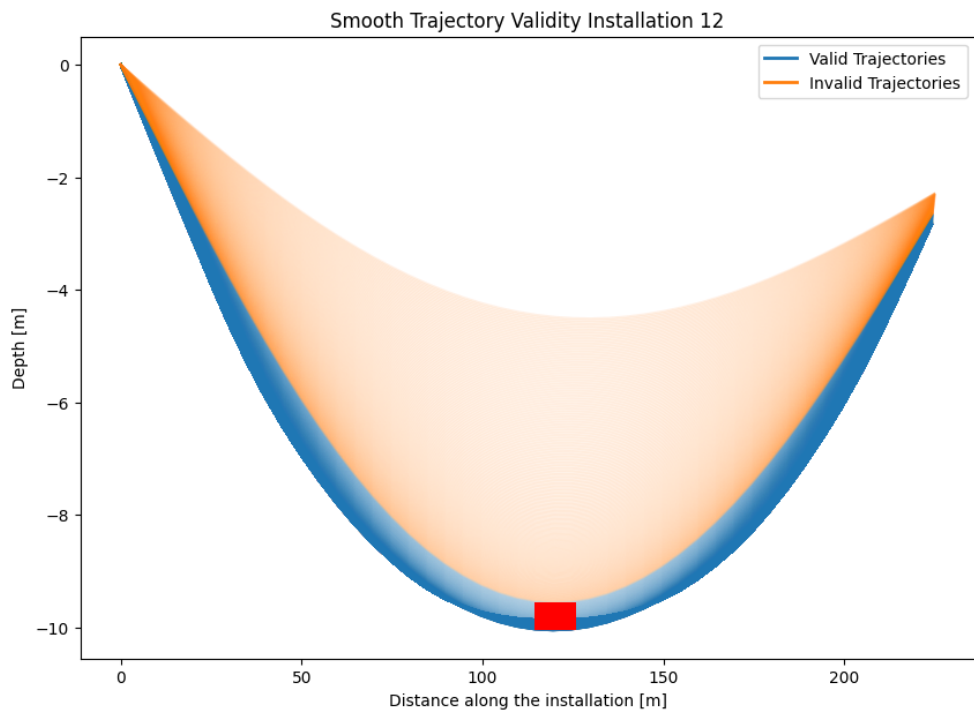


Figure 5.7: Plot showing the valid and invalid generated trajectories

### 5.2.2 Influence of trajectory with real ballast and specific gravity of slurry data

By varying the magnitude of the smoothing factor mentioned in Section 5.2.1, while keeping all of the other parameters constant, it was possible to observe the influence of trajectory accuracy/ smoothness on the maximal pulling forces occurring during the installations under consideration. In Figures 5.8 through 5.10, the smoothness

of the trajectory is varied for different installations. In two out of three mentioned figures a clear trend can be seen, where with increasing the smoothness of the bore, the required maximal force to pull the product pipe in decreases. It can also be seen that the extent of the path accuracy influence depends on the length of the installation under consideration, which remains as an observation in line with logic. In case of installation 12, the reverse of previously mentioned trend can be observed, where the smoothing factor impacts the maximal pulling force like in the other plots up to a certain point after which the relationship inverts causing the pulling forces to increase. The reason for said irregularity in project 12 was not identified and creates an opportunity for further research.

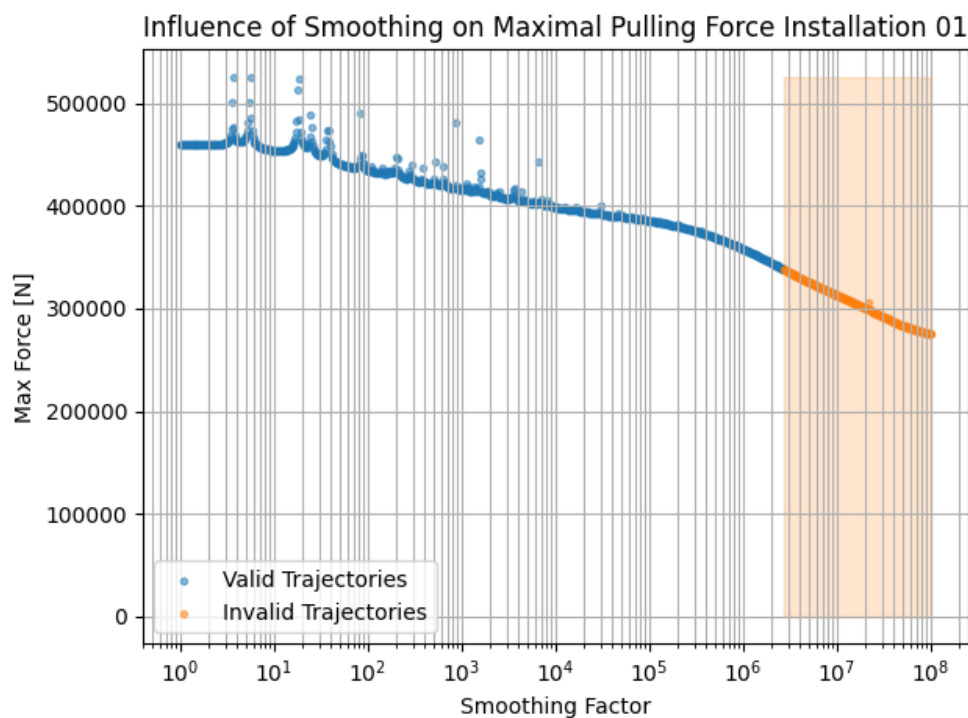


Figure 5.8: Plot showing the relationship between maximal pulling force and trajectory smoothing factor with real ballasting and specific gravity of slurry data

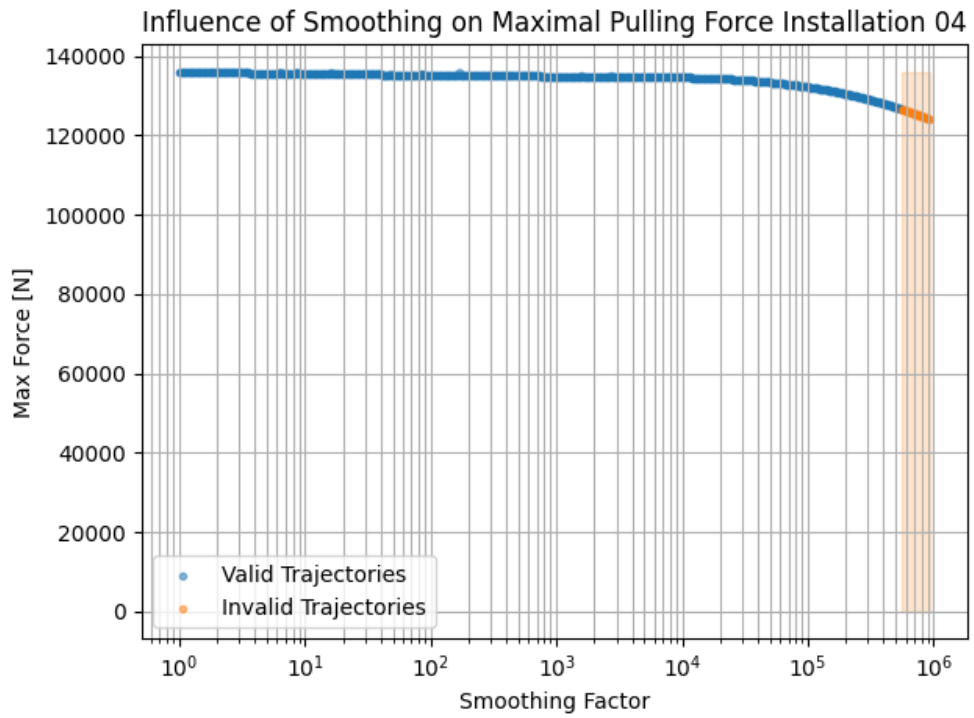


Figure 5.9: Plot showing the relationship between maximal pulling force and trajectory smoothing factor with real ballasting and specific gravity of slurry data

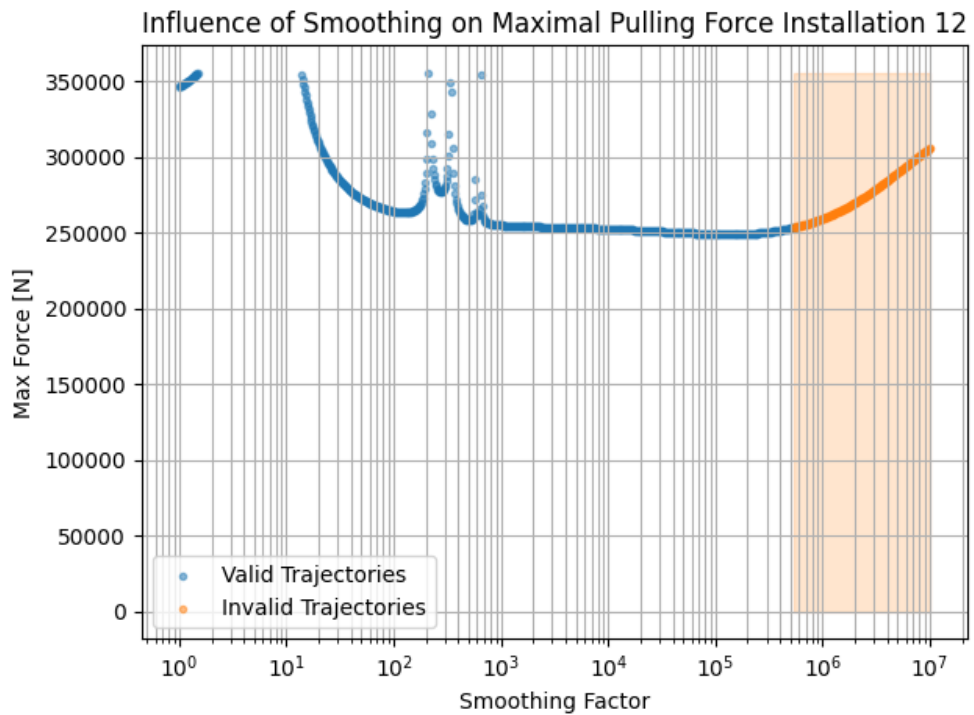


Figure 5.10: Plot showing the relationship between maximal pulling force and trajectory smoothing factor with real ballasting and specific gravity of slurry data

### 5.2.3 Influence of trajectory with optimal ballast and specific slurry gravity data

In this section the situation is analogical to the one previously mentioned in Section 5.2.2, changing only the values of ballasting and specific slurry gravity to optimal

ones. The relationship between the smoothing factor and maximal pulling force occurring can be witnessed in Figures 5.11 through 5.13. In comparison to previously observed Figures 5.8 through 5.10, the ones under consideration now show a similar trend, however the changes to the pulling force with increasing smoothing factor have a lower magnitude than before, which was expected as with appropriate buoyancy of the pipe achieved, the governing factor of friction between the product pipe and the bore itself has a smaller effect on the pulling forces than in case of sub-optimal buoyancy. Additionally, the plot for installation 12 once again differs, however this time the difference can be seen between itself and its predecessor (Figure 5.10) and not the other figures in this section. It can be seen that the trend is in line with logic, yet the maximal occurring force value decreases down to a certain niveau rapidly staying constant afterwards. Such behaviour can be explained by considering the length of the installation leading to the conclusion that correct ballasting and mud balance proves more crucial than the influence of smoother pathing, which is in line with expectations. Furthermore, the peaks in maximal pullback force in Figures 5.11 and 5.13 can be attributed to the inner trigonometrical workings of the model. It can be expected that in these cases the proposed smoothed trajectory introduces unexpected slope angles (most likely in around critical points) leading to changes in the magnitude of the maximal pulling force. Moreover, additional figures visualising the maximal pulling force with different trajectories can be found in Appendix B. Finally the calculated Pearson correlation factor between the smoothing factor and maximal pulling forces occurring in the installations can be seen in Table 5.2. Said correlation factors indicate what was previously observed, an inverse relationship between the smoothing factor and maximal pulling forces, however correlation values were found to be of small magnitude.

Table 5.1: Pearson correlation factor found for smoothing factor and maximal pulling force

Parameter/ Installation	01	04	12
Smoothing factor and maximal pulling force	-0.1537	-0.0501	-0.0509

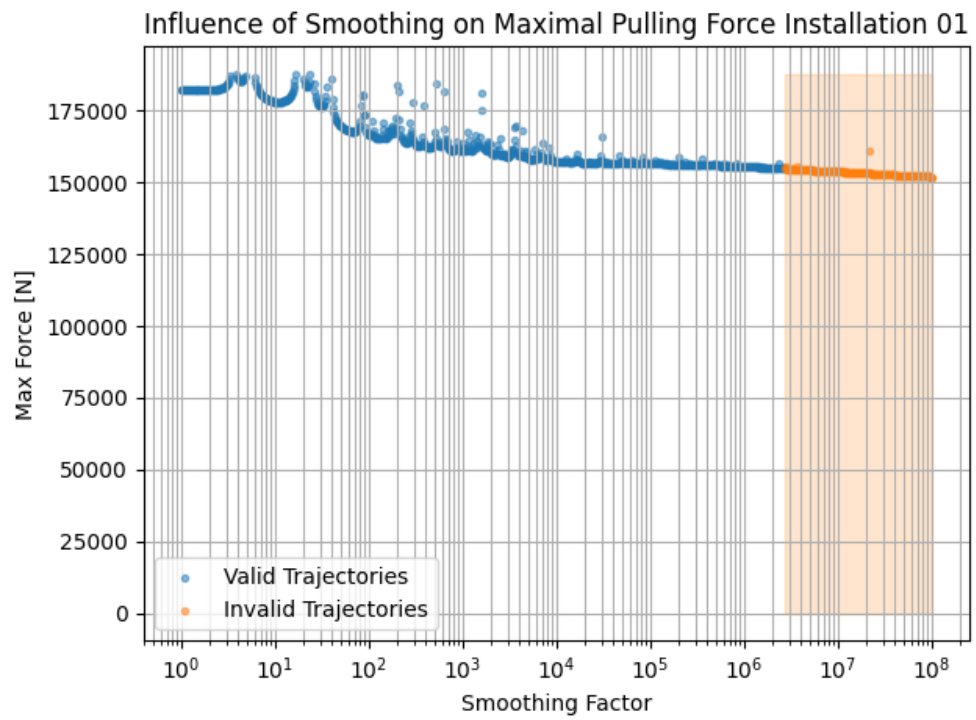


Figure 5.11: Plot showing the relationship between maximal pulling force and trajectory smoothing factor with optimal ballasting and specific gravity of slurry data

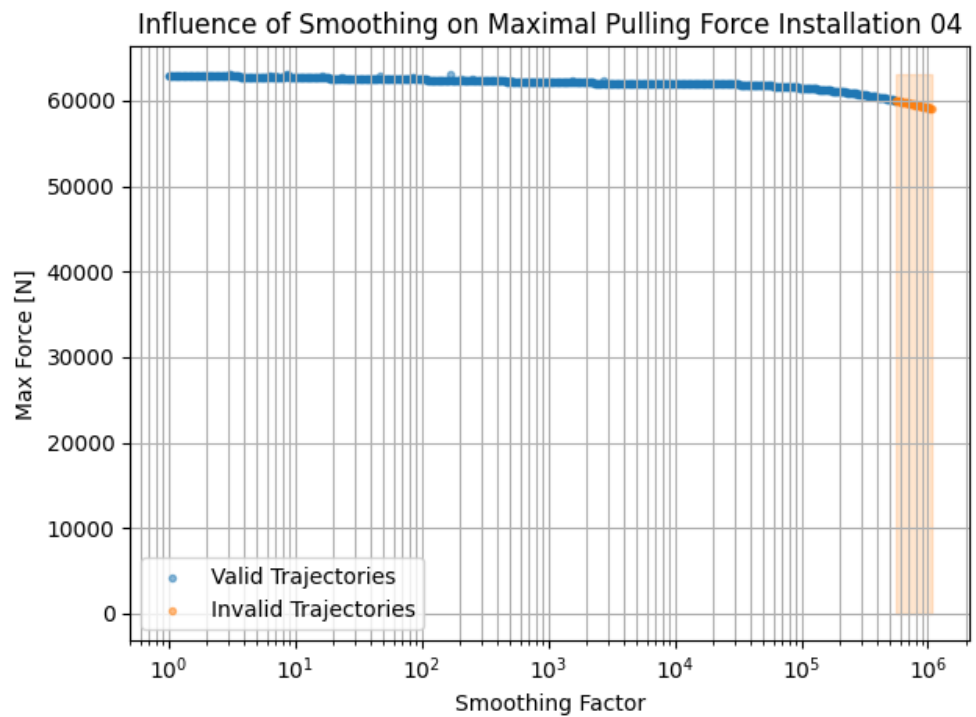


Figure 5.12: Plot showing the relationship between maximal pulling force and trajectory smoothing factor with optimal ballasting and specific gravity of slurry data

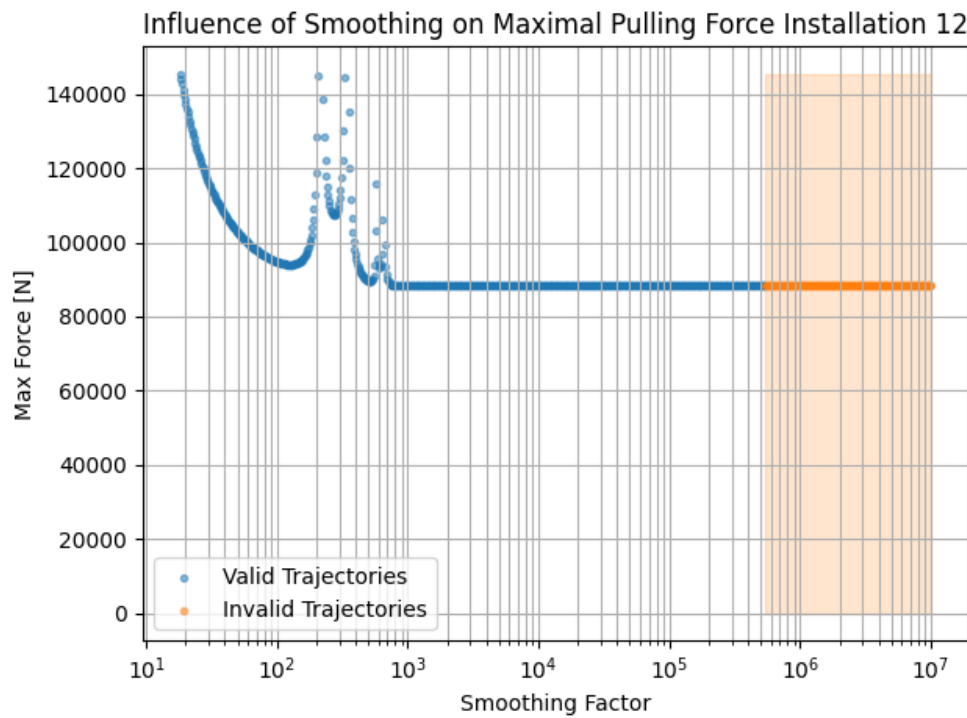


Figure 5.13: Plot showing the relationship between maximal pulling force and trajectory smoothing factor with optimal ballasting and specific gravity of slurry data

### 5.3 INFLUENCE OF BALLAST AND SPECIFIC GRAVITY OF THE SLURRY ON THE PULLING FORCE

Looking at Figures 5.14 through 5.16 a clear relationship can be seen between the specific gravity of the slurry and ballasting of the pipe. In all of the cases areas seen having the lowest magnitudes of maximal pullback forces are ones that also have a relatively low magnitudes of effective vertical forces (due to self unit weight) acting on the product pipe. For example, path marked with dark blue color in Figure 5.14, upon substituting adequate values into Equation 3.26, yields:

Table 5.2: Example unit weight of ballasted product pipe for certain ballast and specific gravity of slurry values for Installation 01

<b>Ballast [-]</b>	0.48	0.55	0.68	0.77	0.88	1.0
<b>Specific gravity of slurry [-]</b>	1.05	1.2	1.3	1.4	1.5	1.6
<b>Ballasted pipe unit weight [kN/m]</b>	0.5	0.49	0.49	0.49	0.49	0.49

In case of installation 01 and 12 a path of optimal values leading to the lowest possible maximal pullback forces can be observed, however in case of installation 04 such path is missing. Aforementioned phenomenon can be explained with the product pipe material in use, while in installations 01 and 12 steel was utilized, in installation 04, HDPE piping was pulled in. Due to the differences in material properties, most importantly self weight, a different approach should have been taken. It would have been beneficial in this case to use a different ballasting fluid instead of water. In this case if the product pipe was filled with drilling mud with a higher unit weight than water, it would have resulted in effective buoyancy being smaller leading to the lowest maximal pullback forces and a visualisation much more similar to the ones for installations 01 and 12. Figures 5.14 through 5.16 were created

by randomly varying ballast and specific gravity of slurry parameters, followed by recalculation of the maximal pullback force occurring. With such a method potentially impractical combinations of said parameters were taken under consideration and plotted, along with the more probable ones. This approach resulted in plots showing clear trends. Furthermore, through calculating the Pearson correlation factors between the specific gravity of the slurry, ballasting and maximal pulling forces (seen in Table 5.3). It was found that, while increase in ballasting tended to decrease the overall maximal pulling forces, increasing the specific gravity of the slurry had an inverse effect, however to a lower extent.

Table 5.3: Pearson correlation factor found for ballasting, specific gravity of the slurry and maximal pulling force

Parameter/ Installation	01	04	12
Ballasting and maximal pulling force	-0.552	-0.7428	-0.1775
Specific gravity of the slurry and maximal pulling force	0.2654	0.6672	0.0586

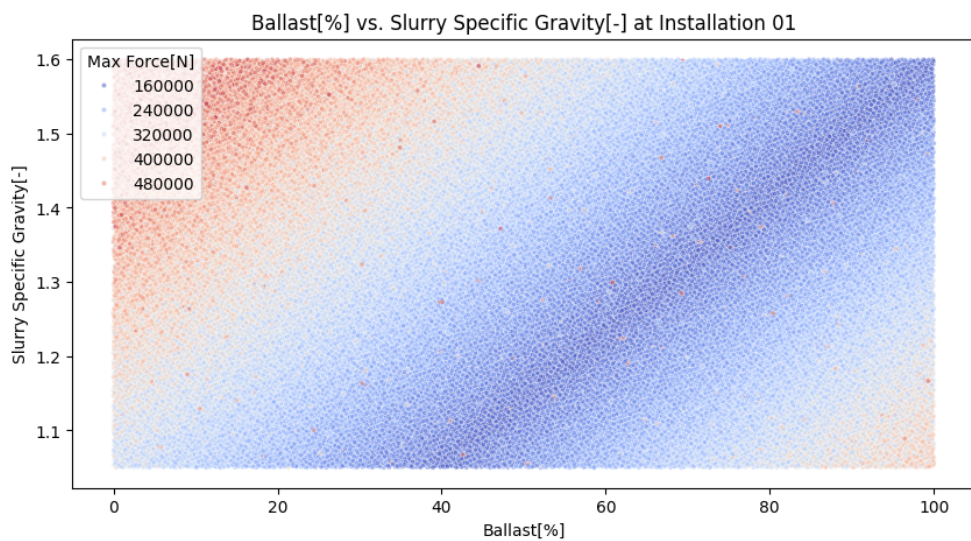


Figure 5.14: Plot showing the relationship between specific gravity of slurry, ballasting and the maximal pulling forces

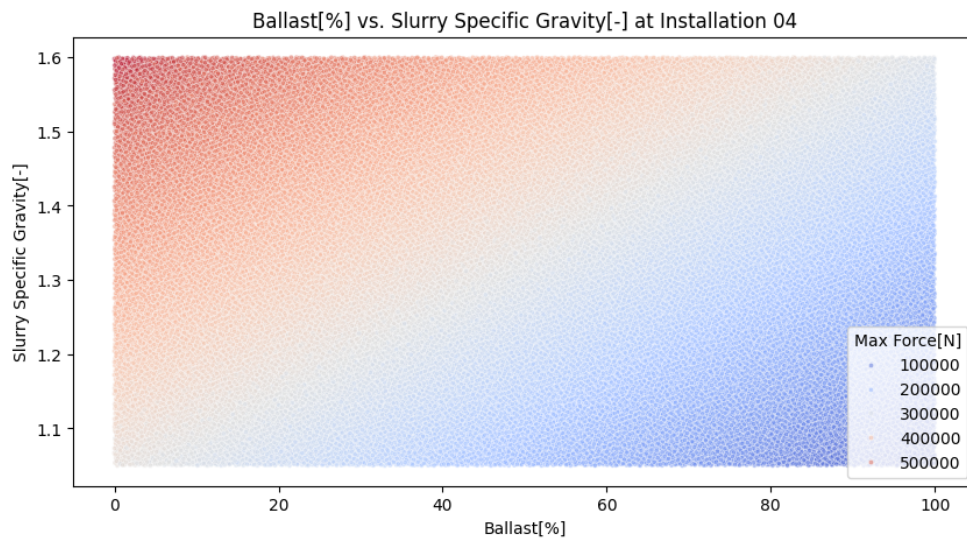


Figure 5.15: Plot showing the relationship between specific gravity of slurry, ballasting and the maximal pulling forces

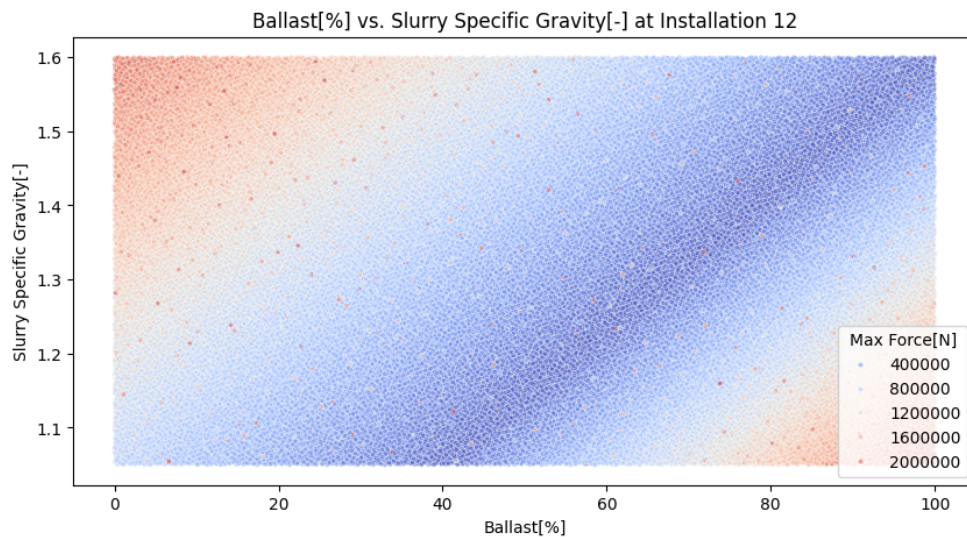


Figure 5.16: Plot showing the relationship between specific gravity of slurry, ballasting and the maximal pulling forces

## 5.4 ADDITIONAL RELATIONSHIPS BETWEEN PARAMETERS

In this section, in Figures 5.17 through 5.19, the relationship between ballast, smoothing factor and the maximal pulling forces can be observed. In Figures 5.20 through 5.22 the relationship between specific gravity of the slurry, smoothing factor and the maximal pulling forces is present. Such an approach was assumed in order to further analyse the impact of varying accuracy of the alignment, while also changing the other parameters taken into account. In the aforementioned figures a trend can be seen only in cases of installation 01 where increasing the smoothing factor actually decreases the pullback force visibly. Considering such a behaviour it can be concluded that, while the impact of the accuracy of borehole alignment can be seen in case of the longest bore, it remains limited in the shorter installations compared to the influence of ballasting and specific gravity of the slurry balance. Figures 5.17 through 5.19 were created by randomly varying the three main parameters un-

der consideration (two at a time for one plot), followed by maximal pullback force calculation.

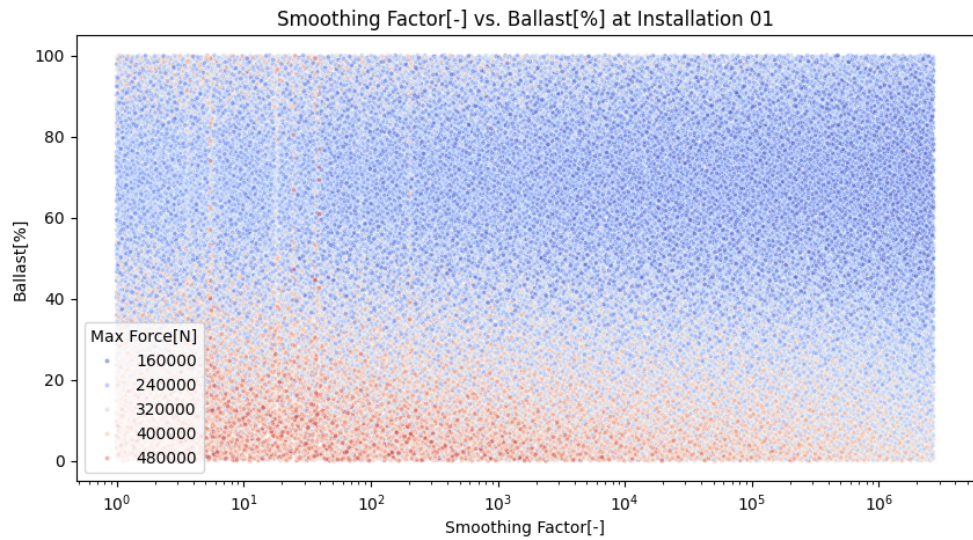


Figure 5.17: Relationship between smoothing factor, ballasting and the maximal pullback force

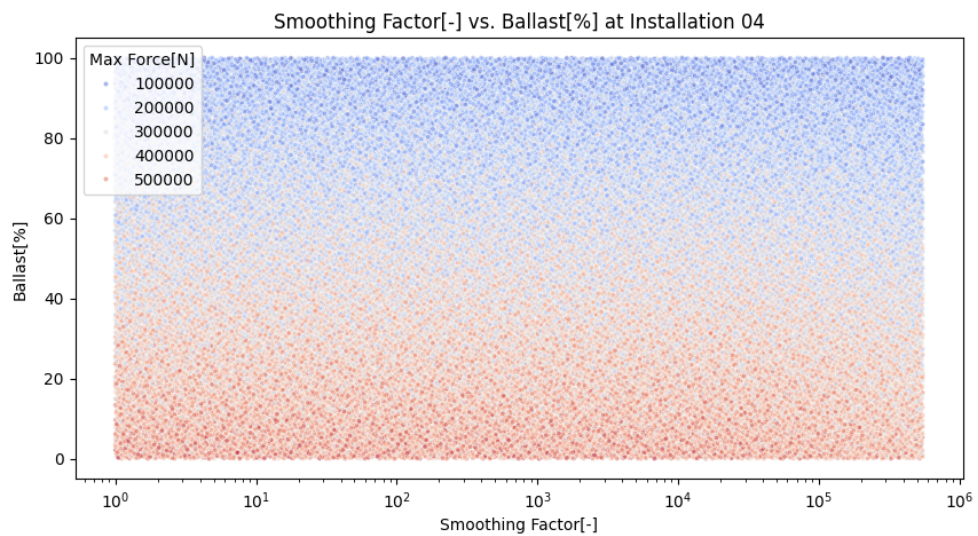


Figure 5.18: Relationship between smoothing factor, ballasting and the maximal pullback force

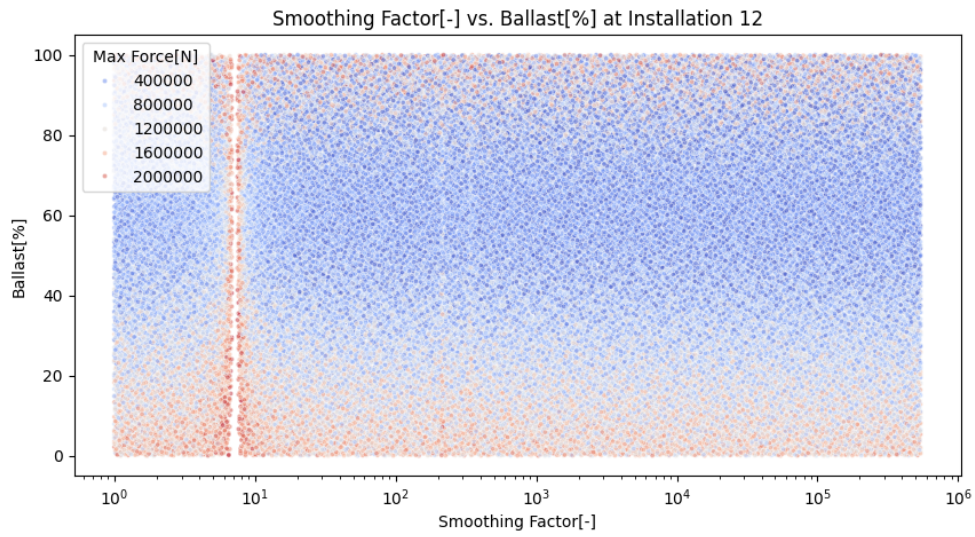


Figure 5.19: Relationship between smoothing factor, ballasting and the maximal pullback force

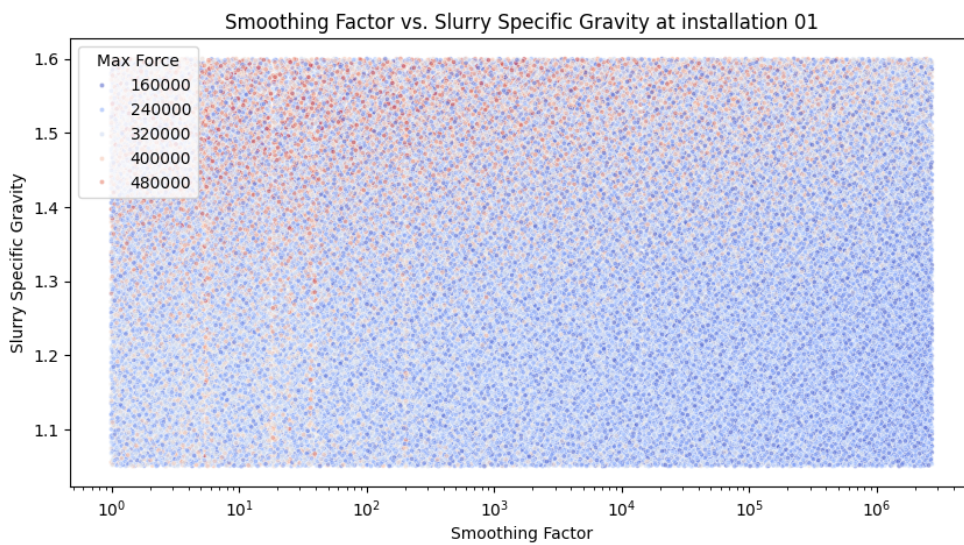
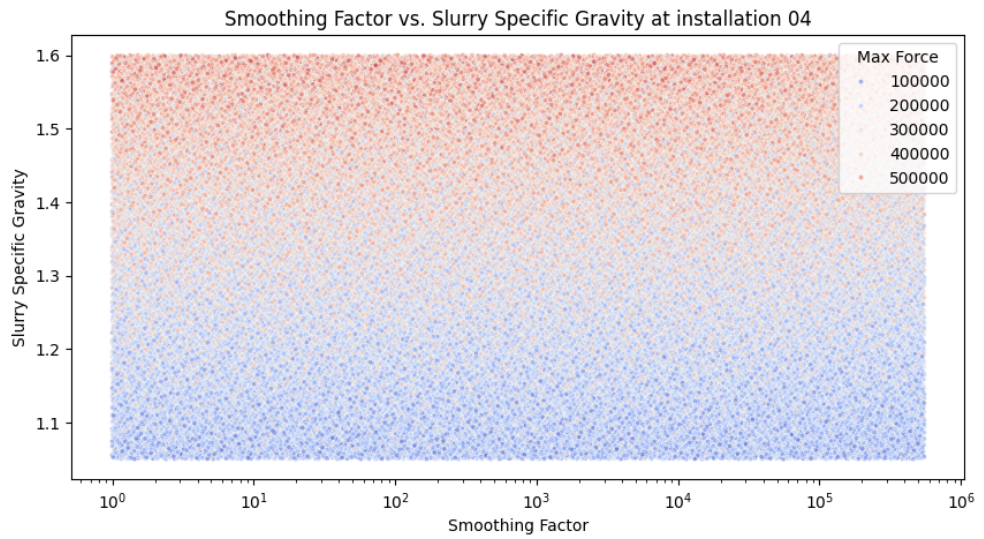
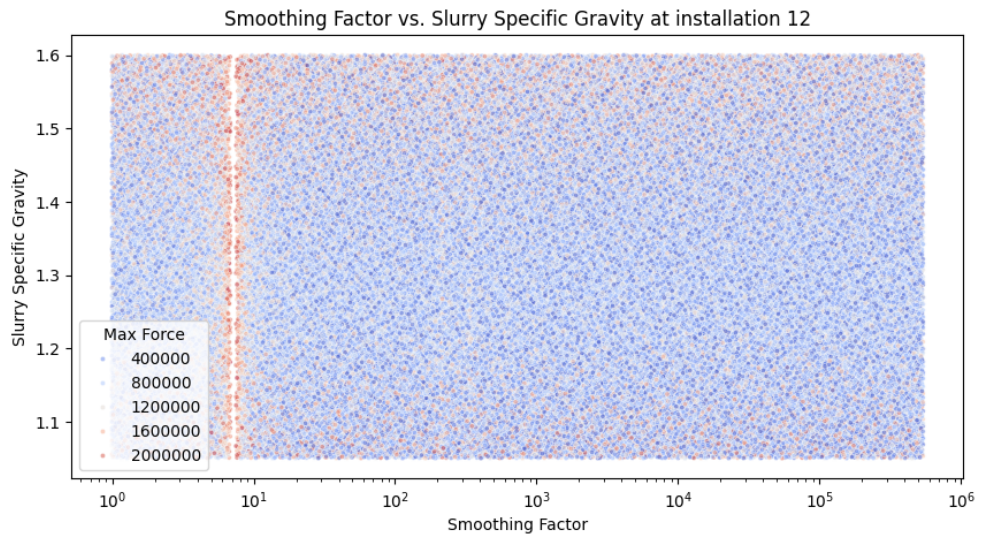


Figure 5.20: Relationship between smoothing factor, slurry specific gravity and the maximal pullback force



**Figure 5.21:** Relationship between smoothing factor, slurry specific gravity and the maximal pullback force



**Figure 5.22:** Relationship between smoothing factor, slurry specific gravity and the maximal pullback force

# 6

## DISCUSSION

In this chapter, discussion on different parts of the research can be seen. Beginning with uncertainties and notes on the data in Section 6.1, through model related concerns in Section 6.2 and limitations to the presented results in Section 6.3, finally to the recommendations for future research in the field 6.4.

### 6.1 DATA AVAILABLE

Firstly, attention should be paid to the data, despite the fact that certain datasets were provided by one organisation, the datasets themselves looked different and more often than not were missing random pieces of information. Regardless of whether the information missing was due to it not being recorded, input correctly or lost in data processing, the general data gathering methodology should be regulated. Out of nine datasets considered for this research, six had to be disregarded due to various discrepancies.

Secondly, in order to develop a more appropriate model for estimating the pullback forces a much larger sample size should be produced, however extracting reliable data in the HDD industry might prove time consuming. Upon accessing a large sample size, a thorough analysis of the magnitude of influence of different parameters on the pullback force can be conducted.

Thirdly, all of the data used in this study was discrete data with irregularly taken sample points leading to higher and lower resolutions along the installations. As it might prove problematic to adjust the data gathering process amongst multiple contractors, an interpolation leading to an equal resampling technique might be beneficial to the overall pullback force estimation process, regardless of the model under consideration.

### 6.2 MODEL EMPLOYED IN THE RESEARCH

Firstly, due to differences between the data available, multiple changes had to be introduced into the original model proposed by Cai [2011]. As the design path and reported (pilot) coordinates were in most cases of insufficient resolution to be applied without utilizing the finite element method present in the original model (not shared). Furthermore, lack of shared validation data, along with the original PipeForce V1 code proved as obstacles in validating and assessing the accuracy of the model proposed in this study.

Secondly, it is worth noting that one of the partial forces being counted into the final pulling force increasing too rapidly to be applied in longer installations can be considered as potentially a crucial shortcoming of the original model. Whether the issue was solved appropriately in this research requires further consideration.

## 6.3 RESULTS

Firstly, it is crucial to point the attention towards the simplification of the complex issue of forces in a bore from a three dimensional problem to two dimensions. Such assumption even with rotating the coordinates in order to minimise the impact of the ignored dimension as it was done in this research, still has most likely influenced the generated outcomes leading to increased discrepancies with the measured data.

Secondly, in multiple plots from Chapter 5 it can be seen that certain portions of data are missing, such a phenomenon might be due to the internal workings of the proposed model, requiring further diagnosing on more data. Moreover, the pulling force decreasing by the end of the installations should not occur and might indicate an issue in calculating the pullback forces in the last section of the installation, as the product pipe is being pulled back up towards the surface.

Thirdly, the proposed method of smoother/ more accurate trajectory generation was not adjusted for the minimal bending radii calculation leading to bore paths, which according to the proposed model can be considered valid, while exceeding physical capabilities and regulation regarding the drill string and product pipe bending.

Fourthly, considering the simplifications and assumptions applied in this research, pullback forces calculated by the model manifest in an expected manner. Furthermore, visual analysis of the influence of trajectory accuracy/ smoothness, ballasting and specific gravity of slurry prove in line with the current knowledge. Upon comparing the proposed model with others mentioned in Chapter 3 it stands out as the only one analysing the influence of chosen parameters based on the measured product pipe placement. Instead of predicting the pullback forces, in this case the model was built to show what differences in the pullback forces would occur upon varying of influential parameters.

Lastly, the calculated correlations between the ballast, specific gravity of the slurry, smoothing factor and the maximal force occurring in the installations might be considered inaccurate due to the fact that Pearson correlation coefficient measures linear relationships between two datasets, however looking at the result plots for all of the mentioned parameters and their relationships with the maximal forces, conclusion can be drawn that there are non-linear relations present. Utilization of probability theory of mutual information (MI) could be recommended to better assess the relationships between the parameters taken into account. The comparison of linear correlation and mutual information theory usage can be seen in Figure 6.1.

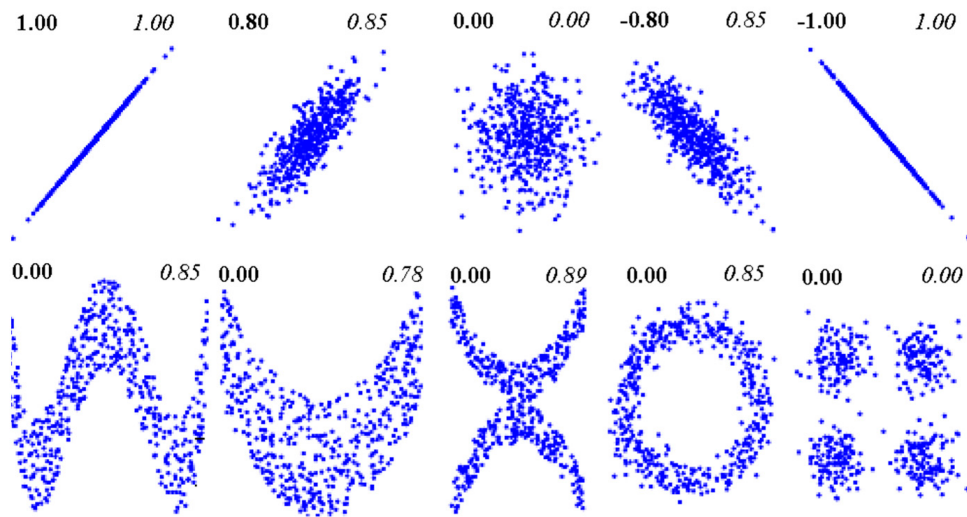


Figure 6.1: Visualisation of linear correlation coefficient and non-linear correlation coefficient obtained from mutual information (Vu [2018])

## 6.4 RECOMMENDATIONS FOR FURTHER RESEARCH

This study was conducted in order to analyse the influence of the accuracy of HDD trajectory amongst other parameters on the pullback forces. To this end initially proposed PipeForce V1 model was changed with accordance to the goal of the study and implemented in Python programming language. While the results thus far can be considered to follow current knowledge in the field of HDD further development is recommended.

As mentioned before, additional attention should be put towards the data gathering and processing stages. Furthermore, turning the model proposed in this research into one that considers all three dimensions should be possible in the future. Adjusting the proposed model (code present in the Appendix A) for the third dimension should prove useful in achieving estimations more similar to the actual ones measured in the field. The model should potentially be expanded to consider the influence posed by factors related to the geological strata being bored, however due to the heterogeneity of the underground domain the reliability of a model adjusted in such a way might come to question, unless site investigation prior to any installations under consideration will be sufficiently thorough. Moreover the model can also be expanded with a higher range of values for the specific gravity of the slurry and ballasting fluid unit weight, leading to better estimations of the most optimal buoyancy combination of the two. Finally, upon accumulating a sufficient amount of installation data, the model can be further refined with the help of machine learning, however such method required as big sample sizes as possible considering the amount of potential parameters differing from between installations.



# 7 | CONCLUSION

Research presented in this paper was aimed to analyse the influence of the accuracy of HDD trajectory and other parameters on the final pullback forces occurring during installations.

The most crucial research questions were:

1. Does the borehole alignment accuracy (smoothness of the bore path) influence the pullback force?
2. Which other soil and pipe parameters influence the pullback force and in what way?

In order to find the answers to those questions data was contributed by Deltares and other anonymous companies in the geotechnical engineering field. At first, information on nine installations were available, out of which only three were suitable for further analysis. Said data was normalized and manipulated in order to be fed into a model proposed in this study. Utilized model was inspired by PipeForce V1, however changes in order to fit the available data and research goals had to be applied. The results shown in this study followed the initial hypothesis that the borehole alignment accuracy has an influence over the pullback force. The alignment accuracy was analysed by creating 1000 paths similar to the original one, yet with varying smoothness and calculating the pullback forces for them. In addition, it was found that ballasting and specific gravity of slurry taken as parameters upon varying also had an influence on the pullback forces. It was found that for smoother trajectories of admissible shape, the maximal pullback force occurring in the installations under consideration had an overall decreasing trend. Moreover, the longer the installation was, the higher the influence of path accuracy was. Additionally, it was found that in cases under consideration, the influence of balancing the ballasting and the specific gravity of slurry parameters was crucial in order to minimise the maximal pullback forces. It was found that regardless of the length of the installation, ballasting and slurry specific gravity remained influential on the outcomes. Furthermore, looking at the Pearson correlation coefficients, ballasting and specific gravity of the slurry have values of higher magnitude than ones related to the accuracy of borehole trajectory. In figures related to ballasting and slurry specific gravity, a clear trend can be seen, that in order to minimise the pullback force, a balance between these parameters needs to result in a small effective vertical force on the product pipe. On top of that, it was also found that the original model which inspired the solution proposed in this research does not accommodate for longer bores through a term increasing in magnitude in quadratic order scaling with the length of the bore.

However, due to the sample size available in this research, the magnitude of influence regarding the parameters under consideration could not be appropriately indicated. Parameter influence over the maximal pullback forces was assessed based on visual inspection of the generated plots along with Pearson correlation factors. Furthermore, the model proposed in this study could not have been compared to its predecessor due to the lack of original PipeForce V1 code and data used to validate it.

In this research it was shown that accuracy of borehole alignment, along with parameters like ballasting and specific gravity of slurry have an influence on the

maximal pullback forces occurring during a HDD installation. This research can be considered as basis for further analysis of influential factors in HDD installations. In the future it is recommended to perform a thorough sensitivity analysis of the model and expand it by acknowledging the third dimension (y-plane) and adding other parameters expected to influence the pullback force.



## A.1 MODEL

```
import numpy as np
import json
import pickle
from copy import deepcopy
import glob as g
from scipy import constants
from scipy.interpolate import make_smoothing_spline
import pandas as pd
import resample
import llp

_DATA_DICT = {}

SMOOTHING_RESOLUTION_M = 0.5
DELTA_COEFFICIENT = 0.05
N_TRAJECTORIES = 10000

class Inst:
    """
    Represents an instance of a model.

    Parameters:
    - json_file (str): The path to the JSON file containing the model data.

    Attributes:
    - json_file (str): The path to the JSON file.
    - Ft (list): The list of Ft values.
    - Fp (list): The list of Fp values.
    - dist (float): The distance value.
    - xd (list): The list of xd values.
    - yd (list): The list of yd values.
    - zd (list): The list of zd values.
    - xr (list): The list of xr values.
    - yr (list): The list of yr values.
    - zr (list): The list of zr values.
    - xm (list): The list of xm values.
    - ym (list): The list of ym values.
    - zm (list): The list of zm values.
    - Q (list): The list of Q values.
    - x_rod (list): The list of x_rod values.
    - y_rod (list): The list of y_rod values.
    - z_rod (list): The list of z_rod values.
    - x_rotated (list): The list of x_rotated values.
    - y_rotated (list): The list of y_rotated values.
    - z_rotated (list): The list of z_rotated values.
    - wp (None or any): The wp value.
    - D_m (None or any): The D_m value.
    - d_m (None or any): The d_m value.
    - E_mod_N_per_m2 (None or any): The E_mod_N_per_m2 value.
    - Db_m (None or any): The Db_m value.
    - YP (None or any): The YP value.
    - PV (None or any): The PV value.
    - Cp (None or any): The Cp value.
    - critical_points (None or any): The critical_points value.
    """
```

```

def __init__(self, json_file):
    with open(json_file, 'r') as f:
        data = json.load(f)
    self.json_file = json_file
    self.Ft = data['Ft']
    self.Fp = data['Fp']
    self.dist = data['dist'][0]
    self.xd = data['xd']
    self.yd = data['yd']
    self.zd = data['zd']
    self.xr = data['xr']
    self.yr = data['yr']
    self.zr = data['zr']
    self.xm = data['xm']
    self.ym = data['ym']
    self.zm = data['zm']
    self.Q = data['Q']

    points = np.column_stack([self.xm, self.ym, self.zm])
    dist = self.dist
    new_points = resample.interpolate(points, dist)
    x_rod = new_points[:, 0]
    y_rod = new_points[:, 1]
    z_rod = new_points[:, 2]
    self.x_rod = x_rod
    self.y_rod = y_rod
    self.z_rod = z_rod

    xys = np.column_stack([x_rod, y_rod, z_rod])
    rotated_xys = llp.norm_rot_3d_to_2d_array(xys)
    self.x_rotated = rotated_xys[:, 0]
    self.y_rotated = rotated_xys[:, 1]
    self.z_rotated = rotated_xys[:, 2]

    self.wp = None
    self.D_m = None
    self.d_m = None
    self.E_mod_N_per_m2 = None
    self.Db_m = None
    self.YP = None
    self.PV = None
    self.Cp = None
    self.critical_points = None

    self.smoothed = False
    self.smoothing_factor = None
    self.valid = True

def __repr__(self):
    res = f'Ft: {len(self.Ft)}, '
    res += f'Fp: {len(self.Fp)}, '
    res += f'dist: {self.dist}, '
    res += f'xm: {len(self.xm)}, '
    res += f'ym: {len(self.ym)}, '
    res += f'zm: {len(self.zm)}, '
    res += f'x_rod: {len(self.x_rod)}, '
    res += f'y_rod: {len(self.y_rod)}, '
    res += f'z_rod: {len(self.z_rod)}, '
    res += f'Q: {len(self.Q)}, '
    res += f'wp: {self.wp:.2f}, '
    res += f'critical: {self.critical_points}'
    return res

def create_data_dict():
    """
    Create a dictionary of data from JSON files and auxiliary CSV file.

    Returns:
        data_dict (dict): A dictionary containing data extracted from JSON files.
    """

```

```

if len(_DATA_DICT) > 0:
    return _DATA_DICT

datafiles = g.glob('*.json')
data_dict = {f.split('_')[1].split('.')[0]: Inst(f) for f in datafiles}
keys = sorted(data_dict.keys())
data_dict

aux_df = pd.read_csv('aux.csv', index_col=0).sort_index()
aux_df.columns = aux_df.columns.str.strip()
aux_df['D_m'] = aux_df.D_mm / 1000
aux_df['t_m'] = aux_df.t_mm / 1000
aux_df['d_m'] = aux_df.D_m - 2 * aux_df.t_m
aux_df['wp_N_per_m'] = aux_df.pipe_rho_kN_per_m3 * 1000 * \
    (constants.pi / 4) * (aux_df.D_m**2 - aux_df.d_m**2)
aux_df['Db_m'] = aux_df.D_m * 1.5

for tag in keys:
    data_dict[tag].D_m = aux_df.loc[tag, 'D_m']
    data_dict[tag].d_m = aux_df.loc[tag, 'd_m']
    data_dict[tag].E_mod_N_per_m2 = aux_df.loc[tag,
        'E_mod_N_per_mm2'] * 1e6
    data_dict[tag].Db_m = aux_df.loc[tag, 'Db_m']
    data_dict[tag].YP = aux_df.loc[tag, 'YP']
    data_dict[tag].PV = aux_df.loc[tag, 'PV'] / 1000
    data_dict[tag].Cp = aux_df.loc[tag, 'Cp']
    inst = data_dict[tag]
    inst.wp = aux_df.loc[tag, 'wp_N_per_m']

data_dict['01'].critical_points = [[175.0, -25.7], [1225.0, -24.7]]
data_dict['04'].critical_points = [[110, -19.7], [410, -19.4]]
data_dict['12'].critical_points = [[120, -9.8]]
data_dict['17'].critical_points = [[37.5, -7], [147.5, -7]]
data_dict['20'].critical_points = [[140, -25.5], [640, -24.9]]
data_dict['G1'].critical_points = [[95, -14.7]]
data_dict['G2'].critical_points = [[100, -13.95]]
data_dict['K1'].critical_points = [[72, -8.7]]
data_dict['L1'].critical_points = [[67, -4.82]]

_DATA_DICT.update(data_dict)

return data_dict

class TrajectoryValidator:
    def __init__(self, critical_points, delta_coefficient=0.05):
        self.critical_points = critical_points
        self.delta_coefficient = delta_coefficient

    def check_trajectory_intersects_box(self, x: np.array, y: np.array, point):
        """
        Check if a trajectory intersects a box defined by a given point and delta
        coefficients.

        Parameters:
        - x (np.array): The x-coordinates of the trajectory.
        - y (np.array): The y-coordinates of the trajectory.
        - point (tuple): The center point of the box.

        Returns:
        - bool: True if the trajectory intersects the box, False otherwise.
        """
        total_x = x[-1] - x[0]
        total_y = y.max() - y.min()
        delta_x = total_x * self.delta_coefficient / 2
        delta_y = total_y * self.delta_coefficient / 2

        x_min = point[0] - delta_x
        x_max = point[0] + delta_x
        y_min = point[1] - delta_y

```

```

        y_max = point[1] + delta_y

        x_in_ival = (x_min <= x) & (x <= x_max)
        y_in_ival = (y_min <= y) & (y <= y_max)
        return np.any(x_in_ival & y_in_ival)

def __call__(self, x: np.array, y: np.array):
    """
    Validate a trajectory based on the given x and y coordinates.

    Parameters:
    x (np.array): Array of x-coordinates.
    y (np.array): Array of y-coordinates.

    Returns:
    bool: True if the trajectory is valid, False otherwise.
    """
    intersections = []
    for point in self.critical_points:
        intersections.append(
            self.check_trajectory_intersects_box(x, y, point))
    return all(intersections)

def _make_smooth_trajectory(inst: Inst, smoothing_factor, output_resolution_m=
                            SMOOTHING_RESOLUTION_M):
    """
    Create a smooth trajectory from the given instance.

    Parameters:
    - inst (Inst): The instance to create the trajectory from.
    - smoothing_factor (float): The smoothing factor to use.
    - output_resolution_m (float): The output resolution in meters.

    Returns:
    - tuple: A tuple containing the x and z coordinates of the smooth trajectory.
    """
    x_smooth = np.arange(
        inst.x_rotated[0], inst.x_rotated[-1], output_resolution_m)

    weights = np.ones_like(inst.x_rotated)
    weights[0] = 1e10
    weights[-1] = 1e10

    spline = make_smoothing_spline(
        inst.x_rotated, inst.z_rotated, lam=smoothing_factor, w=weights)
    z_smooth = spline(x_smooth)
    return x_smooth, z_smooth

def bisect(lam0, lam1, inst, validator):
    """
    Perform bisection method to find a root within the given interval.

    Args:
    lam0 (float): The lower bound of the interval.
    lam1 (float): The upper bound of the interval.
    inst: The instance of the class.
    validator (function): A function that validates the trajectory.

    Returns:
    tuple: A tuple containing the lower and upper bounds of the interval
    that encloses the root.

    Raises:
    Exception: If both trajectories are invalid.
    """
    x0, z0 = _make_smooth_trajectory(inst, lam0, SMOOTHING_RESOLUTION_M)
    x1, z1 = _make_smooth_trajectory(inst, lam1, SMOOTHING_RESOLUTION_M)

```

```

tv0 = validator(x0, z0)
tv1 = validator(x1, z1)

if tv0 and tv1:
    return lam0, lam1

if not tv0 and not tv1:
    raise Exception("Both trajectories are invalid")

if tv0:
    return lam0, (lam0 + lam1) / 2

if tv1:
    return (lam0 + lam1) / 2, lam1

def find_lambda(inst: Inst, iterations=64, delta_coefficient=DELTA_COEFFICIENT):
    """
    Find the optimal smoothing factor for the given instance.

    Parameters:
    - inst (Inst): The instance to find the optimal smoothing factor for.
    - iterations (int): The number of iterations to perform.

    Returns:
    - float: The optimal smoothing factor.
    """
    validator = TrajectoryValidator(
        inst.critical_points, delta_coefficient=delta_coefficient)
    lam0 = 0
    lam1 = 1e10

    for _ in range(iterations):
        lam0, lam1 = bisect(lam0, lam1, inst, validator)

    lam = max(lam0, lam1)
    return lam

def smooth_inst(inst: Inst, smoothing_factor, smoothing_resolution_m) -> Inst:
    """
    Smooth the trajectory of the given installation.

    Parameters:
    - inst (Inst): The instance to smooth.
    - smoothing_factor (float): The smoothing factor to use.
    - smoothing_resolution_m (float): The resolution to use for smoothing.

    Returns:
    - Inst: The smoothed instance.
    """
    _inst_copy = deepcopy(inst)
    x, z = _make_smooth_trajectory(
        inst, smoothing_factor, smoothing_resolution_m)

    points = np.column_stack([x, np.zeros_like(x), z])
    dist = inst.dist
    new_points = resample.interpolate(points, dist)
    x_rotated = new_points[:, 0]
    y_rotated = new_points[:, 1]
    z_rotated = new_points[:, 2]

    _inst_copy.x_rotated = x_rotated
    _inst_copy.y_rotated = y_rotated
    _inst_copy.z_rotated = z_rotated
    _inst_copy.smoothed = True
    _inst_copy.smoothing_factor = smoothing_factor

    _inst_copy.Q = inst.Q[:len(x_rotated)]

    return _inst_copy

```

```

def produce_series(inst: Inst, base_path, n_trajectories=N_TRAJECTORIES, delta_coefficient
                  =DELTA_COEFFICIENT, smoothing_resolution_m=
                  SMOOTHING_RESOLUTION_M):
    """
    Produce a series of smoothed trajectories for the given instance.

    Parameters:
    - inst (Inst): The instance to produce the series for.
    - base_path (str): The base path to save the series.
    - n_trajectories (int): The number of trajectories to produce.

    Returns:
    - list: A list of smoothed instances.
    """
    max_smoothing_factor = find_lambda(inst)
    max_log_smoothing_factor = np.ceil(np.log10(max_smoothing_factor)) + 1

    inst_list = []

    smoothing_factors = np.logspace(
        0, max_log_smoothing_factor, n_trajectories)
    validator = TrajectoryValidator(
        inst.critical_points, delta_coefficient=delta_coefficient)
    for i, smoothing_factor in enumerate(smoothing_factors):
        smoothed_inst = smooth_inst(
            inst, smoothing_factor, smoothing_resolution_m)
        if validator(smoothed_inst.x_rotated, smoothed_inst.z_rotated):
            smoothed_inst.valid = True
        else:
            smoothed_inst.valid = False
        inst_list.append(smoothed_inst)

    return inst_list

def produce_series_parallel(params):
    """
    Produce a series of smoothed trajectories in parallel.

    Parameters:
    - params (tuple): A tuple containing the instance, the base path, the number of
                     trajectories, and the delta coefficient.

    Returns:
    - list: A list of smoothed instances.
    """
    return produce_series(**params)

def _delta_l(i, inst: Inst):
    """
    Calculate the change in length (delta L) for a given index i and instance inst.

    Parameters:
    i (int): The index of the element.
    inst (Inst): An instance of the Inst class.

    Returns:
    float: The change in length (delta L) for the given index i and instance inst.
    """
    count = len(inst.x_rotated) - 1
    L = count * inst.dist
    return L - (i+1) * inst.dist

def Tgi(i, inst: Inst):
    """
    Calculate the Tgi value for a given index and installation.

```

```

Parameters:
i (int): The index value.
inst (Inst): The installation object.

Returns:
float: The Tgi value.

"""
mu_g = 0.1
return inst.wp * mu_g * _delta_l(i, inst)

def Tsi(i, inst: Inst):
    """
    Calculate the Tsi value for a given index and instance.

    Parameters:
    i (int): The index value.
    inst (Inst): The instance object.

    Returns:
    float: The calculated Tsi value.
    """
    Fp0_N = 1000*inst.Fp[0]
    I = len(inst.x_rotated)
    Tg0 = Tgi(0, inst)
    return (Fp0_N - Tg0) * (I-i)/I

def _w(inst: Inst, ballast: float, spec_slur: float, water_density_kg_per_m3=1000) ->
    float:
    """
    Calculate the weight of the slurry in the pipe.

    Parameters:
    - inst: An instance of the Inst class.
    - ballast: The water content in the pipe, ranging from 0 to 1 (1 being 100%).
    - spec_slur: The specific density of the slurry relative to water.
    - water_density_kg_per_m3: The assumed density of water in kg/m^3. Default is 1000.

    Returns:
    - The weight of the slurry in the pipe.

    """
    wp = inst.wp
    assert (ballast >= 0) & (ballast <= 1)
    assert spec_slur >= 0
    fw = (constants.pi / 4) * inst.D_m**2 * \
        water_density_kg_per_m3 * spec_slur * constants.g
    fb = (constants.pi / 4) * inst.d_m**2 * \
        water_density_kg_per_m3 * ballast * constants.g
    return wp - fw + fb

def _cos_beta_s_h_k(k, inst: Inst):
    """
    Calculate the cosine of beta_s_h_k.

    Parameters:
    k (int): The index of the current point.
    inst (Inst): An instance of the Inst class.

    Returns:
    float: The cosine of beta_s_h_k.

    """
    x = inst.x_rotated[k+1] - inst.x_rotated[k]
    y = inst.y_rotated[k+1] - inst.y_rotated[k]
    z = inst.z_rotated[k+1] - inst.z_rotated[k]
    result = (x**2+y**2)**0.5 / (x**2+y**2+z**2)**0.5
    return result

```

```

def _sin_beta_s_h_k(k, inst: Inst):
    """
    Calculate the sine of beta for a given index k and instance inst.

    Parameters:
    k (int): The index value.
    inst (Inst): The instance object containing rotated coordinates.

    Returns:
    float: The sine of beta.
    """
    x = inst.x_rotated[k+1] - inst.x_rotated[k]
    y = inst.y_rotated[k+1] - inst.y_rotated[k]
    z = inst.z_rotated[k+1] - inst.z_rotated[k]
    result = z / (x**2+y**2+z**2)**0.5
    return result

def Tbi(i: int, ballast: float, spec_slur: float, inst: Inst, K_c_k=0.5,
        water_density_kg_per_m3=1000):
    """
    Calculate the Tbi value based on the given parameters.

    Parameters:
    i (int): The value of i.
    ballast (float): The ballast value.
    spec_slur (float): The spec_slur value.
    inst (Inst): An instance of the Inst class.
    K_c_k (float, optional): The value of K_c_k. Defaults to 0.5.
    water_density_kg_per_m3 (float, optional): The water density in kg/m^3. Defaults to
        1000.

    Returns:
    float: The calculated Tbi value.
    """
    w = _w(inst, ballast, spec_slur, water_density_kg_per_m3)
    dist_sums = [inst.dist * k for k in range(0, i-1)]

    result = sum(dist_sums[k] * (abs(K_c_k * w * 0.24 * _cos_beta_s_h_k(k, inst)) + w *
        _sin_beta_s_h_k(k, inst))
        for k in range(0, i-1))
    return result

def Tbi_longer_installations(i: int, ballast: float, spec_slur: float, inst: Inst, K_c_k=0
        .5, water_density_kg_per_m3=1000):
    """
    Calculate the Tbi value based on the given parameters.

    Parameters:
    i (int): The value of i.
    ballast (float): The ballast value.
    spec_slur (float): The spec_slur value.
    inst (Inst): An instance of the Inst class.
    K_c_k (float, optional): The value of K_c_k. Defaults to 0.5.
    water_density_kg_per_m3 (float, optional): The water density in kg/m^3. Defaults to
        1000.

    Returns:
    float: The calculated Tbi value.
    """
    w = _w(inst, ballast, spec_slur, water_density_kg_per_m3)
    dist_sums = [inst.dist for k in range(0, i-1)]

    result = sum(dist_sums[k] * (abs(K_c_k * w * 0.24 * _cos_beta_s_h_k(k, inst)) + w *
        _sin_beta_s_h_k(k, inst))

```

```

        for k in range(0, i-1)
    return result

def _F2(i: int, inst: Inst) -> float:
    """
    Calculate the deflection forces for one beam.

    Parameters:
    i (int): The index of the beam.
    inst (Inst): An instance of the Inst class containing the necessary data.

    Returns:
    float: The deflection forces for the specified beam.
    """
    xs = inst.x_rotated
    ys = inst.y_rotated
    zs = inst.z_rotated

    assert i > 0, "We're omitting the first rod"
    assert i < len(xs) - 3, "We're omitting the last rod"

    a = np.array([xs[i-1], ys[i-1], zs[i-1]])
    b = np.array([xs[i], ys[i], zs[i]])
    c = np.array([xs[i+1], ys[i+1], zs[i+1]])
    d = np.array([xs[i+2], ys[i+2], zs[i+2]])

    s1, s2 = llp.get_slopes(a, b, c, d)

    E = inst.E_mod_N_per_m2
    I = np.pi/64 * (inst.D_m**4 - inst.d_m**4)

    P = llp.deflection_forces(inst.dist, s1, s2, E, I)

    return P

def F2(i: int, inst: Inst, K_ci=0.5) -> float:
    """
    Calculate the total friction force exerted on an object at index i.

    Parameters:
    i (int): The index of the object.
    inst (Inst): An instance of the Inst class.
    K_ci (float, optional): A coefficient value. Default is 0.5.

    Returns:
    float: The total force exerted on the object.
    """
    mu_bi = 0.24
    if i == 0:
        return 0
    i = min(i, len(inst.x_rotated) - 3)
    forces = [abs(_F2(j, inst=inst)) for j in range(1, i)]
    # we can potentially change the K_ci value
    return sum(forces) * K_ci * mu_bi

def _Q_m3_per_s(inst):
    """
    Convert the flow rate from liters per minute to cubic meters per second.

    Parameters:
    inst (object): An instance of the class containing the attributes 'x_rotated' and
    'Q'.

    Returns:
    numpy.ndarray: An array of flow rates converted to cubic meters per second.
    """
    assert len(inst.x_rotated) == len(inst.Q)

```

```

        return np.array(inst.Q) / 1000 / 60

def _va(inst: Inst):
    """
    Calculate the value of _va.

    Parameters:
    inst (Inst): An instance of the Inst class.

    Returns:
    float: The calculated value of _va.
    """
    num = 1.272 * _Q_m3_per_s(inst)
    denom = inst.Db_m ** 2 - inst.D_m ** 2
    return num / denom

def _dp_dz(inst: Inst):
    """
    Calculate the derivative of pressure with respect to depth.

    Parameters:
    inst (Inst): An instance of the Inst class.

    Returns:
    float: The derivative of pressure with respect to depth.
    """
    term1 = 47.82 * (inst.PV * _va(inst)) / ((inst.Db_m - inst.D_m) ** 2)
    term2 = 6 * inst.YP / (inst.Db_m - inst.D_m)
    return term1 + term2

def _P1(i: int, inst: Inst):
    """
    Calculate the value of P1 based on the given index and instance.

    Parameters:
    i (int): The index used to calculate the segments.
    inst (Inst): The instance containing the necessary data.

    Returns:
    float: The calculated value of P1.
    """
    segments = _dp_dz(inst)[i] * inst.dist
    return inst.Cp * sum(segments)

def Tdi(i: int, inst: Inst):
    """
    Calculate the total segments for Tdi.

    Parameters:
    i (int): The value of i.
    inst (Inst): An instance of the Inst class.

    Returns:
    float: The total segments for Tdi.
    """
    segments_tot = _P1(i, inst) * (0.465 * 1/2 * np.pi *
                                   (inst.Db_m - inst.D_m)**2 + np.pi/4 * inst.D_m**2)
    # segments_tot = inst.YP * inst.D_m / \
    #     (inst.D_m + inst.Db_m) * i * inst.dist + sum(inst.PV * _va(inst)[i])
    return segments_tot

def F1_vec(inst: Inst, ballast: float, spec_slur: float, K_c_k=0.5, K_ci=0.5) -> np.array:
    """
    Calculate the force vector F1.

    Args:
    """

```

```

    inst (Inst): The instance object.
    ballast (float): The ballast value.
    spec_slur (float): The specific slurry value.
    K_c_k (float, optional): The K_c_k value. Defaults to 0.5.
    K_ci (float, optional): The K_ci value. Defaults to 0.5.

Returns:
    np.array: The force vector F1.
"""

force_vec = [
    Tgi(_i, inst) + Tsi(_i, inst) + Tbi(_i, ballast=ballast, spec_slur=spec_slur,
        inst=inst, K_c_k=K_c_k) + Tdi(_i, inst) + F2(_i, inst=inst, K_ci=K_ci)
    for _i in range(len(inst.x_rotated))
]

force_cumsum = np.cumsum(force_vec)

gamma_s_si = np.zeros_like(force_cumsum)
for i in range(1, len(inst.x_rotated) - 1):
    point_i0 = inst.x_rotated[i-1], inst.z_rotated[i-1]
    point_i1 = inst.x_rotated[i], inst.z_rotated[i]
    point_i2 = inst.x_rotated[i+1], inst.z_rotated[i+1]

    # assuming all angles are close to zero
    v1 = np.array(point_i1) - np.array(point_i0)
    v2 = np.array(point_i2) - np.array(point_i1)
    angle_r = np.arccos(
        np.dot(v1, v2) / (np.linalg.norm(v1) * np.linalg.norm(v2)))
    gamma_s_si[i] = angle_r

result = np.cumsum(force_vec * (np.exp(0.24 * 0.5 * gamma_s_si) - 1))
return result

def pulling_forces_short(inst: Inst, ballast: float, spec_slur: float):
    """
    Calculate the pulling forces.

    Parameters:
    inst (Inst): The instance object.
    ballast (float): The ballast value.
    spec_slur (float): The specific slurry value.

    Returns:
    np.array: The pulling forces.
    """
    K_c_k = 0.5
    K_ci = 0.5

    Tgi_vec = np.array([Tgi(_i, inst) for _i in range(len(inst.x_rotated))])
    Tsi_vec = np.array([Tsi(_i, inst) for _i in range(len(inst.x_rotated))])
    Tbi_vec = np.array([Tbi(_i, ballast=ballast, spec_slur=spec_slur,
        inst=inst, K_c_k=K_c_k) for _i in range(len(inst.x_rotated))])
    Tdi_vec = np.array([Tdi(_i, inst) for _i in range(len(inst.x_rotated))])
    F2_vec = np.array([F2(_i, inst=inst, K_ci=K_ci)
        for _i in range(len(inst.x_rotated))])

    force_vec = Tgi_vec + Tsi_vec + Tbi_vec + Tdi_vec + F2_vec
    f1_vec = F1_vec(inst, ballast, spec_slur, K_c_k, K_ci)
    pulling_force = force_vec + f1_vec

    result = {
        'Tgi': Tgi_vec,
        'Tsi': Tsi_vec,
        'Tbi': Tbi_vec,
        'Tdi': Tdi_vec,
        'F2': F2_vec,
        'F1': f1_vec,
        'pulling_force': pulling_force
    }
}

```

```

    return result

def pulling_forces_long(inst: Inst, ballast: float, spec_slur: float):
    """
    Calculate the pulling forces.

    Parameters:
    inst (Inst): The instance object.
    ballast (float): The ballast value.
    spec_slur (float): The specific slurry value.

    Returns:
    np.array: The pulling forces.
    """
    K_c_k = 0.5
    K_ci = 0.5

    Tgi_vec = np.array([Tgi(_i, inst) for _i in range(len(inst.x_rotated))])
    Tsi_vec = np.array([Tsi(_i, inst) for _i in range(len(inst.x_rotated))])
    Tbi_vec = np.array([Tbi_longer_installations(_i, ballast=ballast, spec_slur=spec_slur,
                                                inst=inst, K_c_k=K_c_k) for _i in range(len(inst.x_rotated))])
    Tdi_vec = np.array([Tdi(_i, inst) for _i in range(len(inst.x_rotated))])
    F2_vec = np.array([F2(_i, inst=inst, K_ci=K_ci)
                       for _i in range(len(inst.x_rotated))])

    force_vec = Tgi_vec + Tsi_vec + Tbi_vec + Tdi_vec + F2_vec
    f1_vec = F1_vec(inst, ballast, spec_slur, K_c_k, K_ci)
    pulling_force = force_vec + f1_vec

    result = {
        'Tgi': Tgi_vec,
        'Tsi': Tsi_vec,
        'Tbi': Tbi_vec,
        'Tdi': Tdi_vec,
        'F2': F2_vec,
        'F1': f1_vec,
        'pulling_force': pulling_force
    }

    return result

def pulling_forces(inst: Inst, ballast: float, spec_slur: float):
    """
    Calculates the pulling forces based on the given parameters.

    Parameters:
    - inst (Inst): The instance of the Inst class.
    - ballast (float): The ballast value.
    - spec_slur (float): The specific slur value.

    Returns:
    - The pulling forces calculated based on the given parameters.
    """
    magic_number = 400
    if inst.x_rotated.max() < magic_number:
        return pulling_forces_short(inst, ballast, spec_slur)
    else:
        return pulling_forces_long(inst, ballast, spec_slur)

def max_pulling_force(inst: Inst, ballast: float, spec_slur: float):
    return pulling_forces(inst, ballast, spec_slur)['pulling_force'].max()

```

## A.2 BEAM CALCULATION

```

import numpy as np

def deflection_leq0(x, L, s1, s2, E, I):
    """
    Calculates the deflection of a beam with a linearly varying distributed load
    when the position x is less than or equal to the point of zero deflection.

    Parameters:
    x (float): The position along the beam.
    L (float): The length of the beam.
    s1 (float): The value of the slope at the left end of the beam.
    s2 (float): The value of the slope at the right end of the beam.
    E (float): The modulus of elasticity of the beam material.
    I (float): The moment of inertia of the beam cross-section.

    Returns:
    float: The deflection of the beam at the given position x.

    """
    def _l(L, s1, s2):
        return (-L * s1 - 2 * L * s2) / (s1 - s2)

    def _f(L, s1, s2, E, I):
        return 6 * E * I * L * s2 * (s1 - s2) / ((pow(L, 2) - pow(-L * s1 - 2 * L * s2, 2) / pow(s1 - s2, 2)) *
        (-L * s1 - 2 * L * s2))

    l = _l(L, s1, s2)
    F = _f(L, s1, s2, E, I)

    if x <= l:
        return -1.0 / 6.0 * F * x * (L - l) * (pow(L, 2) - pow(x, 2) - pow(L - l, 2)) / (E * I * L)
    else:
        new_l = L - l
        new_x = L - x
        return -1.0 / 6.0 * F * new_x * (L - new_l) * (pow(L, 2) - pow(new_x, 2) - pow(L - new_l, 2)) / (E * I * L)

def deflection_forces(L, s1, s2, E, I):
    """
    Calculates the deflection forces for a beam.

    Parameters:
    L (float): Length of the beam.
    s1 (float): The value of the slope at the left end of the beam.
    s2 (float): The value of the slope at the right end of the beam.
    E (float): Young's modulus of the material.
    I (float): Moment of inertia of the beam.

    Returns:
    float: The deflection forces.

    """
    def _f(L, s1, s2, E, I):
        return 6 * E * I * L * s2 * (s1 - s2) / ((pow(L, 2) - pow(-L * s1 - 2 * L * s2, 2) / pow(s1 - s2, 2)) *
        (-L * s1 - 2 * L * s2))

    F = _f(L, s1, s2, E, I)
    return F

def norm_3d_to_2d(a3d, b3d, c3d):
    """
    Converts three 3D points to their corresponding 2D points in a normalized coordinate
    system.

    Parameters:
    a3d (numpy.ndarray): The coordinates of point A in 3D space.
    b3d (numpy.ndarray): The coordinates of point B in 3D space.

```

```

    c3d (numpy.ndarray): The coordinates of point C in 3D space.

Returns:
tuple: A tuple containing the 2D coordinates of point A, point B, and point C,
       respectively.
"""
"""
Converts three 3D points to their corresponding 2D points in a normalized coordinate
system.

Parameters:
a3d (numpy.ndarray): The coordinates of point A in 3D space.
b3d (numpy.ndarray): The coordinates of point B in 3D space.
c3d (numpy.ndarray): The coordinates of point C in 3D space.

Returns:
tuple: A tuple containing the 2D coordinates of point A, point B, and point C,
       respectively.
"""

a = a3d
b = b3d
c = c3d

cT = c - a
bT = b - a
aT = a - a

x, y = cT[0], cT[1]
angle = np.arctan2(y, x)
rot_matrix = np.array([[np.cos(angle), -np.sin(angle)], [np.sin(angle), np.cos(angle)]])

cT_rot = np.array(list(np.matmul([cT[0], cT[1]], rot_matrix)) + [cT[2]])
bT_rot = np.array(list(np.matmul([bT[0], bT[1]], rot_matrix)) + [bT[2]])
aT_rot = np.array(list(np.matmul([aT[0], aT[1]], rot_matrix)) + [aT[2]])

c_rot = cT_rot + a
b_rot = bT_rot + a
a_rot = aT_rot + a

a_xz = np.array([a_rot[0], a_rot[2]])
b_xz = np.array([b_rot[0], b_rot[2]])
c_xz = np.array([c_rot[0], c_rot[2]])

return a_xz, b_xz, c_xz

def norm_rot_3d_to_2d_array(point_array: np.array) -> np.array:
    """
    Normalize and rotate a 3D point array to a 2D point array.

    Args:
        point_array (np.array): The input 3D point array.

    Returns:
        np.array: The normalized and rotated 2D point array.
    """
    a = point_array[0, :]
    point_array_T = point_array - a
    cT = point_array_T[-1, :]
    x, y = cT[0], cT[1]
    angle = np.arctan2(y, x)
    rot_matrix = np.array([[np.cos(angle), -np.sin(angle)], [np.sin(angle), np.cos(angle)]])
    point_array_T_rot = np.column_stack([np.matmul(point_array_T[:, :2], rot_matrix),
                                         point_array_T[:, 2]])

    return point_array_T_rot

def get_slope(a, b, c):
    """
    Calculates the slope between three points in 3D space.

```

```

Parameters:
a (numpy.ndarray): The coordinates of point A in 3D space.
b (numpy.ndarray): The coordinates of point B in 3D space.
c (numpy.ndarray): The coordinates of point C in 3D space.

Returns:
float: The slope between points A, B, and C.

"""
a, b, c = norm_3d_to_2d(a, b, c)
v1 = a - b
v2 = c - b
v1_len = np.sqrt(v1.dot(v1))
v2_len = np.sqrt(v2.dot(v2))
cos_b = sum(v1 * v2) / (v1_len * v2_len)
b_rad = np.arccos(cos_b)
b_deg = b_rad * 180 / np.pi
alpha_rad = 0.5 * (np.pi - b_rad)
alpha_deg = alpha_rad * 180 / np.pi

dot = v1[0]*v2[0] + v1[1]*v2[1]
det = v1[0]*v2[1] - v1[1]*v2[0]
angle_rad = np.arctan2(det, dot)
if angle_rad > 0:
    return np.tan(alpha_rad)
else:
    return -np.tan(alpha_rad)

def get_slopes(a, b, c, d):
    """
    Calculate the slopes between four points.

    Parameters:
    a (float): The first point.
    b (float): The second point.
    c (float): The third point.
    d (float): The fourth point.

    Returns:
    tuple: A tuple containing the slopes between (a, b, c) and (b, c, d).
    """
    s1 = get_slope(a, b, c)
    s2 = get_slope(b, c, d)
    return s1, s2

```

## A.3 DATA RESAMPLING

```

import numpy as np
from scipy.interpolate import interp1d

def euclidean_distance(x, y):
    """
    Calculate the Euclidean distance between two 1D numpy arrays.

    Parameters:
    x (numpy.ndarray): The first input array.
    y (numpy.ndarray): The second input array.

    Returns:
    float: The Euclidean distance between x and y.

    Raises:
    AssertionError: If either x or y is not a 1D numpy array.
    AssertionError: If x and y are not of equal size.

```

```

"""
assert isinstance(x, np.ndarray) and isinstance(
    y, np.ndarray), "Both inputs must be numpy arrays"
assert x.ndim == 1 and y.ndim == 1, "Both inputs must be 1D arrays"
assert x.size == y.size, "Both inputs must be of equal size"
return np.sqrt(np.sum((x - y) ** 2))

def distances(x: np.array, dist=euclidean_distance):
    """
    Calculate the distances between consecutive elements in an array.

    Parameters:
    x (np.array): The input array.
    dist (function, optional): The distance function to use. Defaults to
        euclidean_distance.

    Returns:
    np.array: An array containing the distances between consecutive elements in x.
    """
    result = [0]
    for i in range(1, len(x)):
        result.append(dist(x[i-1], x[i]))
    return np.array(result)

def interpolate(x, new_dist):
    """
    Interpolates the given numpy array 'x' to a new distance 'new_dist'.

    Parameters:
    - x (numpy.ndarray): The input numpy array to be interpolated.
    - new_dist (float): The new distance between interpolated points.

    Returns:
    - numpy.ndarray: The interpolated numpy array.

    Raises:
    - AssertionError: If 'x' is not a numpy array or if 'new_dist' is not positive.
    """
    assert isinstance(x, np.ndarray), "Input must be a numpy array"
    assert new_dist > 0, "New distance must be positive"

    curr_dists = distances(x)
    curr_grid = curr_dists.cumsum()
    total_curr_dist = curr_grid.max()

    num_of_segments = int(total_curr_dist / new_dist)
    new_grid = np.cumsum([0] + num_of_segments * [new_dist])

    scipy_interp = interp1d(curr_grid, x, axis=0)(new_grid)
    return scipy_interp

```

B

ADDITIONAL VISUALISATIONS OF  
CHANGING MAXIMAL PULLING  
FORCES WITH VARYING GENERATED  
TRAJECTORIES

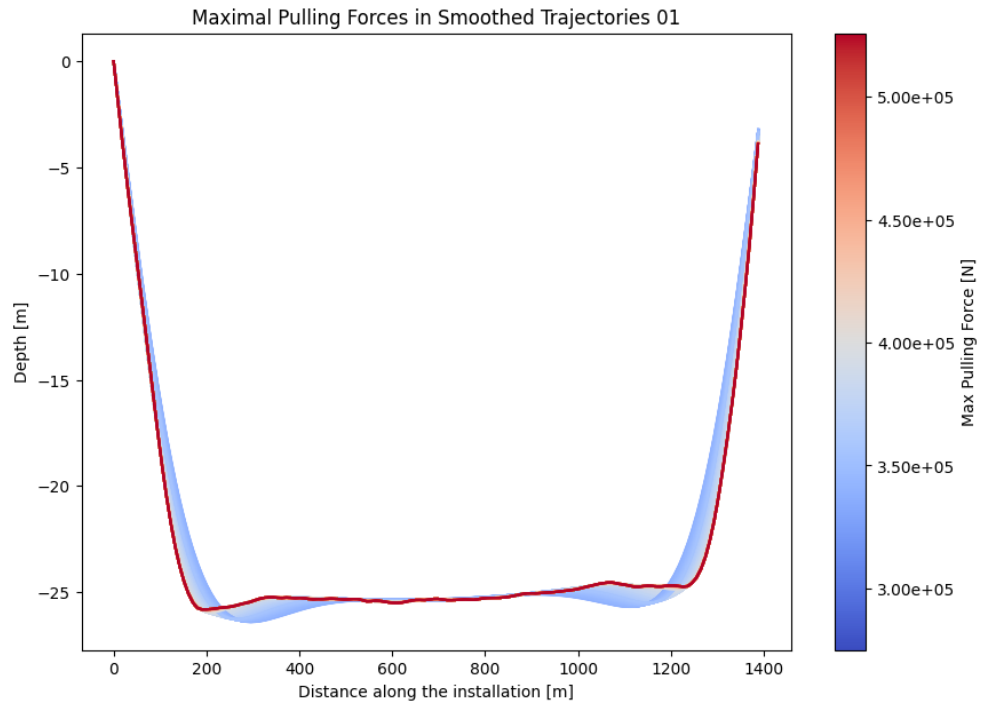


Figure B.1: Plot showing changes in maximal pulling force for varying trajectories with a colorbar for real ballast and specific gravity of slurry values

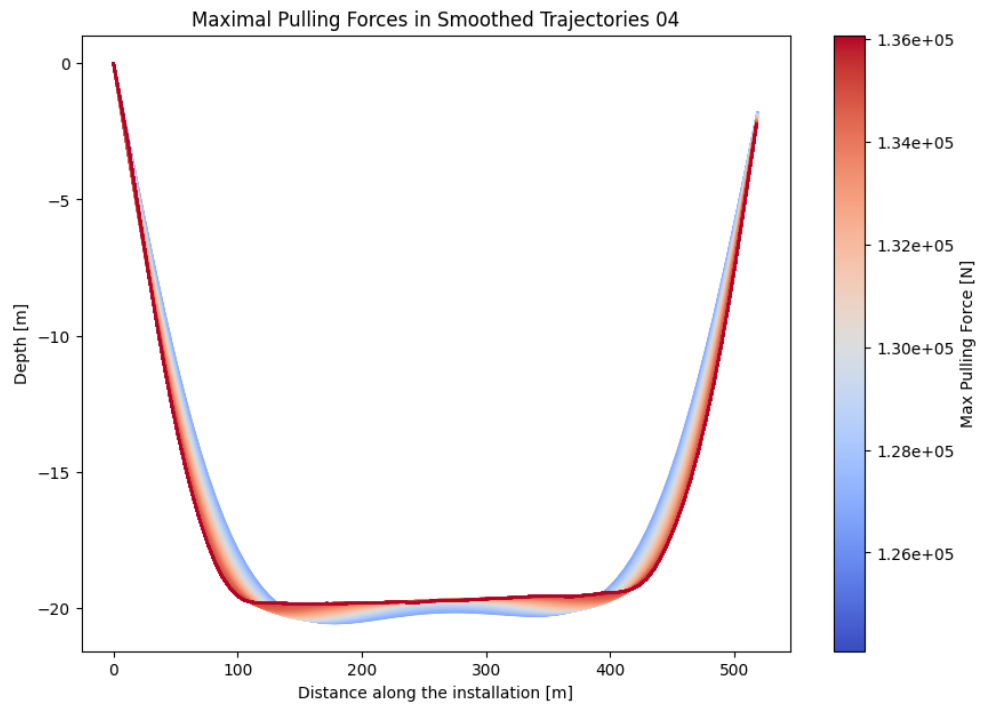


Figure B.2: Plot showing changes in maximal pulling force for varying trajectories with a colorbar for real ballast and specific gravity of slurry values

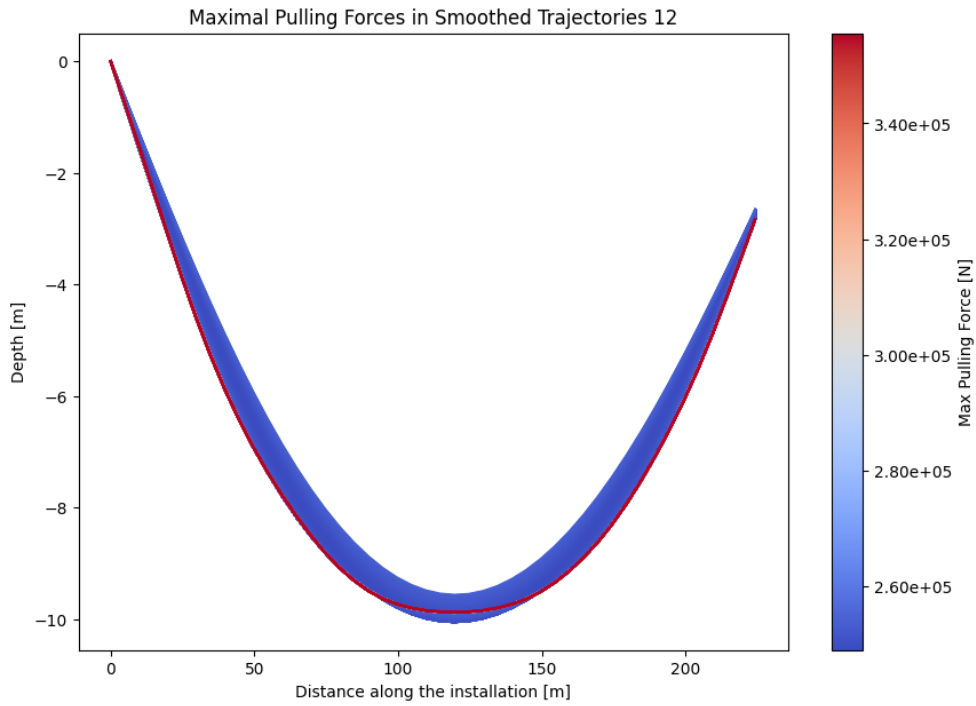


Figure B.3: Plot showing changes in maximal pulling force for varying trajectories with a colorbar for real ballast and specific gravity of slurry values

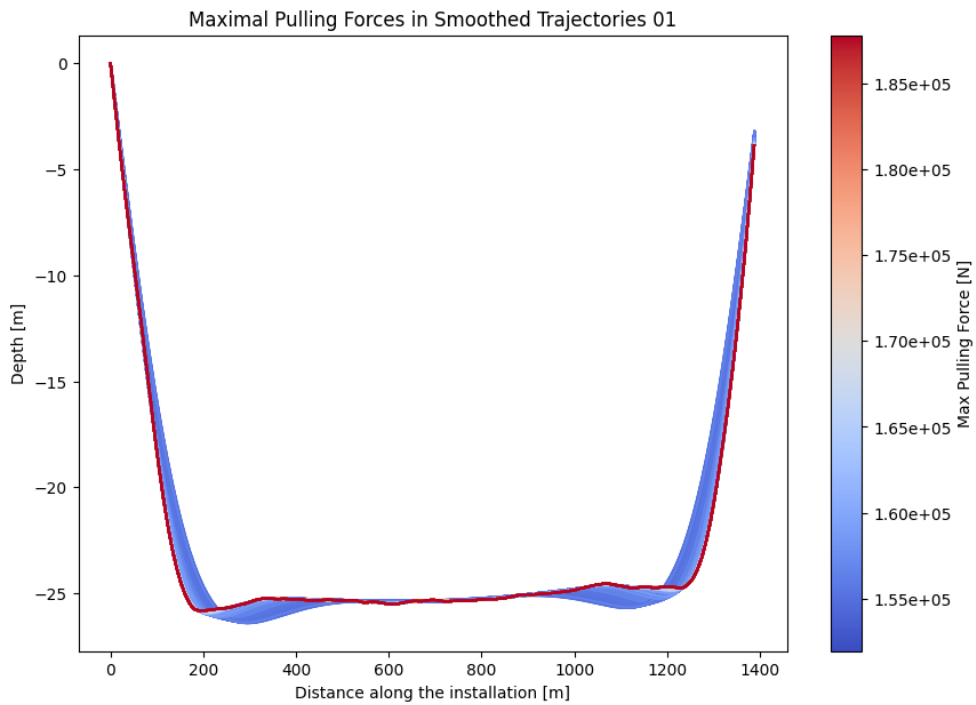


Figure B.4: Plot showing changes in maximal pulling force for varying trajectories with a colorbar for optimal ballast and specific gravity of slurry values

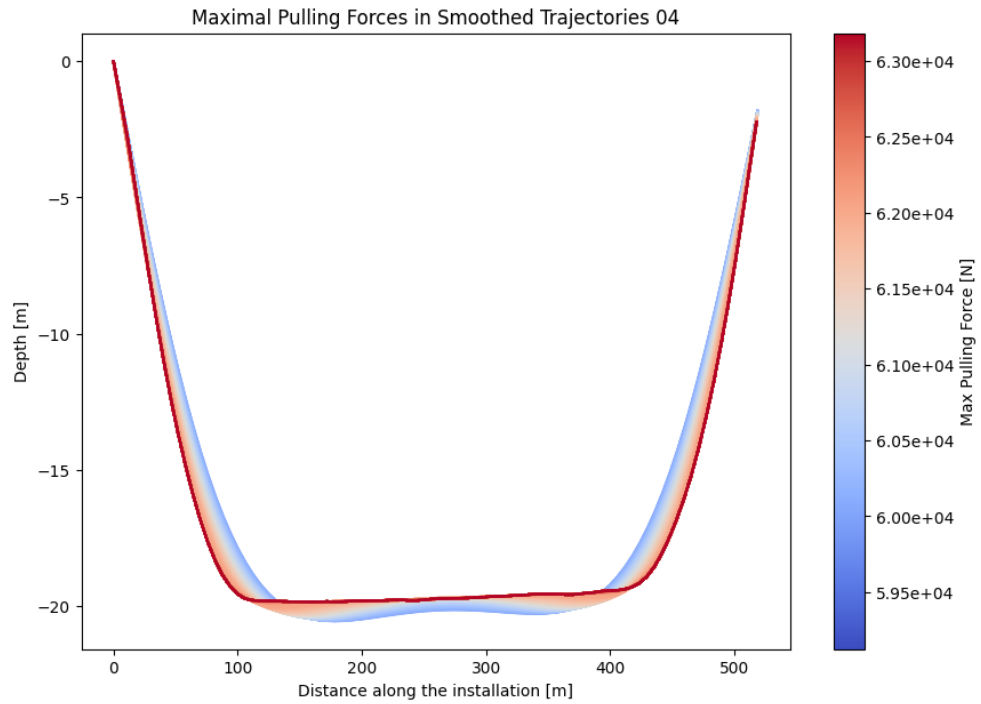


Figure B.5: Plot showing changes in maximal pulling force for varying trajectories with a colorbar for optimal ballast and specific gravity of slurry values

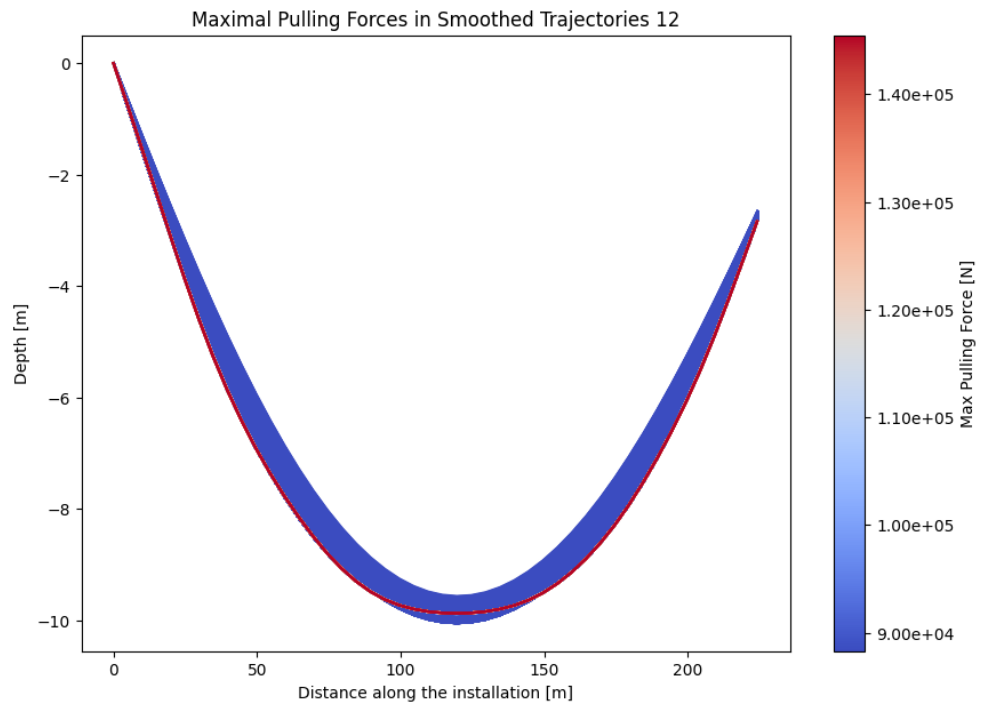


Figure B.6: Plot showing changes in maximal pulling force for varying trajectories with a colorbar for optimal ballast and specific gravity of slurry values

## BIBLIOGRAPHY

- Bormill Inc. (2019). Drill pipe. <https://www.malls-12.top/ProductDetail.aspx?iid=138703249&pr=59.88>.
- Broere, W. & van der Woude, S. (2021). Trenchless technology cie5741. Distributed at University of Technology Delft.
- Cai, L. & Xu, G. . P. M. . K. M. (2017). Horizontal directional drilling pulling forces prediction methods – a critical review. *Tunnelling and Underground Space Technology*, 69:85–93.
- Cai, L. & Polak, M. (2011). A theoretical solution to predict pulling forces in horizontal directional drilling installations. *Tunnelling and Underground Space Technology*, 83:313–323.
- Carpenter, R. (2011). 13th annual directional drilling survey: Mixed market recovery for hdd. *Underground Construction*, 66:24–28.
- Drilling Contractors Association (DCA) (2009). Dca technical guidelines. information and recommendations for planning, construction and documentation of hdd projects. DCA Conference.
- Drilling Contractors Association (DCA) (2022). Dca europe 26th annual congress dca workshop 2022 accuracy for hdd drillings. Shown at DCA congress.
- Drillingbits.eu (2019). Horizontal directional drilling parts for vermeer, ditch witch, tracto-technik. <https://drillingbits.eu/news/compact-reamers-for-hdd-horizontal-directional-drilling/>.
- F1962, A. (2011). Standard guide for use of maxi-horizontal directional drilling for placement of polyethylene pipe or conduit under obstacles, including river crossings. Company Instruction Manual.
- Farr, A. (2012). A brief history of directional drilling: The birth and development of the hdd market. <https://trenchlesstechnology.com/brief-history-horizontal-directional-drilling/#:~:text=Horizontal%20directional%20drilling%20is%20an,for%20a%20gas%20line%20installation>.
- Fisher, R. & Perkins, S. . W. A. . W. A. (2003). Gaussian smoothing. <https://homepages.inf.ed.ac.uk/rbf/HIPR2/gsmooth.htm>.
- Hijnekamp, T. (2016). Site investigation based on return flow in horizontal directional drilling. <http://resolver.tudelft.nl/uuid:f4768607-964c-43d6-8f14-fab1db0f2328>.
- Huey, D. P. & Hair, J. D. . M. K. B. (1996). Installation loading and stress analysis involved with pipelines installed in horizontal directional drilling. No Dig Conf., North American Society for Trenchless Technology (NASTT).
- Infrasoft (1996). Drillpath: Theory and user’s manual. Company Instruction Manual.
- Internal Sources (2022). Horizontal directional drilling article. *ALL ABOUT PIPELINES*, n.d.:n.d.

- Kezdi, M. (2020). Keeping your pipe straight – swivels play an important role in every hdd project. <https://trenchlesstechnology.com/swivels-play-an-important-role-in-every-hdd-project/>.
- MechaniCalc (n.d.). Beam deflection tables. <https://mechanicalc.com/reference/beam-deflection-tables>.
- Najafi, M. (2010). Trenchless technology piping: Installation and inspection, 1st edition. The McGraw-Hill Companies, Inc.
- NEN (2020). Requirements for pipeline systems - part 1: General requirements. Available at Delft University of Technology.
- Oil & Gas UK (n.d.). Cuttings in circulating drilling fluids. [https://www.rigzone.com/training/insight.asp?insight\\_id=291&c\\_id=](https://www.rigzone.com/training/insight.asp?insight_id=291&c_id=).
- Performance Pipe (1993). Technical expertise: Application for driscopipe in directional drilling and river crossings. Technical Note No. 41.
- Prime Horizontal (n.d.). Drilling tools. <https://primehorizontal.com/drilling-tools/>.
- Puckett, J. (2003). Analysis of theoretical versus actual hdd pulling loads. Conference: Pipeline Engineering and Construction International Conference.
- Rabiei, M. & Yi, Y. . B. A. . C. R. (2016). General method for pullback force estimation for polyethylene pipes in horizontal directional drilling. *Journal of Pipeline Systems Engineering and Practice*, 7:3.
- Rabiei, M. & Yi, Y. . B. A. . C. R. . O. M. (2015). New method for predicting pullback force for pipes installed via horizontal directional drilling (hdd). North American Society for Trenchless Technology (NASTT).
- Shu, B. & Ma, B. (2016). Horizontal directional drilling pulling forces prediction methods – a critical review. *Tunnelling and Underground Space Technology*, 52:1–11.
- Sullivan, D. (2023). Horizontal directional drilling methods: gyro vs. magnetic wireline steering. <https://trenchlesspedia.com/horizontal-directional-drilling-methods-gyro-vs-magnetic-wireline-steering/2/4551>.
- Underground Infrastructure Magazine (2012). Walkover locator tracking systems: Equipment spotlight. *underground infrastructure magazine*, 67:9.
- Vu, T. & Mishra, A. . K. G. (2018). Information entropy suggests stronger non-linear associations between hydro-meteorological variables and ENSO. *Entropy*, 20(1):38.
- Xu, G. & Cai, L. . J. R. . W. Z. (2018). Numerical simulation of pipe-soil interaction during pulling back phase in horizontal directional drilling installations. *Tunnelling and Underground Space Technology*, 76:194–201.
- Yang, C. J. & Zhu, W. D. . Z. W. H. . Z. X. H. . R. G. X. (2014). Determination of pipe pullback loads in horizontal directional drilling using an advanced computational dynamic model. *Journal of Engineering Mechanics*, 8:140.
- Łopata P. & Orłowicz G., W. R. . S. K. . (2020). The catenary method as an alternative to the horizontal directional drilling trajectory design in 2d space. *Energies* 2020, 13(5):1112.

## COLOPHON

This document was typeset using L<sup>A</sup>T<sub>E</sub>X. The document layout was generated using the `arsclassica` package by Lorenzo Pantieri, which is an adaption of the original `classicthesis` package from André Miede.



